

AE 721 Report 10 RAIDER Weapon System Design



Anthony Mistretta, Ben Svoboda,
Andrew Dodge, Jonathan Guzman,
Jack Barland, Peter Dillon
Instructor: Dr. Barrett



Department of Aerospace Engineering
December 4, 2023

Table of Contents

	Page #
List of Tables.....	iv
List of Figures	v
List of Symbols	vi
List of Symbols Continued.....	vii
List of Symbols Continued.....	viii
1 Previous RAIDER Work.....	1
2 General RAIDER Layout.....	3
3 Flight Assumptions and Mission Profile.....	4
4 RAIDER Design for Mach 4 at Burnout Altitude, Cruise Initiation Point	5
4.1 Determination of Required Thrust at Cruise Initiation Point	5
4.2 Assumptions	7
4.3 Calculate A_o and A_{IT}	8
4.4 Calculate Combustor Inlet Mach number, M_3 , Combustor Inlet Area, A_3 , Exit Mach Number, M_4 , and Pressure, P_4	9
4.5 Calculate Speed of Sound in Combustion Chamber.....	10
4.6 Calculate Combustion Speed, V_4	11
4.7 Calculate Combustion Chamber Length, L_c	11
4.8 Determine Throat Area	11
4.9 Design the Expansion Bell/Nozzle	11
4.10 Determine Engine Thrust and I_{sp}	12
5 Design Iteration and Optimization.....	14
5.1 Iteration 1	14
5.2 Iteration 2.....	19
5.3 Iteration 3.....	23
5.4 Iteration 4.....	28
5.5 Iteration 5.....	33
5.6 Summary of Iterations	38
6 Final RAIDER Weapon CAD Figures.....	39



Table of Contents Continued

	Page #
6.1 Fully Collapsed/Stowed.....	39
6.2 Separated.....	40
6.3 Dash and Terminal Configuration	42
7 Summary and Recommendations.....	45
7.1 Summary.....	45
7.2 Recommendations.....	46
7.3 Section Responsibilities.....	46
8 References	47
Appendix A: AE 721 Report 6 Raider AIM-9 Benchmark and Aerodynamic Properties I, Reverse & Proverse Engineering	

See Ref. 1 for AIM-9X (Raytheon image) cover image.



List of Tables

	Page #
Table 1: Reference values for Thrust Calculations (Appendix A)	5
Table 2 Summary of AIM9 Raider Iterations.....	38



List of Figures

	Page #
Figure 1: RAIDER AIM-9 Missile Full Scale Model Held by Team Members (Ref. 3).....	2
Figure 2: AIM-9 RAIDER Layout	3
Figure 3: Mission Profile for the AIM-9 RAIDER (Ref. 4, Ref. 5).....	4
Figure 4: CL, CN, CA, CD, L/D vs. Angle of Attack at Mach 4 (Appendix A).....	7
Figure 5: Expansion Bell Design.....	12
Figure 6 Iteration 1 Side View	18
Figure 7 Iteration 1 Inlet Detail View	18
Figure 8 Iteration 1 Nozzle Detail View	19
Figure 9 Iteration 2 Side View	22
Figure 10 Iteration 2 Inlet Detail View	23
Figure 11 Iteration 2 Nozzle Detail View	23
Figure 12 Iteration 3 Side View	27
Figure 13 Iteration 3 Inlet Detail View	27
Figure 14 Iteration 3 Nozzle Detail View	28
Figure 15 Iteration 4 Side View	32
Figure 16 Iteration 4 Inlet Detail View	32
Figure 17 Iteration 4 Nozzle Detail View	33
Figure 18 Iteration 5 Side View	37
Figure 19 Iteration 5 Inlet Detail View	37
Figure 20 Iteration 5 Nozzle Detail View	38
Figure 21: Front, Top, Side and Isometric View of Stowed Configuration	39
Figure 22: Labeled Isometric Stowed Configuration Cut away	40
Figure 23 Front, Top, Side and Isometric View of Separated Configuration	41
Figure 24 Labeled Isometric Cut away of Separated Configuration	42
Figure 25: Front, Top, Side, and Isometric Views of Dash and Terminal Configurations .	43
Figure 26 Labeled Isometric Cut away of Dash and Terminal Configuration	44



List of Symbols

<u>Symbol</u>	<u>Description</u>	<u>Units</u>
a	air	(~)
a	Speed of Sound	(ft/s)
A	Area	(ft ²)
c _p	Specific Heat at Constant Pressure	(~)
C*	Characteristic Flow	(ft/s)
C _A	Axial Force Coefficient	(~)
C _D	Coefficient of Drag	(~)
C _L	Coefficient of Lift	(~)
C _N	Normal Force Coefficient	(~)
D	Drag	(lbs)
f	fuel	(~)
g	gravitational constant	(ft/s ²)
H	Heating Value	(BTU/lbm)
I	Impulse	(lbf-s)
L	Length	(ft)
L	Lift	(lbs)
m	mass	(lbm)
M	Mach Number	(~)
p	Pressure	(lbf/ft ²)
r	radius	(in)
R	Universal Gas Constant	(ft-lb/slug-°R)
t	Time	(s)
T	Temperature	(R)
T	Thrust	(lbs)
V	Velocity	(ft/s)
W	Weight	(lb)
Ẇ	Fuel Flow Rate	(lbf/s)



List of Symbols Continued

<u>Greek Symbol</u>	<u>Description</u>	<u>Units</u>
α	Angle of Attack	(deg. or rad.)
γ	Ratio of Specific Heats.....	(~)
Δ	Change in	(~)
ρ	Density	(lb/in ³)

<u>Subscripts</u>	<u>Description</u>	<u>Units</u>
accel	Acceleration	(~)
avg.....	Average.....	(~)
c	Combustion Chamber.....	(~)
C	Combustor Chamber.....	(~)
comb	Combustion.....	(~)
cruise.....	Cruise	(~)
dash.....	Dash	(~)
engine.....	Of the Engine	(~)
f.....	Fuel	(~)
inlet	Inlet.....	(~)
IE.....	Inlet Entrance	(~)
IT.....	Inlet Throat.....	(~)
launch.....	Launch	(~)
Max	Maximum.....	(~)
missile.....	Missile	(~)
non dim.....	Non-Dimensional.....	(~)
o	Free Stream.....	(~)
p	Pressure.....	(~)
p	Propellant	(~)
shock cone	Shock Cone.....	(~)
sp.....	Specific.....	(~)
start	Start of Inlet	(~)



List of Symbols Continued

<u>Subscripts</u>	<u>Description</u>	<u>Units</u>
t	Throat	(~)
TC	Thermal Choking	(~)
1	Inlet	(~)
2	Inlet Exit	(~)
3	Combustor Entrance	(~)
4	Combustor Exit	(~)

<u>Acronyms</u>	<u>Description</u>	<u>Units</u>
AIM	Air Intercept Missile	(~)
CAD	Computer Aided Design	(~)
FL	Flight Level	(~)
RAIDER	Ram Air Inflatable Duct Eccentric Ramjet	(~)
TOF	Time of Flight	(s)
TSFC	Thrust Specific Fuel Consumption	(lbf/lbf-hr)



1 Previous RAIDER Work

This section will present the previous work done on the Ram Air Inflatable Duct Eccentric Ramjet (RAIDER) Air Intercept Missile (AIM)-9 project. The RAIDER AIM-9 work has consisted mainly of benchmarking using the techniques found in Missile Design and System Engineering (Ref. 2) followed by reverse and proverse engineering. This benchmarking was done on the AIM-9X. This includes aircraft performance relating to the buildup of the drag coefficient as well as exploring the tradeoffs between parameters such as aspect ratio, fineness ratio and lift to drag ratio. Other force buildups and predictions include the prediction of normal forces on planar surfaces, normal force coefficient buildup and hinge moment predictions for the AIM-9X. Aerodynamic center predictions for the body and planar surfaces, effects of flares, boattail angle effects and surface planform alternatives were also explored by the team. The last benchmarking done for the AIM-9X was a tail area sizing based on Mach number at various static margins and a complete aerodynamic buildup of the normal force coefficient.

After benchmarking, the AIM-9X was then reverse engineered. A mission profile and payload range diagram were generated followed by approximation of specific impulse and Thrust Specific Fuel Consumption (TSFC). Mission lift to drag ratios were found based on the propellant, missile weights and thrust at different phases in the mission profile. Also, the Mach number, angle of attack and coefficient of lift were found at the cruise condition of Mach 2.5 and altitude of 45,000 ft. The cruise midpoint air density was then found assuming the weight was 50% of the original weight in cruise and the temperature at high altitudes in the troposphere is considered constant. This new mid-point air density led to an updated mission profile altitude of 56,500 ft.

After reverse engineering the AIM-9X, some of the calculated parameters were then used to proverse engineer the new RAIDER AIM-9 missile. This would minimize the size profile of the AIM-9X by incorporating a ramjet engine, then folding canard and tail surfaces to allow for the new RAIDER AIM-9 to be tube launched. The goal of the proverse engineering was to reduce the size and keep the same range of the AIM-9X of 20 miles. This process was iterative and was first designed to a cruise angle of attack of 8 degrees. The subsequent iterations converged on a



linear dimension size reduction of 66.9% of the original AIM-9X and a new weight of 62.6 lbs while keeping the same range of 20 miles.

After the proverse engineering a computer aided design (CAD) model of the new RAIDER AIM-9 was made and materials were purchased to make a full-scale model of the new missile. The constructed model can be seen below in Figure 1 being held by some of the team.



Figure 1: RAIDER AIM-9 Missile Full Scale Model Held by Team Members (Ref. 3)

2 General RAIDER Layout

This section covers the general RAIDER layout. The general layout of the AIM-9 RAIDER, including the inflated ducts, is shown below. The following sections will size subcomponents more specifically.

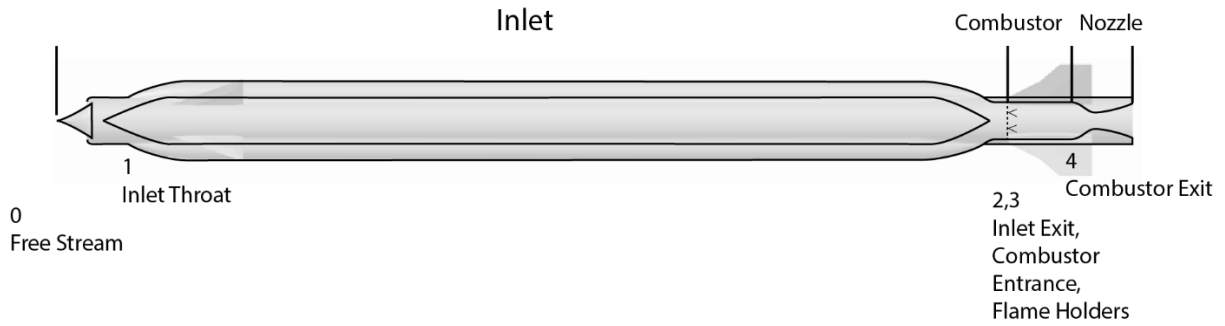


Figure 2: AIM-9 RAIDER Layout

3 Flight Assumptions and Mission Profile

This section covers the flight assumptions and mission profile. For the AIM-9 RAIDER, the missile will be tube launched from an aircraft at an altitude of 56,500 ft at a speed of Mach 2.5. A rocket motor will be used to propel the missile up to an altitude of 80,000 ft and a speed of Mach 4. After this, the ducts for the ramjet are then inflated as the missile cruises for 19.7 miles at Mach 4. The missile then terminally moves to kill the target.

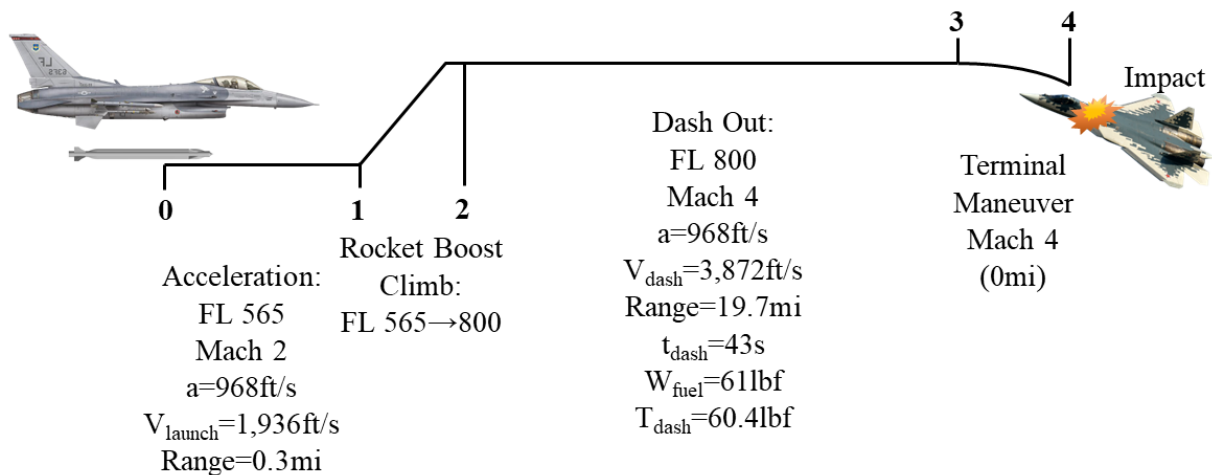


Figure 3: Mission Profile for the AIM-9 RAIDER (Ref. 4, Ref. 5)

Please note that the numbers included in this figure were calculated in section 4.1 as well as Appendix A.



4 RAIDER Design for Mach 4 at Burnout Altitude, Cruise Initiation Point

This section will cover the design of the RAIDER powerplant. Within this section, γ and R are assumed to be 1.4 (~) and 1716 ft-lb/slug-°R, respectively.

4.1 Determination of Required Thrust at Cruise Initiation Point

This subsection will derive the thrust at cruise at the given Mach number of 4 at 80,000 ft. The values for initial launch weight and thrust were previously found using Appendix A. The previously found given values of the missile from this reference that will be used for calculation are seen below.

Table 1: Reference values for Thrust Calculations (Appendix A)

Reference	Value
Launch Weight, W_{Launch}	62.6 lb
Max Thrust of Rocket Propellant, T_{Max}	4,000 lb

The velocity of the missile at Mach 4 at 80,000 ft is found below. The value for temperature is from Appendix B of Ref. 6 at FL 800. The calculations seen below were found using Appendix A.

$$a_0 = \sqrt{\gamma RT_0} = \sqrt{(1.4) \left(1716 \frac{ftlb}{slugR} \right) (390 \text{ }^\circ R)} = 968 \frac{ft}{s} \quad (1)$$

$$V_{dash} = M * a_0 = 4 * 968 \frac{ft}{s} = 3872 \frac{ft}{s} \quad (2)$$

The time to accelerate from the launch velocity to the dash velocity was calculated as shown in Equation 3 using an assumed launch velocity of Mach 2.0.

$$\Delta t = \frac{\Delta V}{a} = \frac{V_{dash} - V_{Launch}}{\frac{T_{Max}}{m_{Launch}}} = \frac{3872 \frac{ft}{s} - 1936 \frac{ft}{s}}{\left(\frac{4,000lb}{\frac{62.6lb}{32.2 \frac{ft}{s}}} \right)} = 0.67s \quad (3)$$

Range was then calculated for the acceleration phase as shown in Equation 4.

$$Range_{accel} = V_{avg} * t_{accel} = \frac{3872 \frac{ft}{s} + 1936 \frac{ft}{s}}{2} * 0.67 s = 1946ft = 0.269 mi \quad (4)$$



Dash range was found simply by subtracting the acceleration range from the known total range of the AIM-9X. Time of flight during the dash phase was calculated as shown in Equation 5.

$$TOF_{dash} = \frac{Range_{dash}}{V_{dash}} = \frac{19.631 \text{ mi} * 5280 \frac{ft}{mi}}{3872 \frac{ft}{s}} = 26.8s \quad (5)$$

From Appendix A, the new fuel weight using jet fuel in dash is 1.47 lb. This value will be used for $W_{f_{dash}}$. The rocket fuel used to get the new AIM-9X up to dash is 10.73 lb, per Appendix A. The specific impulse of the RAIDER engine is assumed to 1,100 s. The thrust required in the dash was calculated as shown in Equation 6.

$$T_{dash} = I_{sp} * \frac{W_{f_{dash}}}{TOF_{dash}} = 1100 \text{ s} * \frac{1.47lb}{26.8 \text{ s}} = 60.4 \text{ lb} \quad (6)$$

Now having the thrust at cruise, the L/D_{cruise} can be found. That equation can be seen below. Note the weights were previously found in Appendix A

$$\frac{L}{D_{Cruise}} = \frac{W_{missile} - (W_f - W_{f_{dash}})}{T_{dash}} = \frac{62.6lb - (10.73lb - 1.74lb)}{60.4lb} = 0.89$$

From Appendix A the cruise angle of attack can be found. Figure 4 below shows the different coefficients compared to angles of attack.



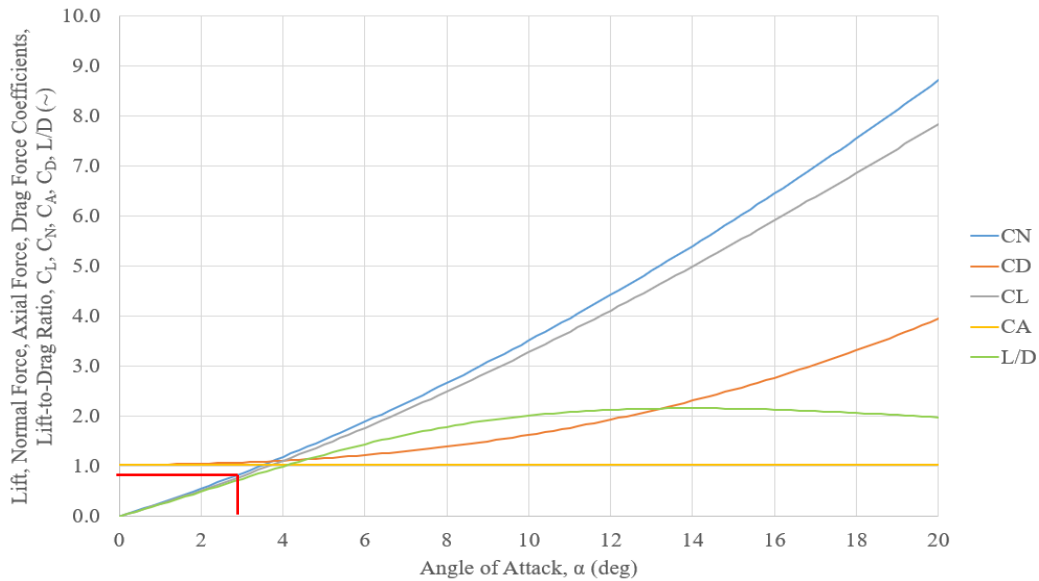


Figure 4: CL, CN, CA, CD, L/D vs. Angle of Attack at Mach 4 (Appendix A)

Since it has been found that $L/D_{cruise} = 0.89$, the α_{cruise} is equal to 2.75 degrees.

4.2 Assumptions

The assumptions that are to be used in these sections are as follows:

- Fuel air ratio of 0.067 (stoichiometric)
- Fuel Heating Value, $H_f = 17,900 \text{ btu/lbm}$, assumed value from Ref. 2.
- $I_{sp} = 1100 \text{ s}$
- $\gamma_0 = 1.4$
- $c_p = 0.302 \frac{\text{btu}}{\text{lbm}^\circ\text{R}}$
- FL 800
- $\rho_0 = 8.6831 \times 10^{-5} \frac{\text{slug}}{\text{ft}^3}$ (Ref. 6)
- $P_0 = 58.125 \frac{\text{lb}}{\text{ft}^2}$ (Ref. 6)
- $T_0 = 390 \text{ }^\circ\text{R}$ (Ref. 6)
- $M_0 = 4$ (~)
- $t_{comb} = 0.001 \text{ s}$ with special fuel additives
- $C^* = 5,200 \frac{\text{ft}}{\text{s}}$



- $g = 32.2 \frac{ft}{s^2}$
- $\gamma_3 = 1.3$

4.3 Calculate A_o and A_{IT}

This section will find the free stream flow area, A_o , and the inlet throat area, A_{IT} . The combustion exit temperature, T_4 , value will be needed for these calculations and can be found using figure 3.25 from Ref. 2. The assumptions and values used in this calculation can be found in section 4.2.

$$T_4 \approx T_o \left\{ 1 + \left[\frac{(\gamma_o - 1)}{2} \right] M_o^2 \right\} + \left(\frac{H_f}{c_p} \right) \left(\frac{f}{a} \right) =$$

$$390R \left\{ 1 + \left[\frac{(1.4 - 1)}{2} \right] 4^2 \right\} + \left(\frac{17,900 \frac{btu}{lbm}}{0.302 \frac{btu}{lbmR}} \right) (0.067) = 5609^\circ R \quad (7)$$

Now having the combustion exit temperature, the free stream flow area can be found. Using figure 3.27 from Ref. 2, the non-dimensional thrust can be found. After finding this value, the free stream flow area can be found. This equation and calculation can be seen below.

$$\frac{T}{p_o A_o} = \gamma_o M_o^2 \left\{ \left\{ \frac{\frac{T_4}{T_o}}{1 + \left[\frac{(\gamma_o - 1)}{2} \right] M_o^2} \right\}^{\frac{1}{2}} - 1 \right\} =$$

$$1.4(4^2) \left\{ \left\{ \frac{\frac{5609^\circ R}{390^\circ R}}{1 + \left[\frac{(1.4 - 1)}{2} \right] 4^2} \right\}^{\frac{1}{2}} - 1 \right\} = 19 \quad (8)$$

The free stream pressure and dash thrust are known values; thus, the free stream flow area can be found. Note that $58.125 \frac{lb}{ft^2} = 0.403 \frac{lb}{in^2}$.

$$A_o = \frac{T}{p_o * T_{non dim}} = \frac{60.4 lb}{0.403 \frac{lb}{in^2} * 19} = 7.89 in^2 \quad (9)$$

Using the free stream flow area into inlet calculated in Equation 9, the inlet sonic throat area can be calculated using Equation 10 and Equation 11 below.



$$\frac{A_{IT}}{A_o} = 1.728(M_{IE})_{Start} [1 + 0.2(M_{IE})_{Start}^2]^{-3} \quad (10)$$

$$A_{IT} = 7.89\{1.728(1.5)[1 + 0.2(1.5)^2]^{-3}\} = 6.71 \text{ in}^2 \quad (11)$$

4.4 Calculate Combustor Inlet Mach number, M_3 , Combustor Inlet Area, A_3 , Exit Mach Number, M_4 , and Pressure, P_4

To begin finding the inlet Mach number the temperature ratio between the combustor exit temperature and the free stream temperature needed to be calculated. This calculation is shown below in Equation 12.

$$\frac{T_4}{T_o} = \frac{5609 \text{ }^\circ R}{390 \text{ }^\circ R} = 14.4 \quad (12)$$

The inlet Mach number was then calculated using the temperature ratio of 14.4 and Equation 13 and was found to be 0.25.

$$(M_3)_{TC} \approx 0.461 \left[\frac{(1 + 0.2M_o^2)}{\left(\frac{T_{4t}}{T_o}\right)} \right]^{\frac{1}{2}} = 0.461 \left[\frac{(1 + 0.2(4)^2)}{14.4} \right]^{\frac{1}{2}} = 0.25 \quad (13)$$

The inlet Mach number calculated in Equation 13 was used to find the combustor inlet area and the calculation is shown below in Equation 14 and Equation 15 and was found to be 16.1 in².

$$\frac{A_{IT}}{A_3} = \frac{1.728M_3}{(1 + 0.2M_3^2)^3} \quad (14)$$

$$A_3 = \frac{6.71 \text{ in}^2 (1 + 0.2(0.25)^2)^3}{1.728(0.25)} = 16.1 \text{ in}^2 \quad (15)$$

To find the combustor exit Mach number the temperature at the combustor inlet was calculated using Equation 16 below.

$$T_3 = [1 + 0.2(4)^2]390 = 1638 \text{ }^\circ R \quad (16)$$

Equations 17 through 21 were used to calculate the combustor exit Mach number which was found to be 1.

$$M_4 \approx \left\{ \frac{\left[-b - (b^2 - 4ac)^{\frac{1}{2}} \right]}{(2a)} \right\}^{\frac{1}{2}} \quad (17)$$



$$a = 1.822 \left(\frac{T_4}{T_3} \right) M_3^2 - 1.175 = 1.822(3.42)(0.25)^2 - 1.175 = -0.785 \quad (18)$$

$$b = 2.70 \left(\frac{T_4}{T_3} \right) M_3^2 = 2.70(3.42)(0.25)^2 = 0.577 \quad (19)$$

$$c = \left(\frac{T_4}{T_3} \right) M_3^2 = 3.42(0.25)^2 = 0.214 \quad (20)$$

$$M_4 \approx \left\{ \frac{\left[-(0.577) - (0.577^2 - 4(-0.785)(0.214))^{\frac{1}{2}} \right]}{2(-0.785)} \right\}^{\frac{1}{2}} = 1.00 \quad (21)$$

Using the combustor exit Mach number calculated in Equation 21, the pressure ratio between the combustor exit and the combustor entrance was found using Equation 22 below.

$$\frac{p_4}{p_3} = \frac{\left\{ 1 + \left[\frac{(\gamma - 1)}{2} \right] M_4^2 \right\}^{\frac{\gamma}{\gamma - 1}}}{(1 + \gamma M_4^2)} = \frac{\left\{ 1 + \left[\frac{1.4 - 1}{2} \right] (1)^2 \right\}^{3.5}}{(1 + 1.4(1)^2)} = 0.789 \quad (22)$$

By utilizing the isentropic pressure relationship, the pressure ratio between the combustor entrance and the inlet can also be found as seen in Equation 23.

$$\frac{p_3}{p_0} = \left\{ 1 + \left[\frac{(\gamma - 1)}{2} \right] M_3^2 \right\}^{\frac{\gamma}{\gamma - 1}} = \left\{ 1 + \left[\frac{(1.3 - 1)}{2} \right] 0.25^2 \right\}^{\frac{1.3}{1.3 - 1}} = 1.04 \quad (23)$$

With this, the pressure at the combustor entrance can be found as seen in Equation 24 and the pressure at the combustor exit can be found using the ratio previously found in Equation 22. This calculation can be seen below in Equation 25.

$$p_3 = p_0(1.04) = 58.125 \text{ lb/ft}^2 * 1.04 = 60.5 \text{ lb/ft}^2 \quad (24)$$

$$p_4 = p_3(0.789) = 60.5 \text{ lb/ft}^2 * 0.789 = 47.7 \text{ lb/ft}^2 \quad (25)$$

4.5 Calculate Speed of Sound in Combustion Chamber

With the calculations shown above, the speed of sound at the combustor exit can be found as shown below in Equation 26 using the assumptions outlined in section 4.2.

$$a_4 = \sqrt{\gamma_4 R_4 T_4} = \sqrt{1.3 * 1716 \frac{\text{ft} * \text{lb}}{\text{slug} * ^\circ\text{R}} * 5,609 ^\circ\text{R}} = 3,537 \frac{\text{ft}}{\text{s}} \quad (26)$$



4.6 Calculate Combustion Speed, V_4

With the speed of sound and the Mach number at the combustor exit known, the velocity at the combustor exit can be solved for as seen below in Equation 27.

$$V_4 = a_4 M_4 = 3,671 \frac{ft}{s} * 1 = 3,537 \frac{ft}{s} \quad (27)$$

4.7 Calculate Combustion Chamber Length, L_c

As shown above, the velocity at the combustor exit was found to be 3,537 ft/s. With this, along with the assumption of the time of combustion as seen in section 4.2, the length of the combustion chamber can be found below in Equation 28.

$$L_c = V_{comb} * t_{comb} = 3,671 \frac{ft}{s} * 0.001 s = 3.54 ft \quad (28)$$

Due to the large combustor chamber length, the team designed the combustor chamber to start in the ducts, so that the rest of the chamber can fit within the length of the missile. This means that combustion will start in the ducts.

4.8 Determine Throat Area

Within this section the propellant weight flow rate during dash will be used, where the propellant weight flow rate is the quantity $W_{f_{dash}}$ divided by TOF_{dash} from section 4.1. The equation for propellant weight flow rate is shown below in Equation 29 from Ref. 2.

$$\dot{W}_p = \frac{gp_c A_t}{C^*} \quad (29)$$

The above equation will be rearranged as seen in Equation 30 and will then be used to solve for the throat area.

$$A_t = \frac{\dot{W}_p C^*}{gp_c} = \frac{1.47 \frac{lb_f}{s} * 5,200 \frac{ft}{s}}{32.2 \frac{ft}{s^2} * 60.5 \frac{psf}}{32.2 \frac{ft}{s^2} * 60.5 \frac{psf}}{32.2 \frac{ft}{s^2} * 60.5 \frac{psf}}} = 0.146 ft^2 = 21.1 in^2 \quad (30)$$

4.9 Design the Expansion Bell/Nozzle

Because the nozzle throat area was determined to be greater than that of the missile cross sectional area, the team had to add a flare to the aft end of the missile with an adaptive expansion bell to accommodate the large, required area. The addition of a flare allowed the team to fit the 21.1 in² nozzle throat, and the adaptive bell allowed for the flow to be properly expanded beyond



that already expanded diameter. The CAD drawing of the expansion bell, in its deployed state can be seen in Figure 5 below.

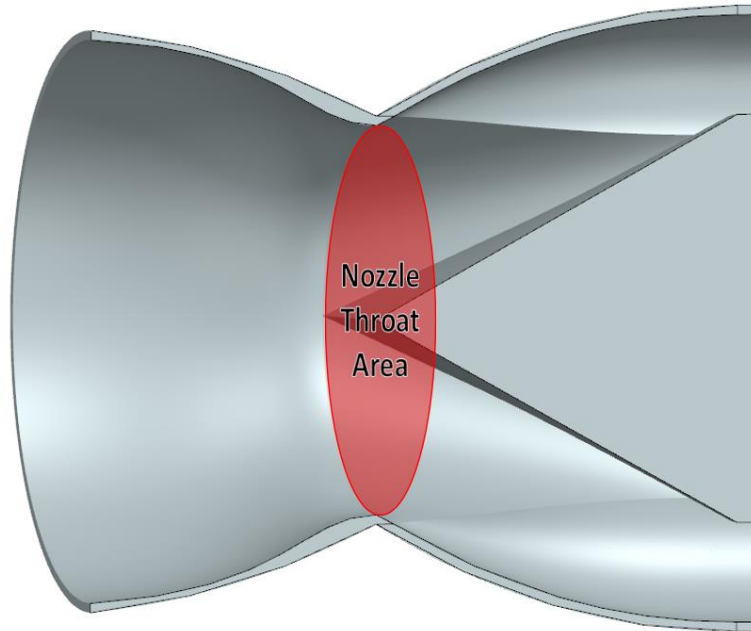


Figure 5: Expansion Bell Design

4.10 Determine Engine Thrust and I_{sp}

With the propulsion system designed the thrust and I_{sp} can be calculated. Equation 31, 32, and 33 below show the prediction of the I_{sp} for the initially designed propulsion system using the values found in the preceding sections.

$$\frac{I_{sp} g_c p T_0}{a_0 H_f} = \frac{M_0 \left(\sqrt{\frac{\left(\frac{T_4}{T_0}\right)}{\left(1 + \left(\frac{\gamma_0 - 1}{2}\right) * M_0^2\right)}} - 1 \right)}{\left(1 + \left(\frac{\gamma_0 - 1}{2}\right) * M_0^2\right) \left(\frac{\left(\frac{T_4}{T_0}\right)}{\left(1 + \left(\frac{\gamma_0 - 1}{2}\right) * M_0^2\right)} - 1 \right)} \quad (31)$$

$$I_{sp} = \frac{M_0 \left(\sqrt{\frac{\left(\frac{T_4}{T_0}\right)}{\left(1 + \left(\frac{\gamma_0 - 1}{2}\right) * M_0^2\right)}} - 1 \right) a_0 H_f}{g c_p T_0 \left(\left(1 + \left(\frac{\gamma_0 - 1}{2}\right) * M_0^2\right) \left(\frac{\left(\frac{T_4}{T_0}\right)}{\left(1 + \left(\frac{\gamma_0 - 1}{2}\right) * M_0^2\right)} \right) - 1 \right)} \quad (32)$$

$$I_{sp} = \frac{4 \left(\sqrt{\frac{\left(\frac{5,609}{390}\right)}{\left(1 + \left(\frac{1.4 - 1}{2}\right) 4^2\right)}} - 1 \right) * 968 * 17,900}{32.2 * 0.302 * 390 \left(\left(1 + \left(\frac{1.4 - 1}{2}\right) * 4^2\right) \left(\frac{\left(\frac{5,609}{390}\right)}{\left(1 + \left(\frac{1.4 - 1}{2}\right) * 4^2\right)} \right) - 1 \right)} = 2,100 \text{ s} \quad (33)$$

Finally, the thrust for the designed propulsion system will be calculated as seen below in Equation 34.

$$T = p_o A_o \gamma_o M_o^2 \left\{ \left(\frac{\frac{T_4}{T_0}}{1 + \left[\frac{\gamma_o - 1}{2}\right] M_o^2} \right)^{\frac{1}{2}} - 1 \right\} =$$

$$58.125 * \frac{7.89}{12^2} * 1.4 * 4^2 \left\{ \sqrt{\left(\frac{\left(\frac{5,609}{390}\right)}{\left(1 + \left(\frac{1.4 - 1}{2}\right) * 4^2\right)} \right)} - 1 \right\} = 61 \text{ lbs} \quad (34)$$

It can be seen above that the thrust generated by the propulsion system is 61 lbs.



5 Design Iteration and Optimization

This section covers the iteration process and optimization of the team's new AIM-9 RAIDER design. To complete the iteration process the same steps shown in section 4 were used.

The variables changed were the following:

- Inlet area;
- Altitude of cruise.

The team is attempted to:

- Minimize inlet throat area which should;
- Minimize fuel consumption and;
- Maximize range.

For the general concept, the team varied the inlet area (reducing it) to minimize the fuel consumption and shrink the expansion bell to a reasonable size. The team also reduced the altitude to increase the thrust and decide the best altitude for cruise. There was no iterative function to convergence in the normal sense, instead, just adjusting assumptions until the team got a more reasonable, desirable outcome. The team also made the effort to maintain thrust required for cruise.

5.1 Iteration 1

To begin iteration one, the team reduced the cruising speed of the RAIDER AIM-9 to Mach 2.5. This is the speed the AIM-9X was assumed to cruise at as seen in Appendix A. To begin this process, the cruise speed was first found. This was done as seen below in Equation 35 using the speed of sound as seen in Equation 1.

$$V = M * a_0 = 2.5 * 968 \frac{ft}{s} = 2,420 \frac{ft}{s} \quad (35)$$

With this velocity, the new TOF was found as seen below in Equation 36.

$$TOF_{dash} = \frac{Range_{dash}}{V_{dash}} = \frac{19.631 \text{ mi} * 5280 \frac{ft}{mi}}{2,420 \frac{ft}{s}} = 42.8s \quad (36)$$



Next, the specific impulse of the engine was calculated. This calculation can be seen below in Equation 37

$$I_{sp} = \frac{M_0 \left(\sqrt{\frac{\left(\frac{T_4}{T_0}\right)}{\left(1 + \left(\frac{\gamma_0 - 1}{2}\right) * M_0^2\right)}} - 1 \right) a_0 H_f}{g c_p T_0 \left(\left(1 + \left(\frac{\gamma_0 - 1}{2}\right) * M_0^2\right) \left(\frac{\left(\frac{T_4}{T_0}\right)}{\left(1 + \left(\frac{\gamma_0 - 1}{2}\right) * M_0^2\right)} - 1 \right) \right)} =$$

$$2.5 \left(\sqrt{\frac{\left(\frac{4849 \text{ }^\circ R}{390 \text{ }^\circ R}\right)}{\left(1 + \left(\frac{1.4 - 1}{2}\right) * 2.5^2\right)}} - 1 \right) 968 \frac{ft}{s} * 17,900 \frac{BTU}{lb}$$

$$32.2 \frac{ft}{s^2} * 0.302 \frac{BTU}{lbm * ^\circ R} * 390 \left(\left(1 + \left(\frac{1.4 - 1}{2}\right) 2.5^2\right) \left(\frac{\left(\frac{4849 \text{ }^\circ R}{390 \text{ }^\circ R}\right)}{\left(1 + \left(\frac{1.4 - 1}{2}\right) * 2.5^2\right)} - 1 \right) \right) \quad (37)$$

$$I_{sp} = 1,350 \text{ s}$$

The thrust required for the dash segment was then calculated in Equation 38.

$$T_{dash} = I_{sp} * \frac{W_f_{dash}}{TOF_{dash}} = 1350 \text{ s} * \frac{1.47lb}{42.8 \text{ s}} = 48.1 \text{ lb} \quad (38)$$

With these values found, the inlet throat area was calculated for these values. This can be seen below in Equation 39 through Equation 43.

$$T_4 \approx T_o \left\{ 1 + \left[\frac{(\gamma_o - 1)}{2} \right] M_o^2 \right\} + \left(\frac{H_f}{c_p} \right) \left(\frac{f}{a} \right) =$$

$$390^\circ R \left\{ 1 + \left[\frac{(1.4 - 1)}{2} \right] 2.5^2 \right\} + \left(\frac{17,900 \frac{btu}{lbm}}{0.302 \frac{btu}{lbmR}} \right) (0.067) = 4,849 \text{ }^\circ R \quad (39)$$



$$\frac{T}{p_o A_o} = \gamma_o M_o^2 \left\{ \left\{ \frac{\frac{T_4}{T_o}}{1 + \left[\frac{(\gamma_o - 1)}{2} \right] M_o^2} \right\}^{\frac{1}{2}} - 1 \right\} =$$

$$1.4(2.5^2) \left\{ \left\{ \frac{\frac{4,849^\circ R}{390^\circ R}}{1 + \left[\frac{(1.4 - 1)}{2} \right] 2.5^2} \right\}^{\frac{1}{2}} - 1 \right\} = 11.8 \quad (40)$$

$$A_o = \frac{T}{p_o * T_{non dim}} = \frac{48.1 lb}{0.403 \frac{lb}{in^2} * 11.8} = 10.1 in^2 \quad (41)$$

$$\frac{A_{IT}}{A_o} = 1.728(M_{IE})_{Start} [1 + 0.2(M_{IE})_{Start}^2]^{-3} \quad (42)$$

$$A_{IT} = 10 in^2 * \{1.728(1.5)[1 + 0.2(1.5)^2]^{-3}\} = 8.5 in^2 \quad (43)$$

With the geometry found, the combustor Mach numbers, geometries, and pressure were found. To begin, the combustor inlet and exit Mach number was found as seen below in Equation 44 through Equation 53.

$$\frac{T_4}{T_o} = \frac{4,849^\circ R}{390^\circ R} = 12.4 \quad (44)$$

$$(M_3)_{TC} \approx 0.461 \left[\frac{(1 + 0.2M_o^2)}{\left(\frac{T_{4t}}{T_o}\right)} \right]^{\frac{1}{2}} = 0.461 \left[\frac{(1 + 0.2(2.5)^2)}{12.4} \right]^{\frac{1}{2}} = 0.20 \quad (45)$$

$$\frac{A_{IT}}{A_3} = \frac{1.728M_3}{(1 + 0.2M_3^2)^3} \quad (46)$$

$$A_3 = \frac{9.27 in^2 (1 + 0.2(0.20)^2)^3}{1.728(0.20)} = 38.2 in^2 \quad (47)$$

$$T_3 = [1 + 0.2(M_o)^2]T_o = [1 + 0.2(2.5)^2]390 = 877^\circ R \quad (48)$$

$$M_4 \approx \left\{ \frac{\left[-b - (b^2 - 4ac)^{\frac{1}{2}} \right]}{(2a)} \right\}^{\frac{1}{2}} \quad (49)$$

$$a = 1.822 \left(\frac{T_4}{T_3}\right) M_3^2 - 1.175 = 1.822(5.53)(0.20)^2 - 1.175 = -0.772 \quad (50)$$



$$b = 2.70 \left(\frac{T_4}{T_3} \right) M_3^2 = 2.70(5.53)(0.20)^2 = 0.597 \quad (51)$$

$$c = \left(\frac{T_4}{T_3} \right) M_3^2 = 3.42(0.20)^2 = 0.137 \quad (52)$$

$$M_4 \approx \left\{ \frac{\left[-0.597 - \sqrt{0.597^2 - 4(-0.772)(0.137)} \right]^{\frac{1}{2}}}{2(-0.772)} \right\}^{\frac{1}{2}} = 0.98 \quad (53)$$

With these Mach numbers found, the pressures at the combustor inlet and exit were then found in Equation 54 Equation 57.

$$\frac{p_4}{p_3} = \frac{\left\{ 1 + \left[\frac{\gamma - 1}{2} \right] M_4^2 \right\}^{\frac{\gamma}{\gamma - 1}}}{(1 + \gamma M_4^2)} = \frac{\left\{ 1 + \left[\frac{1.3 - 1}{2} \right] (0.98)^2 \right\}^{4.33}}{(1 + 1.3(0.98)^2)} = 0.797 \quad (54)$$

$$\frac{p_3}{p_0} = \left\{ 1 + \left[\frac{\gamma - 1}{2} \right] M_3^2 \right\}^{\frac{\gamma}{\gamma - 1}} = \left\{ 1 + \left[\frac{(1.3 - 1)}{2} \right] 0.20^2 \right\}^{\frac{1.3}{1.3 - 1}} = 1.03 \quad (55)$$

$$p_3 = p_0(1.03) = 58.125 \frac{lb}{ft^2} * 1.04 = 59.9 \text{ lb/ft}^2 \quad (56)$$

$$p_4 = p_3(0.789) = 59.9 \text{ lb/ft}^2 * 0.797 = 47.7 \text{ lb/ft}^2 \quad (57)$$

Finally, the geometry of the combustor was calculated as seen below in Equation 58 through Equation 61.

$$a_4 = \sqrt{\gamma_4 R_4 T_4} = \sqrt{1.3 * 1716 \frac{ft * lb}{slug * ^\circ R} * 4,849 ^\circ R} = 3,289 \frac{ft}{s} \quad (58)$$

$$V_4 = a_4 M_4 = 3,289 \frac{ft}{s} * 0.98 = 3,223 \frac{ft}{s} \quad (59)$$

$$L_C = V_{comb} * t_{comb} = 3,223 \frac{ft}{s} * 0.001 s = 3.22 ft \quad (60)$$

$$A_t = \frac{\dot{W}_p C^*}{g p_c} = \frac{1.47 \text{ lbf}}{42.8 \text{ s}} * 5,200 \frac{ft}{s}}{32.2 \frac{ft}{s^2} * 59.9 \text{ psf}} = 0.093 \text{ ft}^2 = 13.3 \text{ in}^2 \quad (61)$$

To accommodate these changes, specifically with the inlet capture area, the missile diameter had to be increased from 3.37in to a minimum of 4.5in. This change allows for the



specified 15.2in^2 for A_0 . It should be noted that this new diameter of 4.5in approaches the original AIM-9X diameter of $\sim 5.04\text{in}$. Again, due to combustion chamber length, combustion would have to occur in the ducts, which should increase in cross sectional area to slow the gas flow and allow for combustion. The side view of the newly sized missile is shown in Figure 6 below.

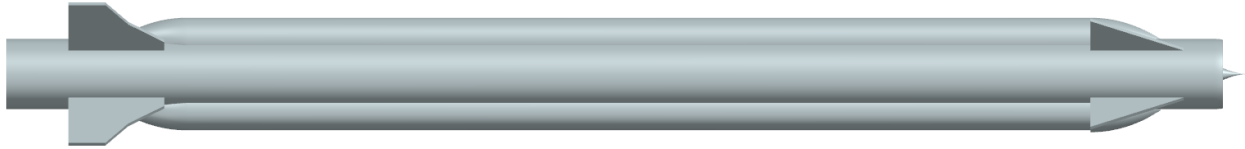


Figure 6 Iteration 1 Side View

The inlet geometry is shown in detail below in Figure 7.

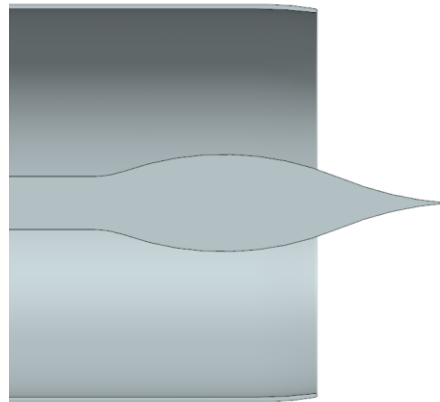


Figure 7 Iteration 1 Inlet Detail View

A detail view of the nozzle geometry is shown in Figure 8 below. As seen, there is little room for exhaust expansion to occur, meaning that the use of a shape memory alloy expanding nozzle flare section would be of benefit to allow for more fully expanded flow.



Figure 8 Iteration 1 Nozzle Detail View

5.2 Iteration 2

Since iteration one's diameter did not fit in the outer mold line from Appendix A, the second iteration decreases the inlet area. The new inlet area was chosen to be 5 in². It should be noted that the cruise Mach number was held at 2.5 and the attitude is at 80,000 ft. The inlet throat area was found using the new inlet capture area shown below in Equation 62.

$$A_{IT} = A_0 * 1.728(M_{IE})_{start} [1 + 0.2(M_{IE})_{start}^2]^{-3} =$$

$$5 \text{ in}^2 * 1.728(1.5)[1 + 0.2 * 1.5^2]^{-3} = 4.25 \text{ in}^2 \quad (62)$$

With the inlet throat area found, the rest of the missile's geometry and thrust were found. To start, the combustion chamber Mach number at the inlet and exit were calculated, shown below in Equation 63 through Equation 72.

$$T_4 \approx T_o \left\{ 1 + \left[\frac{(\gamma_o - 1)}{2} \right] M_o^2 \right\} + \left(\frac{H_f}{c_p} \right) \left(\frac{f}{a} \right) =$$

$$390^\circ R \left\{ 1 + \left[\frac{(1.4 - 1)}{2} \right] 2.5^2 \right\} + \left(\frac{17,900 \frac{\text{btu}}{\text{lbm}}}{0.302 \frac{\text{btu}}{\text{lbm}^\circ R}} \right) (0.067) = 4,849^\circ R \quad (63)$$

$$(M_3)_{TC} \approx 0.461 \left[\frac{(1 + 0.2 * M_o^2)}{\left(\frac{T_{4t}}{T_o} \right)} \right]^{\frac{1}{2}} = 0.461 \left[\frac{1 + 0.2 * 2.5^2}{\frac{4849^\circ R}{390^\circ R}} \right]^{\frac{1}{2}} = 0.196 \quad (64)$$

$$\frac{A_{IT}}{A_3} = \frac{1.728 * M_3}{(1 + 0.2 * M_3^2)^3} = A_{IT} \left[\frac{1.728 * M_3}{(1 + 0.2 * M_3^2)^3} \right]^{-1} \quad (65)$$



$$A_3 = 4.25 \text{ in}^2 \left[\frac{1.728 * 0.196}{(1 + 0.2 * 0.196^2)^3} \right]^{-1} = 12.8 \text{ in}^2 \quad (66)$$

$$T_3 = (1 + 0.2 * M_0^2) * T_0 = (1 + 0.2 * 2.5^2) * 390 \text{ }^\circ\text{R} = 878 \text{ }^\circ\text{R} \quad (67)$$

$$M_4 = \left\{ \frac{[-b - (b^2 - 4 * a * c)]^{\frac{1}{2}}}{2 * a} \right\}^{\frac{1}{2}} \quad (68)$$

$$a = 1.822 * \left(\frac{T_4}{T_3} \right) * M_3^2 - 1.175 = 1.822 * \left(\frac{4,849 \text{ }^\circ\text{R}}{390 \text{ }^\circ\text{R}} \right) * 0.196^2 - 1.175 = -0.788 \quad (69)$$

$$b = 2.70 * \frac{T_4}{T_3} * M_3^2 = 2.70 * \frac{4,849 \text{ }^\circ\text{R}}{390 \text{ }^\circ\text{R}} * 0.196^2 = 0.574 \quad (70)$$

$$c = \frac{T_4}{T_3} * M_3^2 = \frac{4,849 \text{ }^\circ\text{R}}{390 \text{ }^\circ\text{R}} * 0.196^2 = 0.213 \quad (71)$$

$$M_4 = \left\{ \frac{[-0.574 - (0.574^2 - 4 * -0.788 * 0.213)]^{\frac{1}{2}}}{2 * -0.788} \right\}^{\frac{1}{2}} = 0.999 \quad (72)$$

After the combustor inlet and exit Mach numbers were calculated, the pressure at the combustor inlet and exit were calculated in Equation 73 through Equation 76.

$$\frac{p_4}{p_3} = \frac{\left[1 + \left(\frac{\gamma - 1}{2} \right) * M_4^2 \right]^{\frac{\gamma}{\gamma - 1}}}{1 + \gamma * M_4^2} = \frac{\left[1 + \left(\frac{1.4 - 1}{2} \right) * 0.999^2 \right]^{\frac{1.3}{1.3 - 1}}}{1 + 1.3 * 0.999^2} = 0.797 \quad (73)$$

$$\frac{p_3}{p_0} = \left(1 + \frac{\gamma - 1}{2} * M_3^2 \right)^{\frac{\gamma}{\gamma - 1}} = \left(1 + \frac{1.3 - 1}{2} * 0.196^2 \right)^{\frac{1.3}{1.3 - 1}} = 1.03 \quad (74)$$

$$p_3 = p_0 * \frac{p_3}{p_0} = 58.125 \frac{\text{lb}}{\text{ft}^2} * 1.03 = 59.5 \frac{\text{lb}}{\text{ft}^2} \quad (75)$$

$$p_4 = p_3 * \frac{p_4}{p_3} = 59.5 \frac{\text{lb}}{\text{ft}^2} * 0.797 = 47.4 \frac{\text{lb}}{\text{ft}^2} \quad (76)$$

After this, the length of the combustor was calculated and is shown below in Equation 77 through Equation 79.

$$a_4 = \sqrt{\gamma * R * T_4} = \sqrt{1.2 * 1716 \frac{\text{ft} * \text{lb}}{\text{slug} * \text{ }^\circ\text{R}} * 4849 \text{ }^\circ\text{R}} = 3289 \frac{\text{ft}}{\text{s}} \quad (77)$$



$$V_4 = a_4 * M_4 = 3289 \frac{ft}{s} * 0.999 = 3286 \frac{ft}{s} \quad (78)$$

$$L_C = V_4 * t_{comb} = 3286 \frac{ft}{s} * 0.001 s = 3.29 ft \quad (79)$$

After this, the specific impulse of the engine was calculated using Equation 80 below.

$$I_{sp} = \frac{M_0 \left(\sqrt{\frac{\left(\frac{T_4}{T_0}\right)}{\left(1 + \left(\frac{\gamma_0 - 1}{2}\right) * M_0^2\right)}} - 1 \right) a_0 H_f}{g c_p T_0 \left(\left(1 + \left(\frac{\gamma_0 - 1}{2}\right) * M_0^2\right) \left(\frac{\left(\frac{T_4}{T_0}\right)}{\left(1 + \left(\frac{\gamma_0 - 1}{2}\right) * M_0^2\right)} - 1 \right) \right)} =$$

$$2.5 \left(\sqrt{\frac{\left(\frac{4849 \text{ }^\circ R}{390 \text{ }^\circ R}\right)}{\left(1 + \left(\frac{1.4 - 1}{2}\right) * 2.5^2\right)}} - 1 \right) 968 \frac{ft}{s} * 17,900 \frac{BTU}{lb} \quad (80)$$

$$32.2 \frac{ft}{s^2} * 0.302 \frac{BTU}{lbm * \text{ }^\circ R} * 390 \left(\left(1 + \left(\frac{1.4 - 1}{2}\right) 2.5^2\right) \left(\frac{\left(\frac{4849 \text{ }^\circ R}{390 \text{ }^\circ R}\right)}{\left(1 + \left(\frac{1.4 - 1}{2}\right) * 2.5^2\right)} - 1 \right) \right)$$

$$I_{sp} = 1,350 s$$

Using this specific impulse, the time of flight of the engine was calculated. It should be noted that fuel weight was held constant from iteration one. To do this, the thrust during the dash segment was calculated and can be seen below in Equation 81 through Equation 85.

$$\frac{T}{p_o A_o} = \gamma_o M_o^2 \left\{ \left\{ \frac{\frac{T_4}{T_o}}{1 + \left[\frac{\gamma_o - 1}{2}\right] M_o^2} \right\}^{\frac{1}{2}} - 1 \right\} =$$

$$1.4(2.5^2) \left\{ \left\{ \frac{\frac{4,849 \text{ }^\circ R}{390 \text{ }^\circ R}}{1 + \left[\frac{1.4 - 1}{2}\right] 2.5^2} \right\}^{\frac{1}{2}} - 1 \right\} = 11.8 \quad (81)$$



$$T_{dash} = A_0 * p_0 * T_{non\ dim} = 5\ in^2 * 0.402 \frac{lb}{in^2} * 11.8 = 23.8\ lbf \quad (82)$$

$$TOF_{engine} = I_{sp} * \frac{W_{f\ dash}}{T_{dash}} = 1350\ s * \frac{1.47\ lbf}{23.8\ lbf} = 83.4\ s \quad (83)$$

After finding the time of flight, the throat area was calculated.

$$\dot{W}_p = \frac{W_{f\ dash}}{TOF_{engine}} = \frac{1.47\ lb}{83.4\ s} = 0.018\ \frac{lb}{s} \quad (84)$$

$$A_t = \frac{\dot{W}_p * C^*}{g * p_3} = \frac{0.018\ \frac{lb}{s} * 5200\ \frac{ft}{s}}{32.2\ \frac{ft}{s^2} * 59.5\ \frac{lb}{ft^2}} = 0.048\ ft^2 * \frac{144\ in^2}{1\ ft^2} = 6.9\ in^2 \quad (85)$$

While this iteration did decrease the missile size, the time of flight of the engine doubled from the time of flight from iteration one. This means that there is fuel not being used. Thus, another iteration was performed by increasing the size of the inlet capture area.

The result of this iteration was reflected in the CAD model, missile diameter was returned to the original value of 3.37in and the capture area, inlet throat area, and nozzle area were changed to match the results of this section. Combustion chamber length was not modeled in detail, but due to the similarly long combustion chamber length, combustion would have to occur in the ducts.



Figure 9 Iteration 2 Side View

The inlet geometry can be seen below in Figure 10, it is of note that the inlet throat area is small enough that the shock cone tends to fill a large portion of the missile cross sectional area.

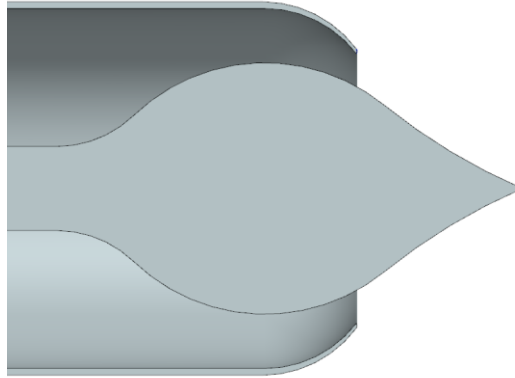


Figure 10 Iteration 2 Inlet Detail View

The nozzle geometry is shown below in Figure 11. As in previous iterations, there is little room for exhaust expansion beyond the nozzle throat. This nozzle could benefit from a shape memory alloy nozzle bell that would expand beyond the missile's outer diameter in flight.

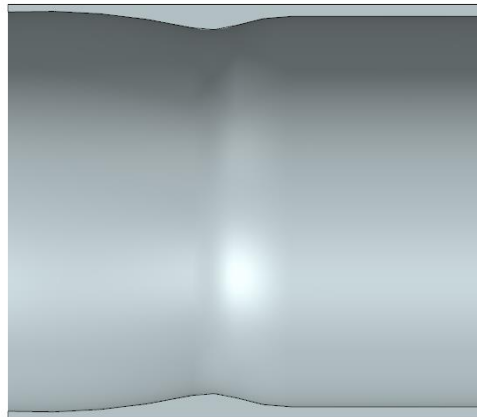


Figure 11 Iteration 2 Nozzle Detail View

5.3 Iteration 3

The third iteration increased the inlet area to decrease the time of flight of the engine. This increased the range of the missile. To decrease the time of flight of the engine, the inlet capture area was increased to 7.5 in^2 . Using this new inlet area, the throat area was found first as shown in Equation 86 below.

$$\begin{aligned}
 A_{IT} &= A_0 * 1.728(M_{IE})_{Start}[1 + 0.2(M_{IE})_{Start}^2]^{-3} = \\
 7.5 \text{ in}^2 * 1.728(1.5)[1 + 0.2 * 1.5^2]^{-3} &= 6.38 \text{ in}^2 \qquad (86)
 \end{aligned}$$



With the inlet throat area found, the rest of the missile's geometry and thrust were found. To start, the combustion chamber Mach numbers at the inlet and exit were calculated and can be shown in Equation 87 through Equation 96.

$$T_4 \approx T_o \left\{ 1 + \left[\frac{(\gamma_o - 1)}{2} \right] M_o^2 \right\} + \left(\frac{H_f}{c_p} \right) \left(\frac{f}{a} \right) =$$

$$390^\circ R \left\{ 1 + \left[\frac{(1.4 - 1)}{2} \right] 2.5^2 \right\} + \left(\frac{17,900 \frac{btu}{lbm}}{0.302 \frac{btu}{lbmR}} \right) (0.067) = 4,849^\circ R \quad (87)$$

$$(M_3)_{TC} \approx 0.461 \left[\frac{(1 + 0.2 * M_o^2)}{\left(\frac{T_{4t}}{T_o} \right)} \right]^{\frac{1}{2}} = 0.461 \left[\frac{1 + 0.2 * 2.5^2}{\frac{4849^\circ R}{390^\circ R}} \right]^{\frac{1}{2}} = 0.196 \quad (88)$$

$$\frac{A_{IT}}{A_3} = \frac{1.728 * M_3}{(1 + 0.2 * M_3^2)^3} = A_{IT} * \left[\frac{1.728 * M_3}{(1 + 0.2 * M_3^2)^3} \right]^{-1} \quad (89)$$

$$A_3 = 6.38 \text{ in}^2 \left[\frac{1.728 * 0.196}{(1 + 0.2 * 0.196^2)^3} \right]^{-1} = 19.3 \text{ in}^2 \quad (90)$$

$$T_3 = (1 + 0.2 * M_o^2) * T_o = (1 + 0.2 * 2.5^2) * 390^\circ R = 878^\circ R \quad (91)$$

$$M_4 = \left\{ \frac{[-b - (b^2 - 4 * a * c)]^{\frac{1}{2}}}{2 * a} \right\}^{\frac{1}{2}} \quad (92)$$

$$a = 1.822 * \left(\frac{T_4}{T_3} \right) * M_3^2 - 1.175 = 1.822 * \left(\frac{4,849^\circ R}{390^\circ R} \right) * 0.196^2 - 1.175 = -0.788 \quad (93)$$

$$b = 2.70 * \frac{T_4}{T_3} M_3^2 = 2.70 * \frac{4,849^\circ R}{390^\circ R} 0.196^2 = 0.574 \quad (94)$$

$$c = \frac{T_4}{T_3} M_3^2 = \frac{4,849^\circ R}{390^\circ R} 0.196^2 = 0.213 \quad (95)$$

$$M_4 = \left\{ \frac{[-0.574 - (0.574^2 - 4 * -0.788 * 0.213)]^{\frac{1}{2}}}{2 * -0.788} \right\}^{\frac{1}{2}} = 0.999 \quad (96)$$

After the combustor inlet and exit Mach numbers were calculated, the pressure at the combustor inlet and exit were calculated using Equation 97 through Equation 100.



$$\frac{p_4}{p_3} = \frac{\left[1 + \left(\frac{\gamma - 1}{2}\right) * M_4^2\right]^{\frac{\gamma}{\gamma - 1}}}{1 + \gamma * M_4^2} = \frac{\left[1 + \left(\frac{1.4 - 1}{2}\right) * 0.999^2\right]^{\frac{1.3}{1.3 - 1}}}{1 + 1.3 * 0.999^2} = 0.797 \quad (97)$$

$$\frac{p_3}{p_0} = \left(1 + \frac{\gamma - 1}{2} * M_3^2\right)^{\frac{\gamma}{\gamma - 1}} = \left(1 + \frac{1.3 - 1}{2} * 0.196^2\right)^{\frac{1.3}{1.3 - 1}} = 1.03 \quad (98)$$

$$p_3 = p_0 * \frac{p_3}{p_0} = 58.125 \frac{lb}{ft^2} * 1.03 = 59.5 \frac{lb}{ft^2} \quad (99)$$

$$p_4 = p_3 * \frac{p_4}{p_3} = 59.5 \frac{lb}{ft^2} * 0.797 = 61.0 \frac{lb}{ft^2} \quad (100)$$

After this, the length of the combustor was calculated using Equation 101 through Equation 103.

$$a_4 = \sqrt{\gamma * R * T_4} = \sqrt{1.2 * 1716 \frac{ft * lbf}{slug * ^\circ R} * 4849 ^\circ R} = 3289 \frac{ft}{s} \quad (101)$$

$$V_4 = a_4 * M_4 = 3289 \frac{ft}{s} * 0.999 = 3286 \frac{ft}{s} \quad (102)$$

$$L_C = V_4 * t_{comb} = 3286 \frac{ft}{s} * 0.001 s = 3.29 ft \quad (103)$$

After this, the specific impulse of the engine was calculated using Equation 104 below.

$$I_{sp} = \frac{M_0 \left(\sqrt{\frac{\left(\frac{T_4}{T_0}\right)}{\left(1 + \left(\frac{\gamma_0 - 1}{2}\right) * M_0^2\right)}} - 1 \right) a_0 H_f}{g_{c_p} T_0 \left(\left(1 + \left(\frac{\gamma_0 - 1}{2}\right) * M_0^2\right) \left(\frac{\left(\frac{T_4}{T_0}\right)}{\left(1 + \left(\frac{\gamma_0 - 1}{2}\right) * M_0^2\right)} - 1 \right) \right)} =$$



$$2.5 \left(\sqrt{\frac{\left(\frac{4849^\circ R}{390^\circ R}\right)}{\left(1 + \left(\frac{(1.4-1)}{2}\right) * 2.5^2\right)}} - 1 \right) 968 \frac{ft}{s} * 17,900 \frac{BTU}{lb}$$

$$32.2 \frac{ft}{s^2} * 0.302 \frac{BTU}{lbm * ^\circ R} * 390 \left(\left(1 + \left(\frac{(1.4-1)}{2}\right) 2.5^2\right) \left(\frac{\left(\frac{4849^\circ R}{390^\circ R}\right)}{\left(1 + \left(\frac{(1.4-1)}{2}\right) * 2.5^2\right)} \right) - 1 \right) \quad (104)$$

$$I_{sp} = 1,350 \text{ s}$$

Using this specific impulse, the time of flight of the engine was calculated. To do this, the thrust during the dash segment was calculated using Equation 105 through Equation 109.

$$\frac{T}{p_o A_o} = \gamma_o M_o^2 \left\{ \left\{ \frac{\frac{T_4}{T_o}}{1 + \left[\frac{(\gamma_o - 1)}{2}\right] M_o^2} \right\}^{\frac{1}{2}} - 1 \right\} =$$

$$1.4(2.5^2) \left\{ \left\{ \frac{\frac{4,849^\circ R}{390^\circ R}}{1 + \left[\frac{(1.4-1)}{2}\right] 2.5^2} \right\}^{\frac{1}{2}} - 1 \right\} = 11.8 \quad (105)$$

$$T_{dash} = A_o * p_o * T_{non dim} = 7.5 \text{ in}^2 * 0.402 \frac{lb}{\text{in}^2} * 11.8 = 35.7 \text{ lbf} \quad (106)$$

$$TOF_{engine} = I_{sp} * \frac{W_{f dash}}{T_{dash}} = 1350 \text{ s} * \frac{1.47 \text{ lbf}}{35.7 \text{ lbf}} = 55.6 \text{ s} \quad (107)$$

After finding the time of flight, the throat area was calculated using Equation 108 and Equation 109.

$$\dot{W}_p = \frac{W_{f dash}}{TOF_{engine}} = \frac{1.47 \text{ lb}}{55.6 \text{ s}} = 0.026 \frac{lb}{s} \quad (108)$$

$$A_t = \frac{\dot{W}_p * C^*}{g * p_3} = \frac{0.026 \frac{lb}{s} * 5200 \frac{ft}{s}}{32.2 \frac{ft}{s^2} * 59.5 \frac{lb}{ft^2}} = 0.072 \text{ ft}^2 * \frac{144 \text{ in}^2}{1 \text{ ft}^2} = 10.3 \text{ in}^2 \quad (109)$$

This time of flight is still higher than the time of flight found in iteration one. Additionally, the cross-sectional area of the throat is increasing as the inlet capture area



increases. The engine is also burning the fuel more efficiently than what is needed for the mission. This is resulting in an inefficient iteration of the missile. The following iterations instead change the altitude.

The results of this iteration were reflected in the CAD model, specifically the capture area, inlet throat area, and nozzle area were changed to match the results of this section. Combustion chamber length was not modeled in detail, but due to the similarly long combustion chamber length, combustion would have to occur in the ducts. A side view of this missile iteration is shown in Figure 12.

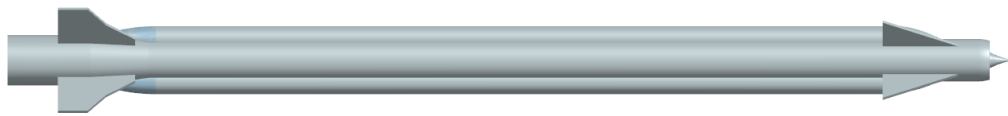


Figure 12 Iteration 3 Side View

The inlet geometry is shown below in Figure 13. Compared to the previous iteration the shock cone for this third iteration does not take up as much of the missile cross sectional area.

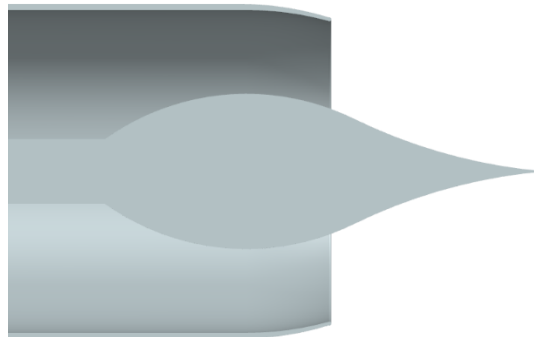


Figure 13 Iteration 3 Inlet Detail View

A detail view of the nozzle geometry is shown in Figure 14 below. Similar to previous iterations there is little room for exhaust expansion to occur, meaning that the use of a shape memory alloy expanding nozzle flare section would be of benefit to allow for more fully expanded flow.

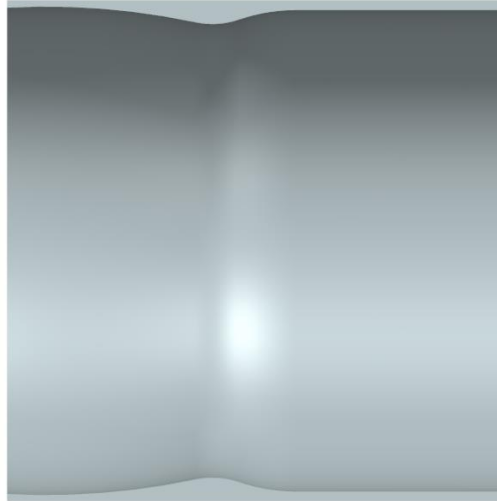


Figure 14 Iteration 3 Nozzle Detail View

5.4 Iteration 4

For the fourth iteration, the engagement altitude of the RAIDER AIM-9 was decreased to 30,000 ft. The reason for this decrease in altitude was to more accurately represent a dogfighting altitude as well as decrease geometry of critical aspects of the missile, such as the inlet area and combustion chamber. All other variables previously found in section 5.3 remained the same. To begin this process, the cruise speed was found first. The first variable that needed to be solved for was the speed of sound at the chosen 30,000 ft which can be seen below in Equation 110. The values for temperature and pressure at 30,000 ft was found from Ref. [6].

$$a_0 = \sqrt{\gamma RT_0} = \sqrt{(1.4) \left(1716 \frac{ftlb}{slugR} \right) (412 \text{ }^\circ R)} = 995 \frac{ft}{s} \quad (110)$$

The next variable that needed to be found was the cruise velocity of the RAIDER AIM-9 at 30,000 ft. This calculation is shown below in Equation 111.

$$V = M * a_0 = 2.5 * 995 \frac{ft}{s} = 2,488 \frac{ft}{s} \quad (111)$$

The combustion exit temperature was calculated using Equation 112 below in Equation 112.



$$T_4 \approx T_o \left\{ 1 + \left[\frac{(\gamma_o - 1)}{2} \right] M_o^2 \right\} + \left(\frac{H_f}{c_p} \right) \left(\frac{f}{a} \right) =$$

$$412^\circ R \left\{ 1 + \left[\frac{(1.4 - 1)}{2} \right] 2.5^2 \right\} + \left(\frac{17,900 \frac{btu}{lbm}}{0.302 \frac{btu}{lbmR}} \right) (0.067) = 4,898^\circ R \quad (112)$$

With dash velocity, I_{sp} , and the new TOF was found as seen below in Equation 113 and Equation 114.

$$TOF_{dash} = \frac{Range_{dash}}{V_{dash}} = \frac{19.631 \text{ mi} * 5,280 \frac{ft}{mi}}{2,488 \frac{ft}{s}} = 41.66 \text{ s} \quad (113)$$

$$I_{sp} = \frac{M_o \left(\sqrt{\frac{\left(\frac{T_4}{T_o} \right)}{\left(\left(1 + \left(\frac{\gamma_o - 1}{2} \right) * M_o^2 \right) \right)} - 1 \right) a_o H_f}{g c_p T_o \left(\left(1 + \left(\frac{\gamma_o - 1}{2} \right) * M_o^2 \right) \left(\frac{\left(\frac{T_4}{T_o} \right)}{\left(\left(1 + \left(\frac{\gamma_o - 1}{2} \right) * M_o^2 \right) \right)} - 1 \right) \right)} =$$

$$\frac{2.5 \left(\sqrt{\frac{\left(\frac{4898^\circ R}{412^\circ R} \right)}{\left(\left(1 + \left(\frac{1.4 - 1}{2} \right) * 2.5^2 \right) \right)} - 1 \right) 995 \frac{ft}{s} * 17,900 \frac{BTU}{lb}}{32.2 \frac{ft}{s^2} * 0.302 \frac{BTU}{lbm * ^\circ R} * 412 \left(\left(1 + \left(\frac{1.4 - 1}{2} \right) 2.5^2 \right) \left(\frac{\left(\frac{4898^\circ R}{412^\circ R} \right)}{\left(\left(1 + \left(\frac{1.4 - 1}{2} \right) * 2.5^2 \right) \right)} - 1 \right) \right)} \quad (114)$$

$$I_{sp} = 1,327 \text{ s}$$

Next, the thrust required for dash was calculated using the I_{sp} as previously seen calculated in Equation 114. The new calculation can be seen below in Equation 115.

$$T_{dash} = I_{sp} * \frac{W_f_{dash}}{TOF_{dash}} = 1,327 \text{ s} * \frac{1.47 lb}{41.66 \text{ s}} = 46.8 \text{ lb} \quad (115)$$

The inlet throat area was calculated using Equation 116 through Equation 119.



$$\frac{T}{p_o A_o} = \gamma_o M_o^2 \left\{ \left\{ \frac{\frac{T_4}{T_o}}{1 + \left[\frac{(\gamma_o - 1)}{2} \right] M_o^2} \right\}^{\frac{1}{2}} - 1 \right\} =$$

$$1.4(2.5^2) \left\{ \left\{ \frac{\frac{4,898^\circ R}{412^\circ R}}{1 + \left[\frac{(1.4 - 1)}{2} \right] 2.5^2} \right\}^{\frac{1}{2}} - 1 \right\} = 11.4 \quad (116)$$

$$A_o = \frac{T}{p_o * T_{non dim}} = \frac{46.8 lb}{4.37 \frac{lb}{in^2} * 11.4} = 0.939 in^2 \quad (117)$$

$$\frac{A_{IT}}{A_o} = 1.728(M_{IE})_{Start} [1 + 0.2(M_{IE})_{Start}^2]^{-3} \quad (118)$$

$$A_{IT} = 0.939 * \{1.728(1.5)[1 + 0.2(1.5)^2]^{-3}\} = 0.8 in^2 \quad (119)$$

With the geometry found, the combustor Mach numbers, geometries, and pressure can be found. To begin, the combustor inlet and exit Mach number was calculated using Equation 120 through Equation 129 below.

$$\frac{T_4}{T_o} = \frac{4,898^\circ R}{390^\circ R} = 12.6 \quad (120)$$

$$(M_3)_{TC} \approx 0.461 \left[\frac{(1 + 0.2M_o^2)}{\left(\frac{T_{4t}}{T_o}\right)} \right]^{\frac{1}{2}} = 0.461 \left[\frac{(1 + 0.2(2.5)^2)}{12.6} \right]^{\frac{1}{2}} = 0.195 \quad (121)$$

$$\frac{A_{IT}}{A_3} = \frac{1.728M_3}{(1 + 0.2M_3^2)^3} \quad (122)$$

$$A_3 = \frac{0.939 in^2 (1 + 0.2(0.195)^2)^3}{1.728(0.195)} = 2.86 in^2 \quad (123)$$

$$T_3 = [1 + 0.2(M_o)^2]T_o = [1 + 0.2(2.5)^2]412^\circ R = 927^\circ R \quad (124)$$

$$M_4 \approx \left\{ \frac{\left[-b - (b^2 - 4ac)^{\frac{1}{2}} \right]}{(2a)} \right\}^{\frac{1}{2}} \quad (125)$$

$$a = 1.822 \left(\frac{T_4}{T_3} \right) M_3^2 - 1.175 = 1.822(5.28)(0.195)^2 - 1.175 = -0.809 \quad (126)$$



$$b = 2.70 \left(\frac{T_4}{T_3} \right) M_3^2 = 2.70(5.28)(0.195)^2 = 0.542 \quad (127)$$

$$c = \left(\frac{T_4}{T_3} \right) M_3^2 = 5.28(0.195)^2 = 0.20 \quad (128)$$

$$M_4 \approx \left\{ \frac{\left[\frac{-(-0.542) - \sqrt{(-0.542)^2 - 4(-0.809)(0.20)}}{2(-0.809)} \right]^{\frac{1}{2}}}{1} \right\} = 0.967 \quad (129)$$

With these Mach numbers found, the pressures at the combustor inlet and exit were found as seen below in Equation 130 through Equation 133.

$$\frac{p_4}{p_3} = \frac{\left\{ 1 + \left[\frac{(\gamma - 1)}{2} \right] M_4^2 \right\}^{\frac{\gamma}{\gamma - 1}}}{(1 + \gamma M_4^2)} = \frac{\left\{ 1 + \left[\frac{1.3 - 1}{2} \right] (0.967)^2 \right\}^{4.33}}{(1 + 1.3(0.967)^2)} = 0.797 \quad (130)$$

$$\frac{p_3}{p_0} = \left\{ 1 + \left[\frac{(\gamma - 1)}{2} \right] M_3^2 \right\}^{\frac{\gamma}{\gamma - 1}} = \left\{ 1 + \left[\frac{(1.3 - 1)}{2} \right] 0.195^2 \right\}^{\frac{1.3}{1.3 - 1}} = 1.02 \quad (131)$$

$$p_3 = p_0(1.02) = 629.66 \frac{lb}{ft^2} * 1.02 = 642 lb/ft^2 \quad (132)$$

$$p_4 = p_3(0.797) = 642 lb/ft^2 * 0.797 = 512 lb/ft^2 \quad (133)$$

Finally, the geometry of the combustor was calculated as seen below in Equation 134 through Equation 137.

$$a_4 = \sqrt{\gamma_4 R_4 T_4} = \sqrt{1.3 * 1716 \frac{ft * lb}{slug * ^\circ R} * 4,898 ^\circ R} = 3,306 \frac{ft}{s} \quad (134)$$

$$V_4 = a_4 M_4 = 3,306 \frac{ft}{s} * 0.967 = 3,203 \frac{ft}{s} \quad (135)$$

$$L_c = V_{comb} * t_{comb} = 3,203 \frac{ft}{s} * 0.001 s = 3.2 ft \quad (136)$$

$$A_t = \frac{\dot{W}_p C^*}{g p_c} = \frac{1.47 lb f}{41.66 s} * 5,200 \frac{ft}{s}}{32.2 \frac{ft}{s^2} * 642 psf} = 0.00089 ft^2 = 1.27 in^2 \quad (137)$$

This iteration was shown to be successful in decreasing geometry in critical aspects of the missile. The inlet area was found to be $0.939 in^2$, an 87% decrease compared to the previous



iteration. The length of the combustor was found to be 0.09 ft smaller than the missile in the previous iteration.

The capture area, inlet throat area, and nozzle throat area were changed in the CAD model to reflect the results of this iteration. Combustion chamber length was not modeled in detail, but due to the similarly long combustion chamber length, combustion would have to occur in the ducts.

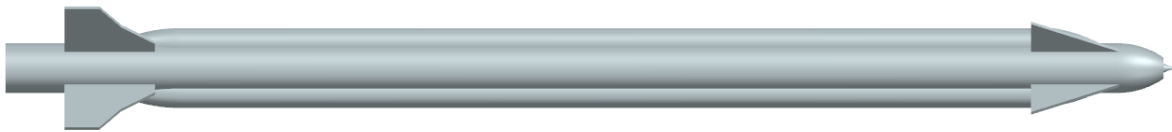


Figure 15 Iteration 4 Side View

The inlet geometry is shown below in Figure 16. Compared to the previous iteration the shock cone for this third iteration takes up slightly more space of the missile cross sectional area.

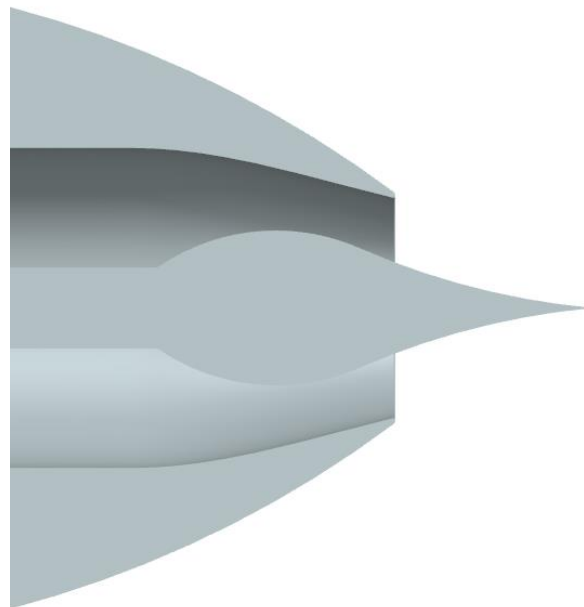


Figure 16 Iteration 4 Inlet Detail View

A detail view of the nozzle geometry is shown in Figure 17 below. Unlike previous iterations the nozzle throat area was smaller allowing room for exhaust expansion to occur. This means that for this iteration a shape memory alloy expanding nozzle flare section would not be necessary.

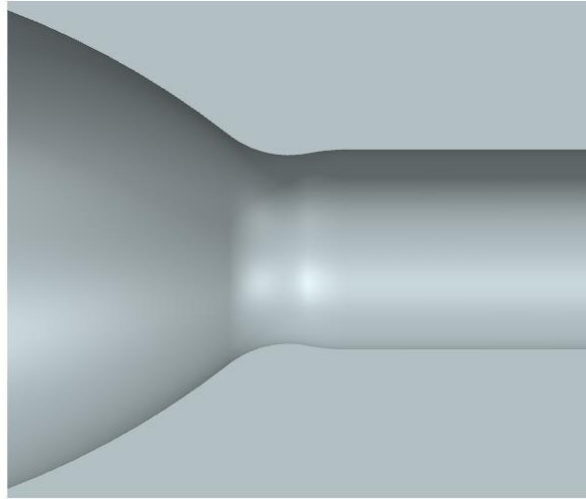


Figure 17 Iteration 4 Nozzle Detail View

5.5 Iteration 5

For iteration 5, the team kept the engagement altitude at 30,000 ft, however, increased the Mach number back to 4.0. This was done to quantify the change in combustor length and inlet area of the RAIDER AIM-9 at a higher Mach number at the lower altitude. The goal of this iteration was to decrease the combustor length and inlet area, as well as increase the dash speed of the missile. All other variables previously found remained the same. To begin this process, the cruise speed was first found. The first variable to be solved was the speed of sound at the prescribed 30,000 ft which can be seen below in Equation 138. The values for temperature and pressure at 30,000 ft were found from Ref. [6].

$$a_0 = \sqrt{\gamma RT_0} = \sqrt{(1.4) \left(1716 \frac{ftlb}{slug^\circ R} \right) (412^\circ R)} = 995 \frac{ft}{s} \quad (138)$$

Next to find is the cruise velocity of the RAIDER AIM-9 at 30,000 ft. This can be seen below in Equation 139.

$$V = M * a_0 = 4 * 995 \frac{ft}{s} = 3,980 \frac{ft}{s} \quad (139)$$

The combustion exit temperature, I_{SP} , and time of flight needs to be found and were calculated using Equation 140 through Equation 142.



$$T_4 \approx T_o \left\{ 1 + \left[\frac{(\gamma_o - 1)}{2} \right] M_o^2 \right\} + \left(\frac{H_f}{c_p} \right) \left(\frac{f}{a} \right) =$$

$$412^\circ R \left\{ 1 + \left[\frac{(1.4 - 1)}{2} \right] 4^2 \right\} + \left(\frac{17,900 \frac{btu}{lbm}}{0.302 \frac{btu}{lbm^\circ R}} \right) (0.067) = 5,702^\circ R \quad (140)$$

$$I_{sp} = \frac{M_o \left(\sqrt{\frac{\left(\frac{T_4}{T_o} \right)}{\left(\left(1 + \left(\frac{\gamma_o - 1}{2} \right) * M_o^2 \right) \right)} - 1 \right) a_o H_f}{g c_p T_o \left(\left(1 + \left(\frac{\gamma_o - 1}{2} \right) * M_o^2 \right) \left(\frac{\left(\frac{T_4}{T_o} \right)}{\left(\left(1 + \left(\frac{\gamma_o - 1}{2} \right) * M_o^2 \right) \right)} - 1 \right) \right)} =$$

$$4.0 \left(\sqrt{\frac{\left(\frac{5702^\circ R}{412^\circ R} \right)}{\left(\left(1 + \left(\frac{1.4 - 1}{2} \right) * 4.0^2 \right) \right)} - 1 \right) 995 \frac{ft}{s} * 17,900 \frac{BTU}{lb}$$

$$32.2 \frac{ft}{s^2} * 0.302 \frac{BTU}{lbm * ^\circ R} * 412 \left(\left(1 + \left(\frac{1.4 - 1}{2} \right) 4.0^2 \right) \left(\frac{\left(\frac{5,702^\circ R}{412^\circ R} \right)}{\left(\left(1 + \left(\frac{1.4 - 1}{2} \right) * 4.0^2 \right) \right)} - 1 \right) \right) \quad (141)$$

$$I_{sp} = 1,130 s$$

$$TOF_{dash} = \frac{Range_{dash}}{V_{dash}} = \frac{19.631 mi * 5280 \frac{ft}{mi}}{3,980 \frac{ft}{s}} = 26.04s \quad (142)$$

Next, the thrust required for dash was calculated using the Isp as seen calculated in Equation 33. This calculation can be seen below in Equation 143.

$$T_{dash} = I_{sp} * \frac{W_f_{dash}}{TOF_{dash}} = 1,130 s * \frac{1.47lb}{26.04 s} = 63.8 lb \quad (143)$$

With these values found, the inlet throat area was calculated for these values. This can be seen below in Equation 144 through Equation 147.



$$\frac{T}{p_o A_o} = \gamma_o M_o^2 \left\{ \left\{ \frac{\frac{T_4}{T_o}}{1 + \left[\frac{(\gamma_o - 1)}{2} \right] M_o^2} \right\}^{\frac{1}{2}} - 1 \right\} =$$

$$1.4(4^2) \left\{ \left\{ \frac{\frac{5,702^\circ R}{390^\circ R}}{1 + \left[\frac{(1.4 - 1)}{2} \right] 4^2} \right\}^{\frac{1}{2}} - 1 \right\} = 18.3 \quad (144)$$

$$A_o = \frac{T}{p_o * T_{non\ dim}} = \frac{63.8\ lb}{4.37 \frac{lb}{in^2} * 18.3} = 0.798\ in^2 \quad (145)$$

$$\frac{A_{IT}}{A_o} = 1.728(M_{IE})_{Start} [1 + 0.2(M_{IE})_{Start}^2]^{-3} \quad (146)$$

$$A_{IT} = 1.48 * \{1.728(1.5)[1 + 0.2(1.5)^2]^{-3}\} = 0.679\ in^2 \quad (147)$$

With the geometry found, the combustor Mach numbers, geometries, and pressure were found. To begin, the combustor inlet and exit Mach number will be found as seen below in Equation 148 through Equation 157.

$$\frac{T_4}{T_o} = \frac{5,702\ ^\circ R}{390\ ^\circ R} = 14.62 \quad (148)$$

$$(M_3)_{TC} \approx 0.461 \left[\frac{(1 + 0.2M_o^2)}{\left(\frac{T_{4t}}{T_o}\right)} \right]^{\frac{1}{2}} = 0.461 \left[\frac{(1 + 0.2(4)^2)}{14.62} \right]^{\frac{1}{2}} = 0.247 \quad (149)$$

$$\frac{A_{IT}}{A_3} = \frac{1.728M_3}{(1 + 0.2M_3^2)^3} \quad (150)$$

$$A_3 = \frac{1.26\ in^2(1 + 0.2(0.247)^2)^3}{1.728(0.247)} = 3.53\ in^2 \quad (151)$$

$$T_3 = [1 + 0.2(M_o)^2]T_o = [1 + 0.2(4)^2]412^\circ R = 1730\ ^\circ R \quad (152)$$

$$M_4 \approx \left\{ \frac{\left[-b - (b^2 - 4ac)^{\frac{1}{2}} \right]}{(2a)} \right\}^{\frac{1}{2}} \quad (153)$$

$$a = 1.822 \left(\frac{T_4}{T_3} \right) M_3^2 - 1.175 = 1.822(3.3)(0.247)^2 - 1.175 = -0.808 \quad (154)$$



$$b = 2.70 \left(\frac{T_4}{T_3} \right) M_3^2 = 2.70(3.3)(0.247)^2 = 0.544 \quad (155)$$

$$c = \left(\frac{T_4}{T_3} \right) M_3^2 = 3.3(0.247)^2 = 0.201 \quad (156)$$

$$M_4 \approx \left\{ \frac{\left[-(0.544) - (0.544^2 - 4(-0.808)(0.201))^{\frac{1}{2}} \right]}{2(-0.808)} \right\}^{\frac{1}{2}} = 0.969 \quad (157)$$

With these Mach numbers found, the pressures at the combustor inlet and exit were found as seen below in Equation 158 through Equation 161.

$$\frac{p_4}{p_3} = \frac{\left\{ 1 + \left[\frac{(\gamma - 1)}{2} \right] M_4^2 \right\}^{\frac{\gamma}{\gamma - 1}}}{(1 + \gamma M_4^2)} = \frac{\left\{ 1 + \left[\frac{1.3 - 1}{2} \right] (0.969)^2 \right\}^{4.33}}{(1 + 1.3(0.969)^2)} = 0.797 \quad (158)$$

$$\frac{p_3}{p_0} = \left\{ 1 + \left[\frac{(\gamma - 1)}{2} \right] M_3^2 \right\}^{\frac{\gamma}{\gamma - 1}} = \left\{ 1 + \left[\frac{(1.3 - 1)}{2} \right] 0.247^2 \right\}^{\frac{1.3}{1.3 - 1}} = 1.04 \quad (159)$$

$$p_3 = p_0(1.04) = 629.66 \frac{lb}{ft^2} * 1.04 = 655 \text{ lb/ft}^2 \quad (160)$$

$$p_4 = p_3(0.797) = 655 \text{ lb/ft}^2 * 0.797 = 522 \text{ lb/ft}^2 \quad (161)$$

Finally, the geometry of the combustor was calculated as seen below in Equation 162 through Equation 165.

$$a_4 = \sqrt{\gamma_4 R_4 T_4} = \sqrt{1.3 * 1716 \frac{ft * lb}{slug * ^\circ R} * 5,702 ^\circ R} = 3,567 \frac{ft}{s} \quad (162)$$

$$V_4 = a_4 M_4 = 3,567 \frac{ft}{s} * 0.969 = 3,456 \frac{ft}{s} \quad (163)$$

$$L_C = V_{comb} * t_{comb} = 3,456 \frac{ft}{s} * 0.001 s = 3.46 \text{ ft} \quad (164)$$

$$A_t = \frac{\dot{W}_p C^*}{g p_c} = \frac{1.47 \text{ lbf}}{26.04 \text{ s}} * 5,200 \frac{ft}{s}}{32.2 \frac{ft}{s^2} * 655 \text{ psf}} = 0.0139 \text{ ft}^2 = 2.00 \text{ in}^2 \quad (165)$$



This iteration showed that the higher Mach number at the lower altitude increased the combustion chamber length and area at the throat. This new geometry resulted in the raider configuration shown below in Figure 18.



Figure 18 Iteration 5 Side View

The inlet section has shrunk considerably from previous iterations and is shown below in Figure 19. This newly shrunk inlet may allow thermal seekers to reside in the unused portion of the nose as opposed to the previous thoughts of placing sensors within the shock cone.

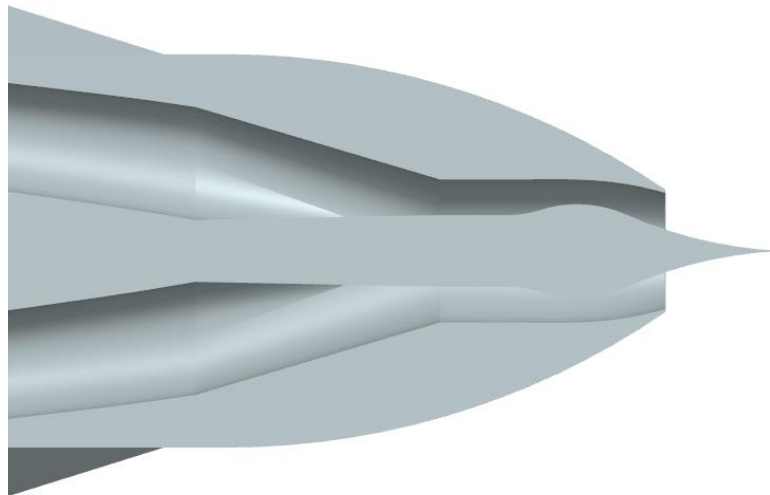


Figure 19 Iteration 5 Inlet Detail View

The nozzle geometry has changed minimally from iteration 4. The revised throat area is shown below in Figure 20.

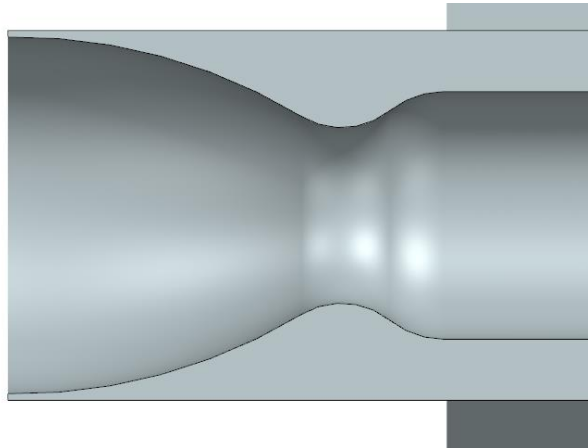


Figure 20 Iteration 5 Nozzle Detail View

As seen in Figure 18 through Figure 20, the throat area, inlet area, and combustion chamber length are still reasonable values. These geometries allow for an expansion bell to fit within the missile without the need for additional complex shape memory alloy parts.

5.6 Summary of Iterations

The changes made in each iteration, and the results of those changes are summarized in the table below. As iterations are made, the area requirements trend down while maintaining the same range.

Table 2 Summary of AIM9 Raider Iterations

Iteration	Diameter	A_0	A_{IT}	L_{combust}	A_{NTH}	Altitude	TOF
0	3.37in	7.89in ²	6.71in ²	3.54ft	21.1in ²	FL800	26.8s
1	4.5in	10.1in ²	8.59in ²	3.22ft	13.3in ²	FL800	42.8s
2	3.37in	5.00in ²	4.25in ²	3.28ft	6.898in ²	FL800	83.4s
3	3.37in	7.50in ²	6.38in ²	3.29ft	10.3in ²	FL800	55.6s
4	3.37in	0.939in ²	0.8in ²	3.20ft	1.27in ²	FL300	41.7s
5	3.37in	0.798in ²	0.679in ²	3.46ft	2.00in ²	FL300	26.0s



6 **Final RAIDER Weapon CAD Figures**

This section covers the CAD modeling of the final configuration of the RAIDER AIM-9 from Section 5.5. This final configuration will be shown in three different configurations which are stowed, separated, and terminal.

6.1 **Fully Collapsed/Stowed**

This section shows the stowed configuration of iteration 5. Figure 21 below shows the front, top, side and isometric view of the stowed configuration of iteration 5. The red component below is the rocket motor to get the missile up to cruise speed.

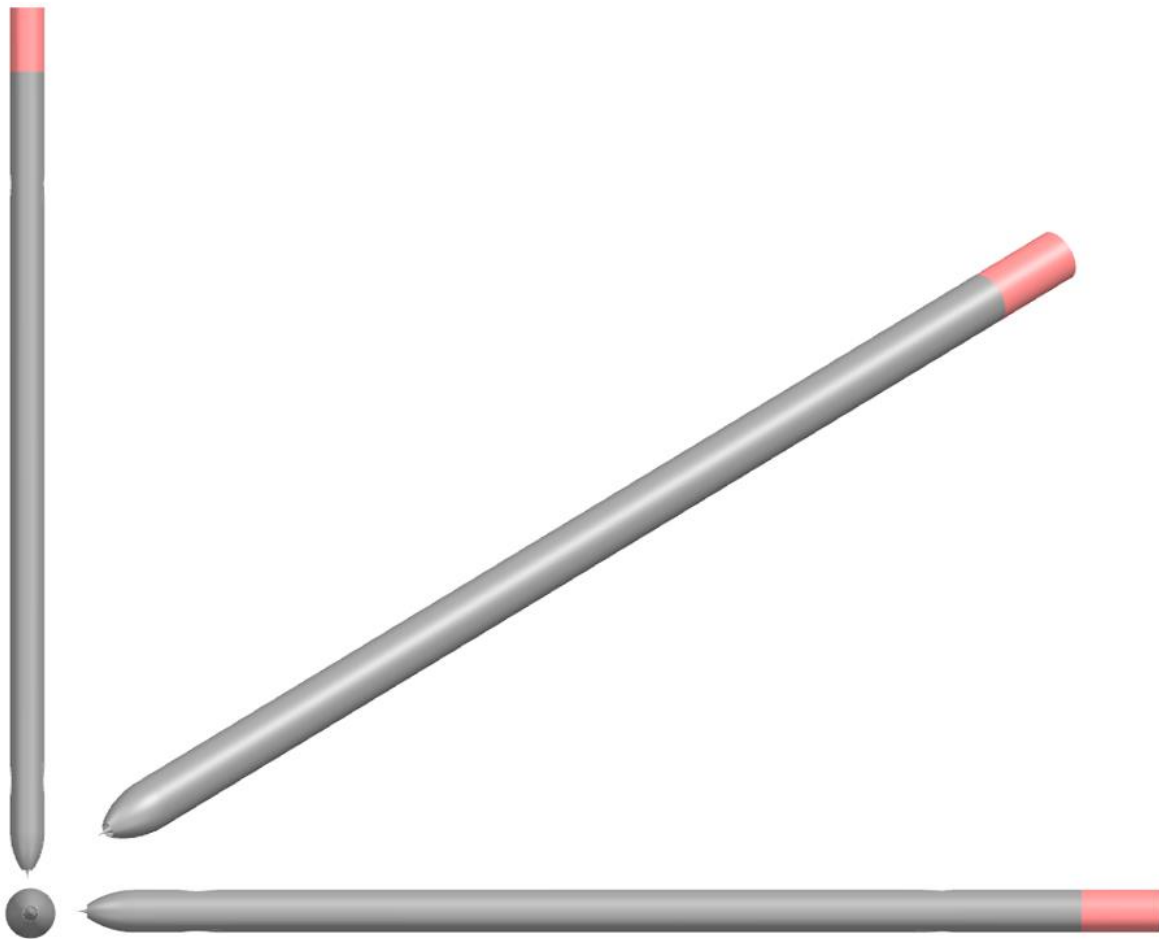


Figure 21: Front, Top, Side and Isometric View of Stowed Configuration

A cut away section view is also shown. Below in Figure 22 is the labeled cutaway isometric view of the stowed configuration of iteration 5. The red section below is the rocket

motor, and the tail fins, canards and ducts are stowed, hence why they are not shown. The sections shown below are:

- The rocket motor;
- Expansion bell;
- Converging combustor section;
- Stowed duct section;
- Inlet diverging ducts;
- Inlet throat section.

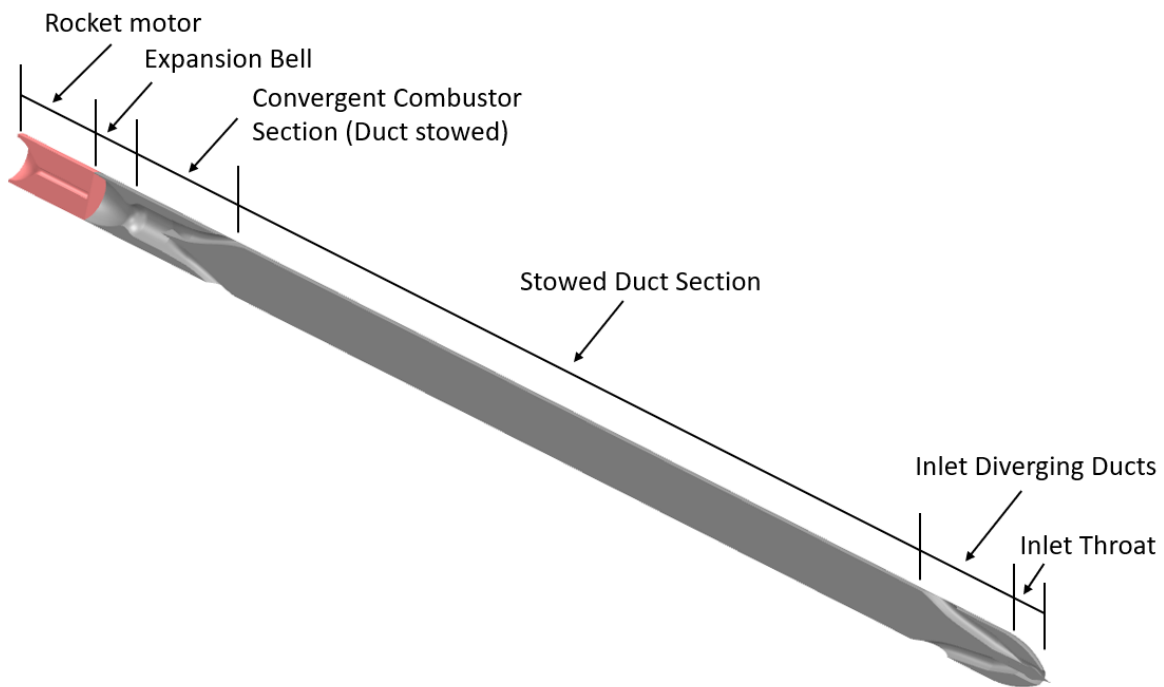


Figure 22: Labeled Isometric Stowed Configuration Cut away

6.2 Separated

This section shows the CAD model of iteration 5 during the separated phase. This phase of flight shows the missile immediately after booster separation. Below in Figure 23 is a top, front, side and isometric view of iteration 5 in the separated configuration just after the rocket motor has dropped off. The tail fins, canards and ducts are still stowed.

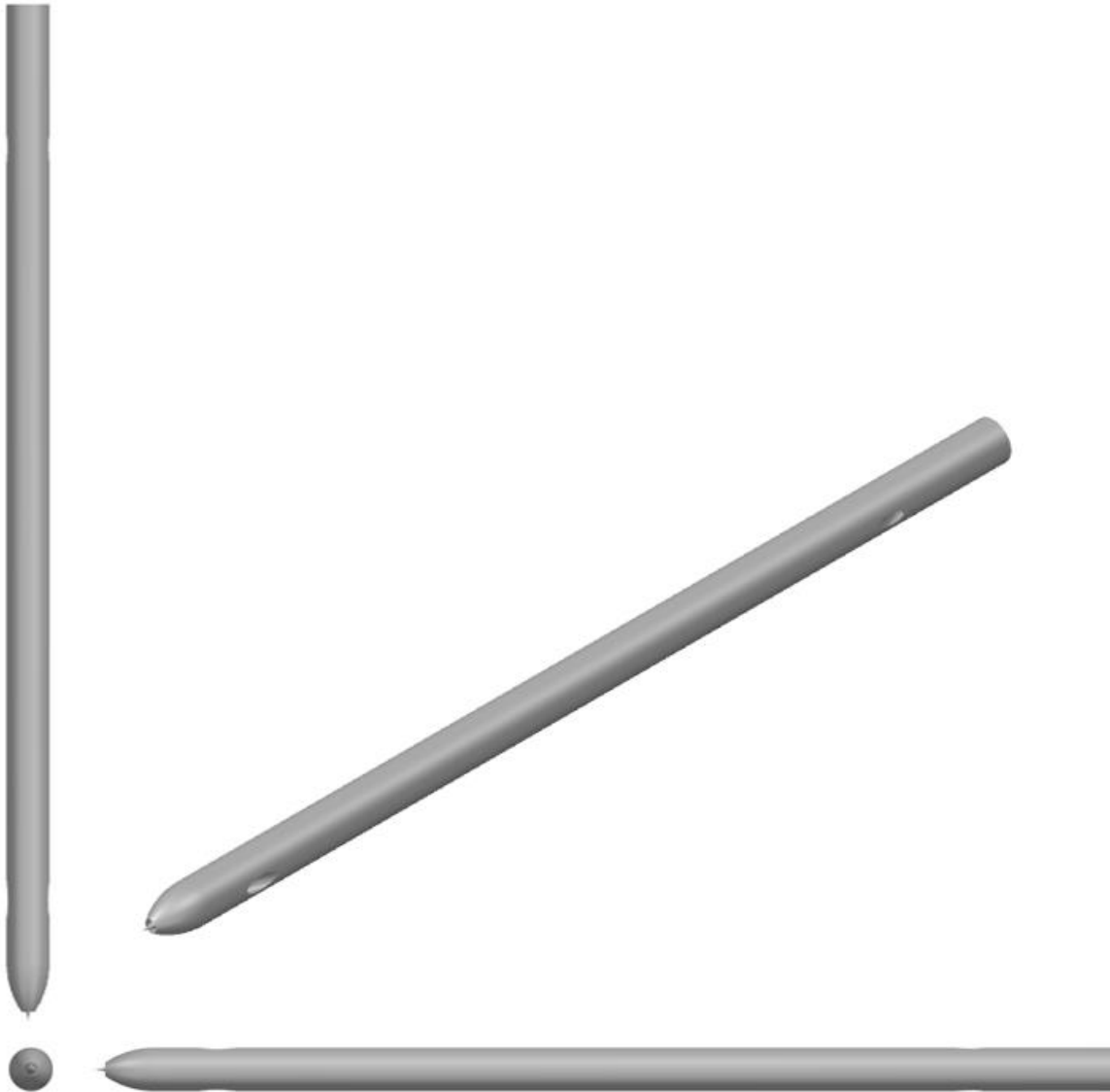


Figure 23 Front, Top, Side and Isometric View of Separated Configuration

An isometric cut away section is also shown. Below, in Figure 24, a cutaway isometric view is shown consisting of the different sections of the separated configuration of iteration 5. The tail fins, canards and ducts are still stowed as this is after the rocket motor has just dropped off. The sections shown below are:

- The Expansion bell;
- Converging combustor section;
- Stowed duct section;

- Inlet diverging ducts;
- Inlet throat section.

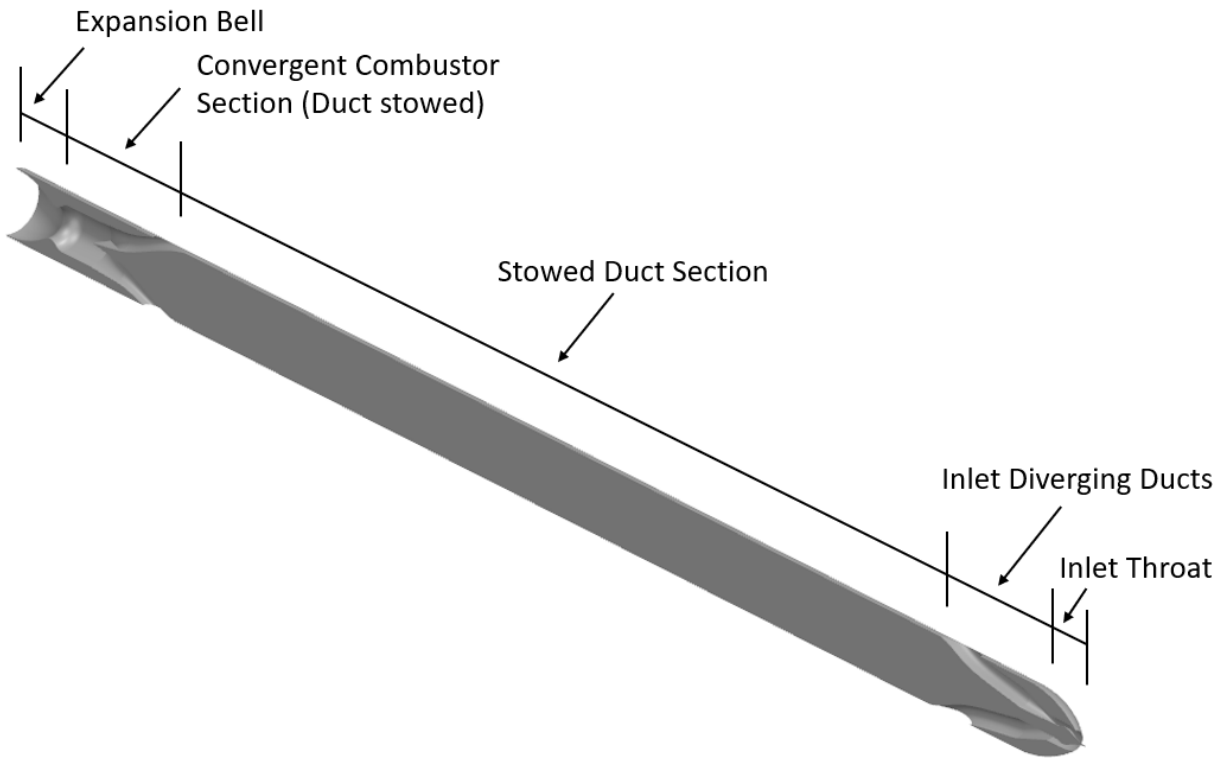


Figure 24 Labeled Isometric Cut away of Separated Configuration

6.3 Dash and Terminal Configuration

This section shows the dash and terminal configurations of iteration 5. Figure 25 below show a front, top, side, and isometric view of iteration 5. This is after the tail fins, canards and ducts are deployed.

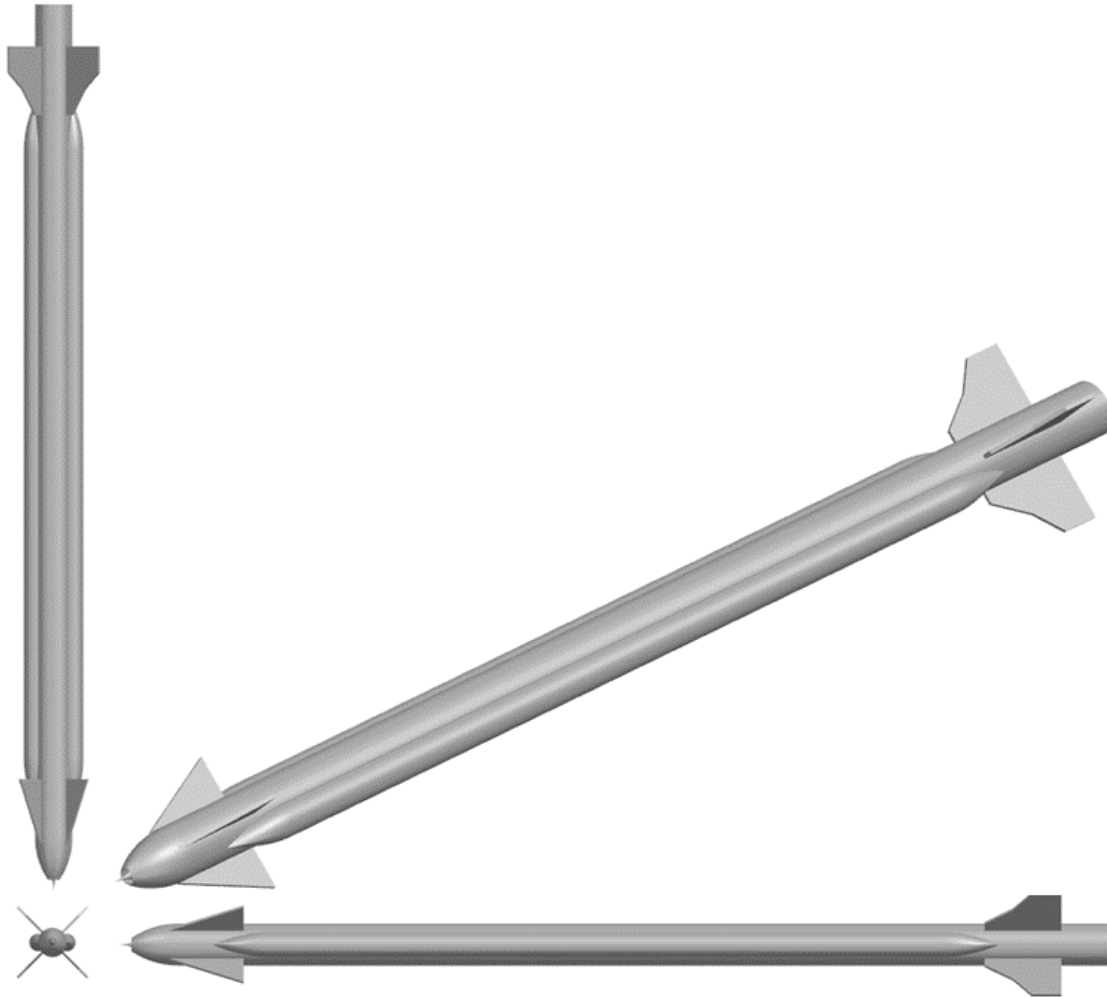


Figure 25: Front, Top, Side, and Isometric Views of Dash and Terminal Configurations

A labeled isometric cut away of iteration 5 is also shown for the dash and terminal configurations in Figure 26 below. In these configurations the ducts and control surfaces are fully deployed.

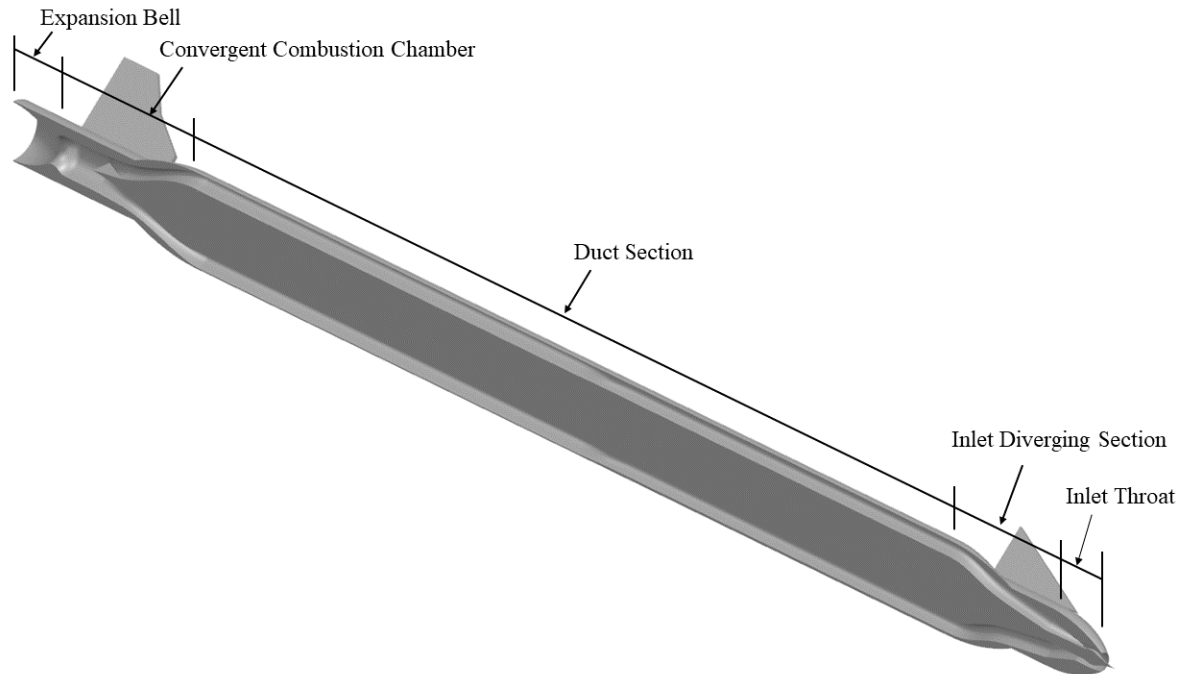


Figure 26 Labeled Isometric Cut away of Dash and Terminal Configuration

The cut away above highlights the inlet section, duct section, combustion chamber, and nozzle of this iteration of the RAIDER AIM-9.

7 Summary and Recommendations

7.1 Summary

In summary:

- The cruise L/D at FL 800 is 0.89;
- The cruise angle of attack at FL 800 is 2.75 degrees;
- The required thrust at cruise is 60.4 lbf;
- The free stream flow area is 7.89 in²;
- The inlet throat area is 6.71 in²;
- The combustor inlet Mach number is 0.25;
- The combustor inlet area is 16.1 in²;
- The exit Mach number is 1.00;
- The exit pressure is 0.82 lb/ft²;
- The combustor chamber for the powerplant design is 3.54 ft long;
- Combustion will begin within the inflatable ducts;
- The throat area was calculated to be 21.1 in²;
- The missile configuration must be changed to conform to the ramjet design.
- Iteration 1 showed:
 - Decreasing the Mach number to 2.5 decreased the specific impulse, but the inlet area and inlet throat area do not conform to the outer mold line dimensions in Appendix A;
- Iteration 2 showed:
 - At 80,000 ft, Mach 2.5, and a chosen inlet area of the 5 in² was able to size the missile to the outer mold line defined in Appendix A;
 - The new engine will burn the fuel in 83.4 seconds, which is more than the time of flight of the mission;
- Iteration 3 showed:
 - At 80,000 ft, Mach 2.5, and a chosen inlet area of the 7.5 in² was able to size the missile to the outer mold line defined in Appendix A



- The new engine will burn the fuel in 55.6 seconds, which is more than the time of flight of the mission;
- Changing the inlet capture area is an inefficient way to size the missile
- Iteration 4 showed:
 - At 30,000 ft and Mach 2.5, the inlet area is 80% with respect to iteration 3.
- Iteration 5 showed:
 - At 30,000 ft and Mach 2.5, the combustion chamber length is within 10% with respect to iteration 3.
- At an altitude of 30,000 ft and Mach 4, all geometry is within design limitation.

7.2 **Recommendations**

The authors recommend that:

- Combustion starts in the ducts to keep the combustor chamber length within the profile of the existing missile;
- A flare be added to the missile to incorporate a larger expansion nozzle;
- A shape memory alloy nozzle be used to expand the flow from the nozzle throat area that was calculated.

7.3 **Section Responsibilities**

This section outlines the contributions of each group member:

- Jack Barland: Sections 1, 6.1, 6.2, CAD Iteration 5, 7.1, 7.2, Report formatting.
- Peter Dillon: Section 3, 7.1, 7.2, Iteration 2, Iteration 3.
- Andrew Dodge: Sections 4.4, 4.5, 4.6, 4.7, 4.8, 4.10, Iteration 1.
- Jonathan Guzman: Sections 4.3, 4.4, 5.6, 6.3, 7.1, CAD Iteration 3 and 4, Report Formatting.
- Anthony Mistretta: Sections 4.1, 4.2, 4.3, Iteration 4, Iteration 5.
- Ben Svoboda: Sections 2, 4.9, CAD Iteration 1 and 2, Section 6.2 figures.



8 References

1. Parsch, A., “Raytheon (Philco/General Electric) AAM-N-7/GAR-8/AIM-9 Sidewinder,” *Designation-Systems, Designation-Systems.net* [<http://designation-systems.net/dusrm/m-9.html>] Lawrence, Kansas 66044, 10 September 2023, 5:30 pm.
2. Fleeman, Eugene L., “*Missile Design and System Engineering*,” American Institute of Aeronautics and Astronautics, Inc, 2012, Chapter 2.
3. Barrett, R., “The RAIDER AIM-9 Team at the NDIA Air Armament Symposium with Their Missile Model,” 8 November 2023.
4. Anon., “63rd Fighter Squadron (USAF AETC),” *F-16.net*. [https://f-16.net/units_article223.html] Lawrence, Kansas 66044, 16 October 2023, 1:25 pm.
5. Zvereva, A., “Sukhoi Design Bureau, 054, Sukhoi Su-57,” *Flickr*. [<https://www.flickr.com/photos/130961247@N06/49581303977/>] Lawrence, Kansas 66044, 16 October 2023, 1:29 pm.
6. Anderson, J “*Fundamentals of Aerodynamics*” 6th ed., McGraw Hill, New York, 2017, pp 1103-1109.
7. Barrett, R., “Reverse Engineering of Baseline Missiles & Proverse Engineering of RAIDER Missiles,” *AE 721 Design Lab I, aerodoc.tech* [https://www.aerodoc.tech/files/ugd/aae7b4_12ea37f6b05e4c3da2bc53a6efa1d936.pdf] Lawrence, Kansas 66044, 16 October 2023, 12:30 pm.
8. Slater, J. W. “Design and Analysis Tool for External-Compression Supersonic Inlets,” *50th AIAA Aerospace Sciences Meeting*, AIAA, Nashville Tennessee, 9 January 2012, [<https://doi.org/10.2514/6.2012-16>].
9. Barrett, R., “Technical Consultation Regarding RAIDER Powerplant Design,” University of Kansas Aerospace Engineering Department – In Person, 28 November 2023, 2:15 – 2:30 pm.



**Appendix A: AE 721 Report 6 Raider AIM-9 Benchmark and
Aerodynamic Properties I, Reverse & Proverse Engineering**

Table of Contents

	Page #
List of Tables.....	v
List of Figures	vi
List of Figures Continued	vii
List of Figures Continued	viii
List of Figures Continued	ix
List of Symbols	x
List of Symbols Continued.....	xi
List of Symbols Continued.....	xii
List of Symbols Continued.....	xiii
1 Introduction	1
2 Background Research and State of the Art (SOTA) Technology	2
2.1 Background Research	2
2.2 Engagement History	3
3 Benchmark Round Description & Salient Characteristics	4
3.1 Salient Characteristics	4
4 AIM-9X Performance Analysis	5
4.1 D/C _D Dynamic Pressure.....	5
4.2 Body First Bending Moment	7
4.3 Body C _{Do}	8
4.4 C _{DoBody, Wave}	11
4.5 Boattail Effect.....	13
4.6 Body Normal Force to Aspect Ratio	13
4.7 Relate Body Lift-to-Drag Ratio with Aspect Ratio, Fineness Ratio and Angle of Attack.....	14
4.8 Relate Body Lift-to-Drag Ratio with Dynamic Pressure.....	16
4.9 L/D Comparison	20
5 Body Aerodynamic Center Prediction	21
6 Flare Stabilizer Effects.....	22



7	Normal Force Prediction for Surfaces.....	25
	7.1 Non-dimensional C_N Slope with Angle of Attack	25
	7.2 Normal Force Coefficient Prediction of Surfaces	29
8	Aerodynamic Center Prediction for Planar Surfaces	34
9	Hinge Moment Prediction	37
	9.1 Hinge Moment Prediction for Fleeman Missile	37
	9.2 Hinge Moment Prediction for AIM-9X Block II.....	39
10	Planar Surface Drag Prediction.....	42
	10.1 Zero Lift Drag Coefficient Increase due to Increasing Planform Area.....	42
	10.2 Supersonic Drag of Planar Surfaces of AIM-9X	44
	10.3 L/D of AIM 9X with Respect to Local Angle of Attack	46
11	Surface Planform Geometry and Planform Alternatives	49
12	Tail Area Sizing	51
13	Aerodynamic Configuration Buildup.....	54
	13.1 Normal Force Coefficient Build Up.....	54
14	Reverse Engineering of Baseline System	55
	14.1 Baseline Missile Data.....	55
	14.2 Design Mission Profile.....	55
	14.3 Payload Range Diagram.....	56
	14.4 Propellant Weight	56
	14.5 Approximation of I_{sp} and Thrust Specific Fuel Consumption (TSFC).....	57
	14.6 Estimation of Time of Flight.....	57
	14.7 Mission Profile with Derived Values.....	57
	14.8 Mission L/D	58
	14.9 Empty Weight Ratio.....	58
	14.10 Lift and Drag Expressions with Mach	59
	14.11 Mach and Alpha at L/D Cruise	63
	14.12 $C_{Lcruise}$, L/D_{cruise} , and α_{cruise}	63
	14.13 Cruise Mid-Point Air Density	64
	14.14 Mission Profile with Mid-Point Cruise Detail	64



15	Proverse Engineering of RAIDER	65
15.1	Baseline Aerodynamic and Inertial Information.....	65
15.2	Proposed Changes	65
15.3	New Size Solution.....	65
16	Model CAD and Physical Model Preparation.....	75
16.1	CAD Model of New Form Factor RAIDER	75
16.2	Model BOM.....	77
16.3	Components to be Ordered	77
16.4	STL Files for 3D Printing	78
16.5	Assembly Methods.....	78
17	Conclusions and Recommendations	80
17.1	Conclusions.....	80
17.2	Recommendations.....	82
18	References.....	83

Appendix A: Off Rail Speed Calculations

Appendix B: AIM-9M Weight and Volume Calculations

Appendix C: AIM-9X Volume and Planform Area Calculations

Appendix D: AIM-9X Planar Surface Geometric Calculations

See Ref. 1 for AIM-9X (Raytheon image) cover image.



List of Tables

	Page #
Table 1: Characteristics of AIM-9X Block II (Ref. 4, Ref. 5, Ref. 6, Ref.7).....	3
Table 2: Salient Characteristics of the AIM-9X Block II (Ref. 1, Ref. 6)	4
Table 3: Aspect Ratio and Slender Wing Theory Mach Number Limit.....	26
Table 4: Canard and Tail Aspect Ratios and Limiting Mach Number	27
Table 5: Reverse Engineering Baseline Missile Data (Ref. 1, Ref. 6, Ref. 19)	55
Table 6: Baseline AIM-9X Block II Aerodynamic and Inertial Information.....	65
Table 7: RAIDER AIM-9 Component Volumes.....	74
Table 8 AIM-9X Replacement Model BOM.....	77



List of Figures

	Page #
Figure 1: Drag divided by Drag Coefficient vs. Diameter (Fleeman).....	5
Figure 2: Drag vs. Mach Number at Different Altitudes.....	6
Figure 3: First Mode Body Bending Frequency Trends with AIM-9X as Reference	7
Figure 4: Cross Section of AIM-9L (Ref. 13)	8
Figure 5: Body Zero-Lift Drag Coefficient vs. Mach at 20,000 ft (Fleeman).....	9
Figure 6: Body Zero-Lift Drag Coefficient vs. Mach at 20,000 ft (AIM-9X)	10
Figure 7: Body Zero-Lift Drag Coefficient vs. Mach at 20,000 ft	10
Figure 8: Body Wave Drag Coefficient vs. Mach Number (Fleeman)	11
Figure 9: C_{D_0} Body, Wave for AIM-9X Block II.....	12
Figure 10: C_{D_0} Body, Wave (Fleeman and AIM-9X Block II).....	12
Figure 11: Boattail Effect on Zero-Lift Drag Coefficient vs. Mach Number (Fleeman)	13
Figure 12: Normal Force Coefficient vs. Angle of Attack (Fleeman)	14
Figure 13: L/D vs. Angle of Attack (Fleeman)	15
Figure 14: AIM-9X Block II L/D.....	16
Figure 15: Fleeman Fig. 2.13 and AIM-9X Block II	16
Figure 16: L/D vs. Dynamic Pressure (Fleeman).....	17
Figure 17: Coefficient of Lift vs. Mach Number at Different Altitudes	18
Figure 18: Angle of Attack vs. Mach Number at Different Altitudes.....	19
Figure 19: L/D vs. Mach Number at Different Altitudes	19
Figure 20: AIM-9X Block II Max L/D vs. Body Design (Fleeman).....	20
Figure 21: Aerodynamic Center Shift Due to Angle of Attack Normalized with Length of Nose	21
Figure 22: Distance to AC_{body} /Length of the Nose vs. Angle of Attack	23
Figure 23: Distance to AC_{body} /Length of the Body vs. Angle of Attack	24
Figure 24: Non-Dimensional Normal Force Coefficient Slope with Angle of Attack vs. Mach Number	27
Figure 25: Non-Dimensional Normal Force Coefficient Slope with Angle of Attack vs. Mach Number Overlaid with AIM-9X Canard.....	28



List of Figures Continued

	Page #
Figure 26: Non-Dimensional Normal Force Coefficient Slope with Angle of Attack vs. Mach Number Overlaid with Tail	29
Figure 27: Wing Normal Force Coefficient vs. Effective Angle of Attack	30
Figure 28: Surface Normal Force Coefficient vs. Effective Angle of Attack Overlaid with Canard of AIM-9X Block II	31
Figure 29: Surface Normal Force Coefficient vs. Effective Angle of Attack Overlaid with Tail of AIM-9X Block II	32
Figure 30: Total Normal Force Coefficient of the AIM-9X Block II vs. Local Angle of Attack.....	33
Figure 31: AC of Planar Surfaces vs. Mach Number (Fleeman)	34
Figure 32: AC of Front Planform vs. Mach Number (AIM-9X).....	35
Figure 33: AC of Aft Planform vs. Mach Number (AIM-9X).....	35
Figure 34: AC of Planar Surfaces vs. Mach Number.....	36
Figure 35: Aerodynamic Center of Fleeman's Example Rocket Shifts with Mach Number	38
Figure 36: Figure 2.28 from Ref. 10 Recreated in Excel	39
Figure 37: HM Prediction for the AIM-9X Block II at Different Mach Numbers and Dynamic Pressures.....	40
Figure 38: Skin Friction Drag vs. Missile Area Reference (Fleeman).....	42
Figure 39: AIM 9X Zero Lift Drag from Planform Characteristics	43
Figure 40: AIM 9X Zero Lift Drag Compared to Reference Missiles	43
Figure 41: Planar Surface Wave Drag vs Mach Number Perpendicular to Leading Edge (Fleeman).....	44
Figure 42: Planar Surface Wave Drag vs. Mach Number Perpendicular to Leading Edge (AIM-9X).....	45
Figure 43: Planar Surface Wave Drag vs. Mach Number Perpendicular to Leading Edge (Fleeman and AIM-9X)	46
Figure 44: Lift to Drag Ratio vs. Local Angle of Attack (Fleeman)	47



List of Figures Continued

	Page #
Figure 45: AIM 9X Lift to Drag Ratio vs. Local Angle of Attack.....	48
Figure 46: AIM 9X Lift to Drag Ratio vs. Local Angle of Attack Compared to Baseline Missiles	48
Figure 47: RAIDER AIM-9 Grid Fin with Detailed View.....	49
Figure 48: Critical Mach Number vs. Cell Geometry with AIM-9 RAIDER Grid Fin Geometry	50
Figure 49: Tail Area for Stability Given SM, Baseline Missile	52
Figure 50: Tail Area for Stability Given SM, AIM-9X Full Fuel	53
Figure 51: Tail Area for Stability Given SM, AIM-9X Empty Fuel.....	53
Figure 52: AIM-9X Block II Normal Force Coefficient Build Up	54
Figure 53: AIM-9X Mission Profile (Ref. 20, Ref. 21).....	55
Figure 54: Payload Range Diagram	56
Figure 55: Updated Mission Profile	58
Figure 56: $C_L, C_N, C_A, C_D, L/D$ vs. Angle of Attack at Mach 2.5	60
Figure 57: $C_L, C_N, C_A, C_D, L/D$ vs. Angle of Attack at Mach 2	61
Figure 58: $C_L, C_N, C_A, C_D, L/D$ vs. Angle of Attack at Mach 3	61
Figure 59: $C_L, C_N, C_A, C_D, L/D$ vs. Angle of Attack at Mach 3.5	62
Figure 60: $C_L, C_N, C_A, C_D, L/D$ vs. Angle of Attack at Mach 4.....	63
Figure 61: Mission Profile Updated with Mid-Point Cruise Altitude	64
Figure 62: $C_L, C_N, C_A, C_D, L/D$ vs. Angle of Attack at Mach 2 for RAIDER Variant	66
Figure 63: $C_L, C_N, C_A, C_D, L/D$ vs. Angle of Attack at Mach 2.5 for RAIDER Variant	67
Figure 64: $C_L, C_N, C_A, C_D, L/D$ vs. Angle of Attack at Mach 3 for RAIDER Variant ...	67
Figure 65: $C_L, C_N, C_A, C_D, L/D$ vs. Angle of Attack at Mach 3.5 for RAIDER Variant	68
Figure 66: $C_L, C_N, C_A, C_D, L/D$ vs. Angle of Attack at Mach 4 for RAIDER Variant ...	68
Figure 67: $C_L, C_N, C_A, C_D, L/D$ vs. Angle of Attack at Mach 2 for Resized RAIDER Variant	70
Figure 68: $C_L, C_N, C_A, C_D, L/D$ vs. Angle of Attack at Mach 2.5 for Resized RAIDER Variant	71



List of Figures Continued

	Page #
Figure 69: CL, CN, CA, CD, L/D vs. Angle of Attack at Mach 3 for Resized RAIDER Variant	71
Figure 70: CL, CN, CA, CD, L/D vs. Angle of Attack at Mach 3.5 for Resized RAIDER Variant	72
Figure 71: CL, CN, CA, CD, L/D vs. Angle of Attack at Mach 4 for Resized RAIDER Variant	73
Figure 72 RAIDER AIM-9X Replacement 3 View	75
Figure 73 AIM-9X and RAIDER Replacement Comparison.....	76
Figure 74: RAIDER AIM-9 Color Scheme.....	79



List of Symbols

Symbol

a	Half of the Missile Cross Section Major Axis	(ft)
a	Speed of Sound.....	(ft/s)
A	Area	(ft ²)
A	Aspect Ratio	(~)
b	Half of the Missile Cross Section Minor Axis	(ft)
C _A	Axial Force Coefficient	(~)
C _D	Coefficient of Drag.....	(~)
C _{D0}	Zero Lift Coefficient of Drag	(~)
C _L	Coefficient of Lift.....	(~)
C _N	Normal Force Coefficient.....	(~)
d	Diameter	(ft)
D	Drag	(lbs)
E.....	Modulus of Elasticity	(ksi)
h	Altitude.....	(ft)
h	Height	(ft)
HM.....	Hinge Moment	(in-lb)
I.....	Impulse	(lbf-s)
l.....	Length.....	(~)
L.....	Lift	(lbs)
M.....	Mach Number	(~)
n	number	(~)
N	Normal Force	(lbs)
q	Dynamic Pressure.....	(Psf)
R	Coefficient of Determination	(~)
R	Engagement Range.....	(mi)
S	Area	(~)



List of Symbols Continued

Symbols

t	Thickness	(ft)
t	Time	(s)
T	Temperature	(R)
T	Thrust	(lbs)
V	Velocity	(ft/s)
W	Weight	(lb)
X	Distance	(ft)

Greek Symbols

α	Angle of Attack	(deg. or rad.)
α'	Effective Angle of Attack	(deg. or rad.)
γ	Ratio of Specific Heats	(~)
δ	Leading Edge Section Angle	(deg. or rad.)
Λ	Sweep Angle	(deg. or rad.)
ρ	Density	(lb/in ³)
σ	Density Ratio	(~)
ϕ	Roll Angle	(deg. or rad.)
ω	Frequency	(Hz. or rad/s)

Subscripts

accel	Acceleration	(~)
AIM-9X	AIM-9X	(~)
avg	Average	(~)
B	of the Body	(~)
Base	Base of the Missile	(~)
BB	Body First Bending Moment	(~)
Body	of the Body	(~)
BT	of the Boattail	(~)



List of Symbols Continued

Subscripts

C	of the Canard	(~)
Coast.....	During Coasting Flight.....	(~)
Crit.....	Critical	(~)
cruise.....	Cruise	(~)
dash.....	Dash	(~)
e.....	Effective	(~)
f.....	Fuel.....	(~)
F.....	of the Flare	(~)
Friction.....	Skin Friction.....	(~)
fuel	Fuel.....	(~)
HL.....	Hinge Line	(~)
jet fuel	jet fuel.....	(~)
launch.....	Launch	(~)
LE	Leading Edge	(~)
m	Missile	(~)
mac.....	Mean Aerodynamic Chord.....	(~)
missile.....	Missile	(~)
n	of the Nose	(~)
new	New.....	(~)
old.....	Old	(~)
payload.....	Payload.....	(~)
Powered	During Powered Flight.....	(~)
propellant	Propellant	(~)
RAIDER	RAIDER.....	(~)
Ref.....	Reference Value	(~)
rocket fuel	Rocket Fuel.....	(~)
sp.....	Specific.....	(~)



List of Symbols Continued

Subscripts

Surface	of the Control Surface	(~)
T	of the Tail	(~)
w	Warhead	(~)
W	of the Wing	(~)
warhead	Warhead	(~)
Wave	Due to Shock Wave Formation	(~)

Acronyms

AC	Aerodynamic Center	(~)
AR	Aspect Ratio	(~)
AIM	Air Intercept Missile	(~)
BOM	Bill of Materials	(~)
BVR	Beyond Visual Range	(~)
COM	Center of Mass	(~)
FL	Flight Level	(~)
FY	Fiscal Year	(~)
HM	Hinge Moment	(~)
HOBS	High Off-Boresight	(~)
IR	Infrared	(~)
RAIDER	Ram Air Inflatable Duct Eccentric Ramjet	(~)
SOTA	State of the Art	(~)
STL	Stereolithography	(~)
TOF	Time of Flight	(s)
TSFC	Thrust Specific Fuel Consumption	(lbf/lbf-hr)
US	United States	(~)
USAF	United States Air Force	(~)



1 Introduction

The Ram Air Inflatable Duct Eccentric Ramjet (RAIDER) Air Intercept Missile (AIM)-9 replacement will be intended for all current uses of the latest Sidewinder missile, AIM-9X, but with greater capabilities and mission specifications. This will be done with RAIDER technology. With this technology, the lift of the AIM-9 can be improved drastically. The RAIDER AIM-9 replacement was chosen by the authors because of the extreme capabilities of the current AIM-9. By utilizing RAIDER technology, the team hopes to further advance these capabilities and explore the cutting edge of missile design. Additionally, the RAIDER AIM-9 opens the door to several interesting engineering challenges, such as the use of a ramjet on a missile with off boresight capabilities performing in environments with an angle of attack greater than 90 degrees, exposure to over 60 times the force of gravity, and the use of an infrared (IR) sensor inside a shock cone. Throughout this project, the authors hope to learn more about the development of this technology, and how to improve it to pave the way for the future of missile and munition design and make current platforms of use more efficient.



2 Background Research and State of the Art (SOTA) Technology

This section covers the background research and gives an explanation of the SOTA of the current AIM-9 technology.

2.1 Background Research

Data for the latest version of the AIM-9X, the AIM-9X Block III, is largely unavailable because the Navy's Fiscal Year (FY) 2016 budget cancelled the development effort (Ref. 2). This leaves most of its specifications up to pure speculation based upon the requirements originally developed by the US Navy in 2012. Renewed requests for modifications indicate that a successor to the Block II may focus on a significant increase in range and Beyond Visual Range (BVR) capability. As a result, the data used within this report is focused on the AIM-9X Block II. The Block II has been fielded by the US and its allies since 2015, and the data for it is much more widely available. It is currently fielded on the following platforms (Ref. 2):

- F/A-18C/D Hornet
- F/A-18E/F Super Hornet
- F-15 Eagle
- F-16 Fighting Falcon
- F-15E Strike Eagle
- F-35 Lightning II
- F-22 Raptor

Below in Table 1, the dimensions of the AIM-9X Block II variant are shown. This variant is the SOTA of the AIM-9. The off-rail velocity of the AIM-9X Block II was found using Ref. 3, using the distance traveled off the rail divided by time. The figure referenced, Figure A.1, is shown in Appendix A.

Table 1: Characteristics of AIM-9X Block II (Ref. 4, Ref. 5, Ref. 6, Ref.7)

Range:	22 mi (35.4 km)
Off-Rail Velocity:	115 ft/s (35 m/s)
Unit Cost:	\$400,000-\$500,000
Production Volume (United States Air Force (USAF) and Navy):	11,635 units (through 2035)
Guidance System:	Passive Infrared
Propulsion System:	Solid Rocket Propellant
Launch System:	Rail Launch

2.2 Engagement History

The only publicly known aerial engagements involving the AIM-9X Block II all occurred in February of 2023. Five AIM-9X were launched to engage high altitude balloon targets over Alaska, Canada, Lake Huron, and over the coast of South Carolina. The object over Lake Huron required two AIM-9X to bring down the target, while each of the other engagements only required a single missile to be fired. The missiles were each fired from an F-22, and in the case of the balloon over the coast of South Carolina the F-22 fired from an altitude of 58,000ft to the target at 62,000-65,000ft, potentially marking the highest altitude air-to-air engagement in history (Ref. 8).



3 **Benchmark Round Description & Salient Characteristics**

This section displays the salient characteristics of the AIM-9X Block II.

3.1 **Salient Characteristics**

The following dimensions were what the team will optimize when making the RAIDER variant of the Sidewinder. Table 2 shows the salient characteristics of the missile.

Table 2: Salient Characteristics of the AIM-9X Block II (Ref. 1, Ref. 6)

Length:	9.92 ft (3.02 m)
Finspan:	1.16 ft (0.35 m)
Diameter:	0.42 ft (0.13 m)
Loaded Weight:	191 lbs (86.6 kg)
Warhead Size:	21 lbs (9.4 kg)

The AIM-9X is well-known for its high off-boresight (HOBS) capabilities for target engagement. This capability allows the missile to engage targets not directly in front of the launch aircraft. The seeker is capable of tracking 90 degrees off-boresight targets, and more modern aircraft platforms such as the F-35 with 360 degrees IR sensors allow the missile to fire at targets in any direction as locked using the pilots helmet mounted sight, and even lock-on-after-launch. The missile maneuverability is enabled by clipped forward and rear fins as well as the thrust vector control system (Ref. 9). In the authors' opinion, alternatives to the AIM-9X will need to incorporate this capability.

4 AIM-9X Performance Analysis

This section covers the benchmark AIM-9X missile performance parameters. Various aerodynamic and geometric trends are presented. The following equations are used throughout this chapter and are presented here for ease of reference. Equation 1 was used to calculate the speed of sound.

$$a = \sqrt{\gamma RT} \tag{1}$$

The velocity was then calculated using Equation 2.

$$V = M * a \tag{2}$$

Equation 2 and Equation 3 were used to calculate the dynamic pressure, q , shown below in Equation 3, where ρ is the density at a certain altitude.

$$q = \frac{1}{2} \rho V^2 \tag{3}$$

4.1 D/C_D Dynamic Pressure

Drag and C_D are related to missile diameter at various dynamic pressures in Ref. 10, Figure 2.4, this figure is replicated below in Figure 1:

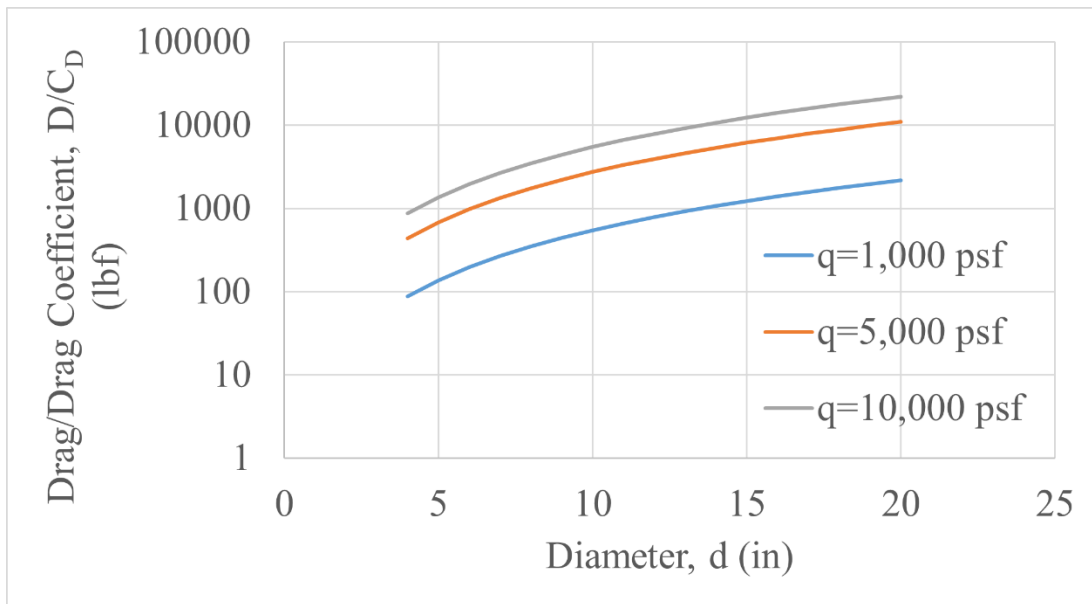


Figure 1: Drag divided by Drag Coefficient vs. Diameter (Fleeman)



This figure is governed by the principal equation in Ref. 10, Equation 4, and is shown below.

$$D = C_D * q * S_{Ref} = C_D * q * S_{Ref} \Rightarrow \frac{D}{C_D} = q * S_{Ref} \quad (4)$$

The reference area was found using Equation 5.

$$S_{Ref} = \frac{\pi}{4} * d^2 \quad (5)$$

These principal equations are used to analyze drag on the AIM-9X at various Mach numbers and altitudes. To find the speed dynamic pressure at each altitude, the standard atmosphere table from Ref. 11. The results of these calculations are shown in Figure 2, assuming $C_D = 0.45$ as instructed.

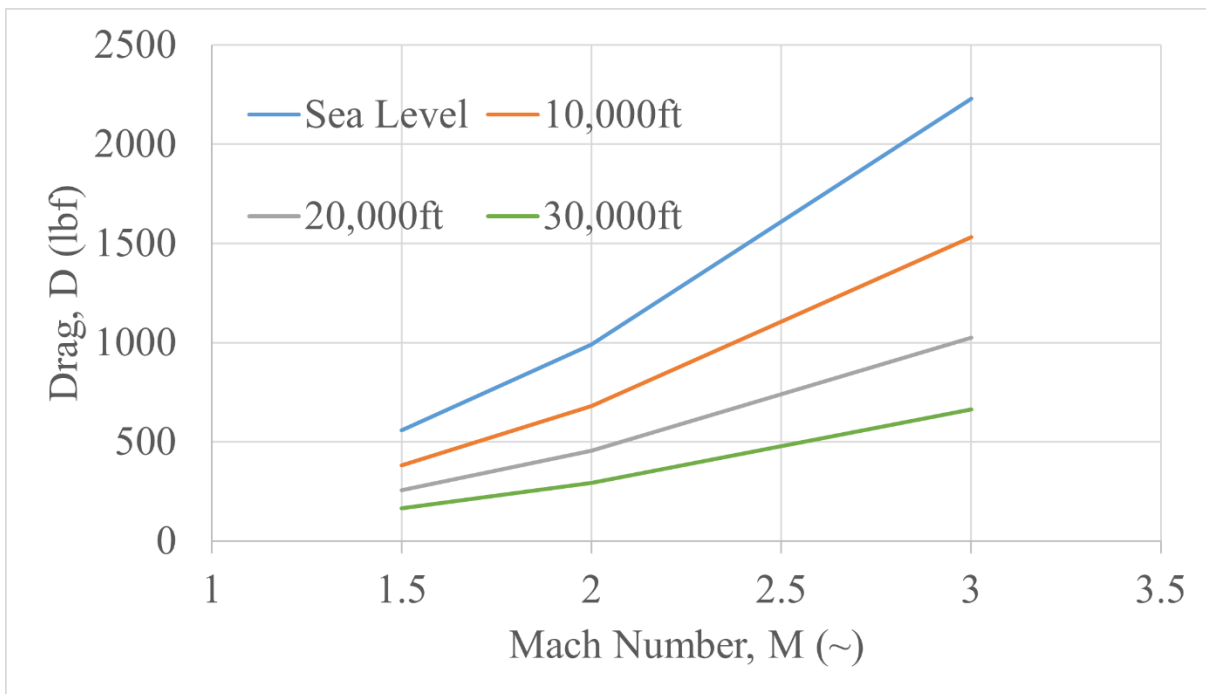


Figure 2: Drag vs. Mach Number at Different Altitudes



4.2 Body First Bending Moment

Calculation of the first bending moment frequency is done using the principal equation from Ref. 10, Equation 6, shown below.

$$\omega_{BB} = 276 * \left\{ \frac{E * t}{W * \left(\frac{l}{d}\right)^3} \right\}^{\frac{1}{2}} \tag{6}$$

This equation is utilized to generate a typical trend for first bending moment frequency compared to l/d in Ref. 10, Figure 2.4. A recreation of these trends is shown below in Figure 3. The AIM-9X is shown on the graph as a point of reference.

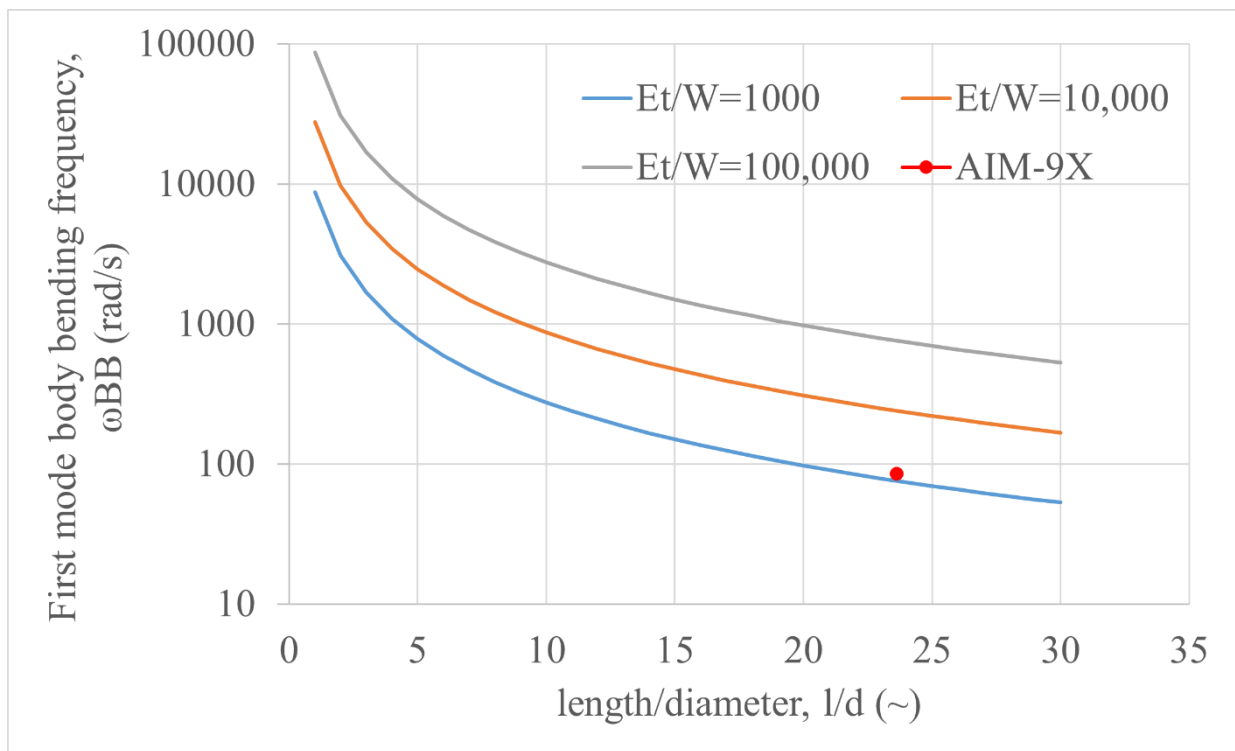


Figure 3: First Mode Body Bending Frequency Trends with AIM-9X as Reference

The calculation for the AIM-9X was done assuming the structure to be made of 4130 structural steel (Ref. 12) and the modulus of elasticity for the steel to be 29,700 ksi (Ref. 13). To approximate the thickness of the wall structures a cross sectional image was found and analyzed as shown below in Figure 4. Knowing the diameter of the missile, we can measure the thickness of the wall and scale it to an assumed 0.2 in wall thickness. The image used for reference is of an AIM-9R, and it was assumed that minimal structural changes were made

between the 9R and 9X variants. This results in a first mode body bending frequency of 85 rad/s.

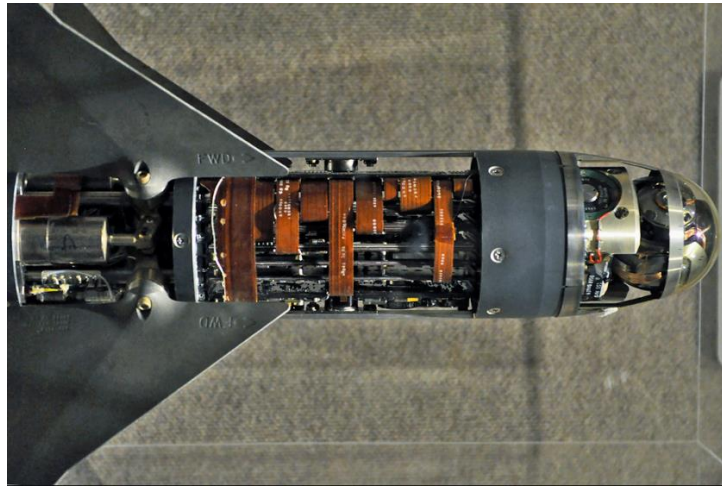


Figure 4: Cross Section of AIM-9L (Ref. 13)

4.3 Body C_{D_0}

This section relates the body zero-lift drag coefficient to the Mach number for the coast and powered condition of a missile. The body zero-lift drag coefficient is found using Equation 7.

$$(C_{D_0})_{Body} = (C_{D_0})_{Body,Friction} + (C_{D_0})_{Base} + (C_{D_0})_{Body,Wave} \quad (7)$$

To find the body zero-lift skin friction drag coefficient, Equation 8 below was used.

$$(C_{D_0})_{Body,Friction} = 0.053 * \left(\frac{l}{d}\right) * \left[\frac{M}{q * l}\right]^{0.2} \quad (8)$$

To find the coast body base drag coefficient for supersonic Mach numbers, Equation 9 below was used.

$$(C_{D_0})_{Base,Coast} = \frac{0.25}{M}, \text{ if } M > 1 \quad (9)$$

To find the coast body base drag coefficient for subsonic Mach numbers, Equation 10 below was used.

$$(C_{D_0})_{Base,Coast} = (0.12 + 0.13 * M^2), \text{ if } M < 1 \quad (10)$$

To find the powered body base drag coefficient for supersonic Mach numbers, Equation 11 below was used.



$$(C_{D_o})_{Base,Powered} = \left(1 - \frac{A_e}{S_{Ref}}\right) * \left(\frac{0.25}{M}\right), \text{ if } M > 1 \quad (11)$$

To find the powered body base drag coefficient for subsonic Mach numbers, Equation 12 below was used.

$$(C_{D_o})_{Base,Powered} = \left(1 - \frac{A_e}{S_{Ref}}\right) * (0.12 + 0.13 * M^2), \text{ if } M < 1 \quad (12)$$

To find the body zero-lift wave drag coefficient for supersonic Mach numbers, Equation 13 below was used. It should be noted there is no body zero-lift wave drag coefficient at subsonic Mach numbers.

$$(C_{D_o})_{Body,Wave} = \left(1.59 + \frac{1.83}{M^2}\right) * \left[\tan^{-1}\left(\frac{0.5}{\frac{l_n}{d}}\right)\right]^{1.69}, \text{ for } M > 1 \quad (13)$$

These equations were used to recreate Fig 2.7 in (Ref. 10) which is shown below in Figure 5.

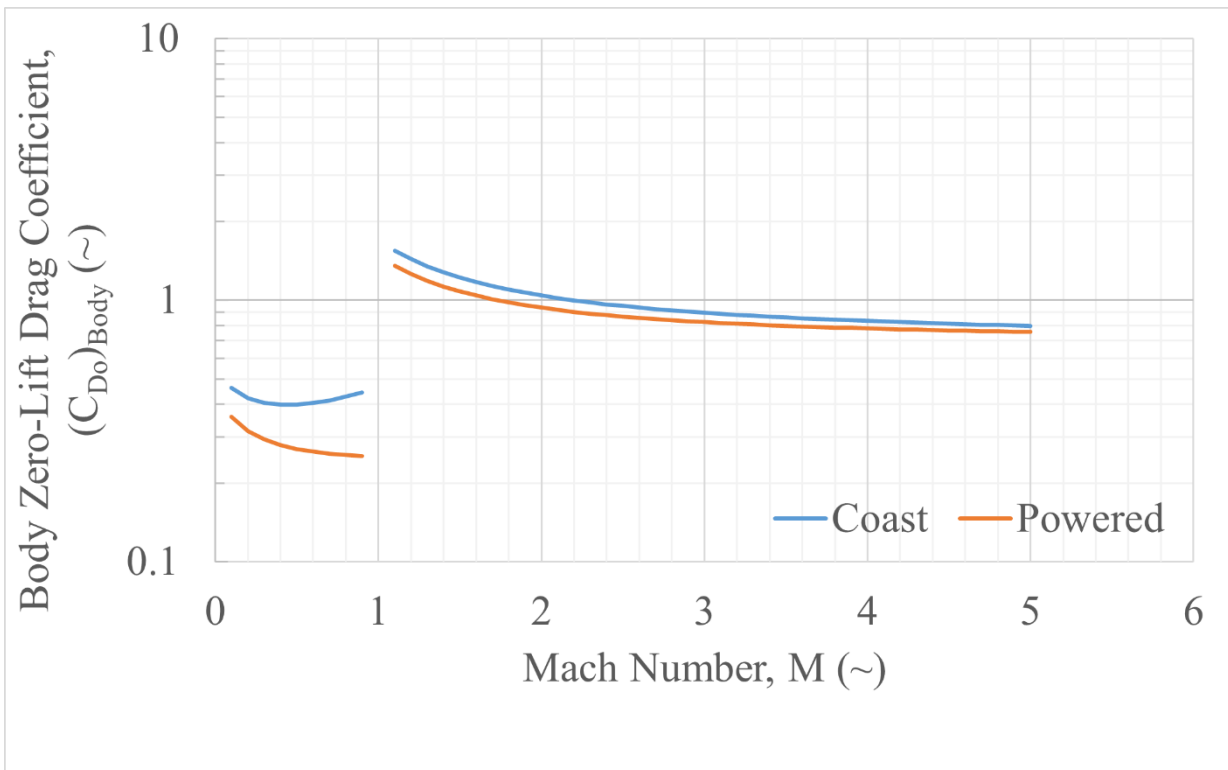


Figure 5: Body Zero-Lift Drag Coefficient vs. Mach at 20,000 ft (Fleeman)



Equation 7 through Equation 13 were then used to recreate the figure for the baseline AIM-9X missile at 20,000 ft, shown in Figure 6.

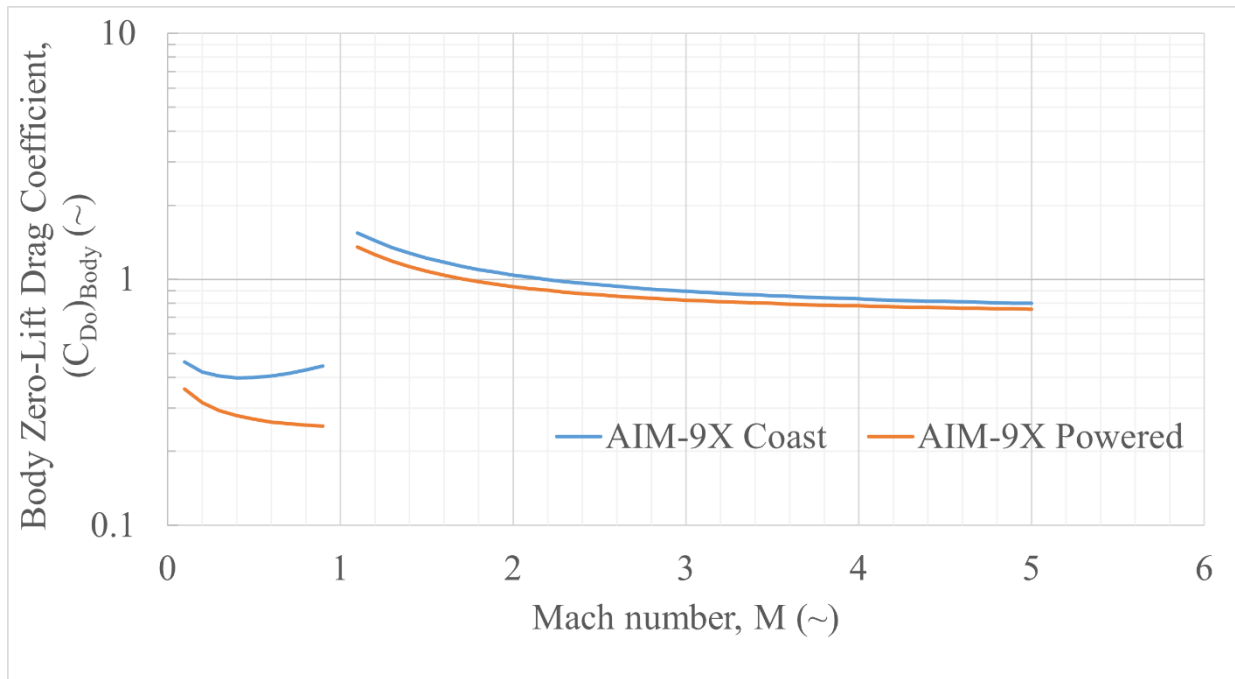


Figure 6: Body Zero-Lift Drag Coefficient vs. Mach at 20,000 ft (AIM-9X)

These figures were then overlaid for comparison in Figure 7.

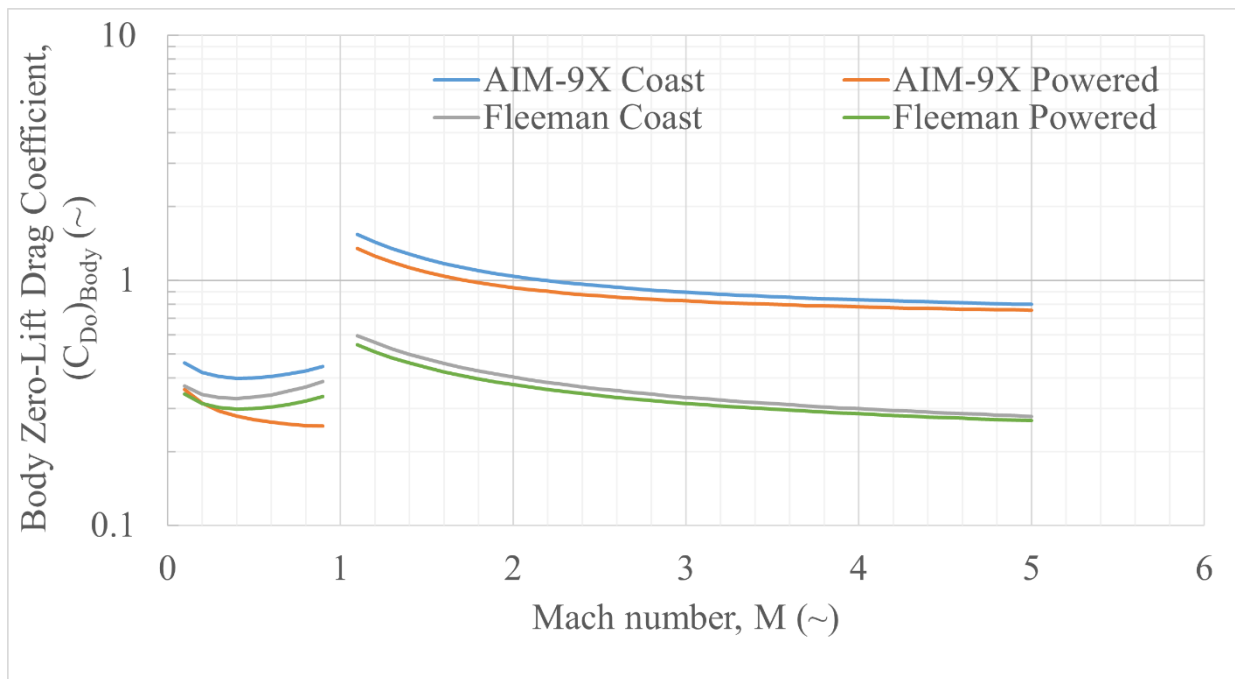


Figure 7: Body Zero-Lift Drag Coefficient vs. Mach at 20,000 ft



The body zero-lift drag coefficient for the AIM-9X at 20,000 ft at an engagement speed of Mach 2.5 is 0.87 for a powered condition and 0.95 for a coast condition.

4.4 C_{DoBody, Wave}

This section recreates Figure 2.8 from Ref. 10. This figure shows the body wave drag coefficient in relation to Mach number. To recreate this graph, Equation 13 was used.

It should be noted that this equation only works when M is greater than one. However, wave drag only occurs when the missile is traveling supersonic. It should also be noted that this equation is dependent on nose fineness ratio. The larger this ratio is, the smaller the drag coefficient is. The graph was recreated, in Figure 8, using fineness ratios of 0.5, 1, 2, 5:

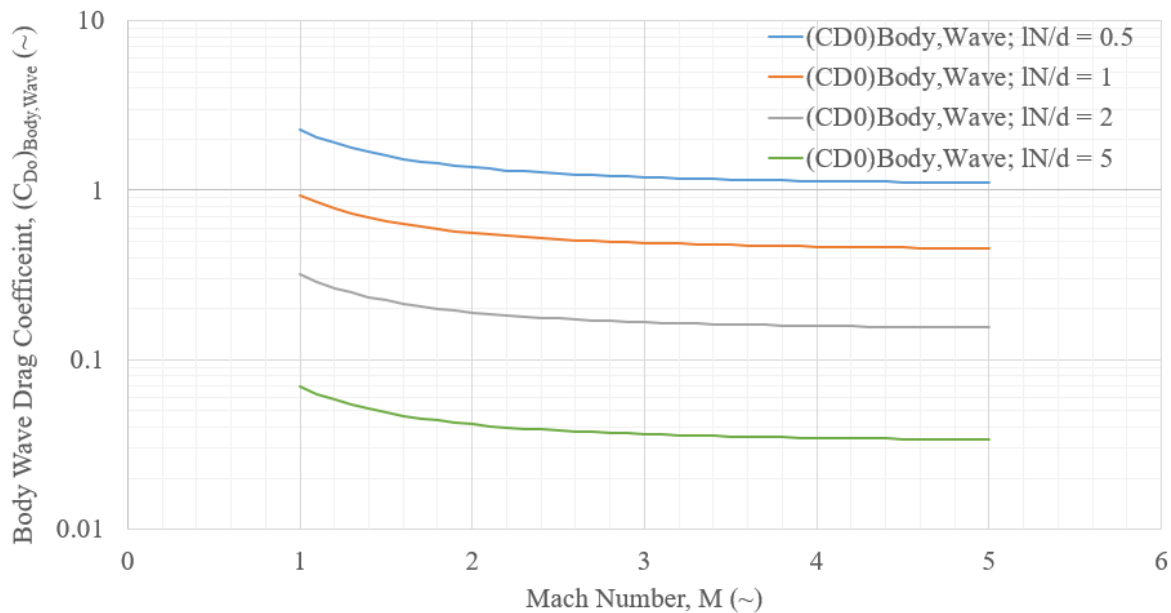


Figure 8: Body Wave Drag Coefficient vs. Mach Number (Fleeman)

To calculate the body, wave drag coefficient of the AIM-9X Block II, the nose fineness was calculated to be 0.83 (Appendix B). Using this nose fineness ratio, the wave body drag coefficient was graphed along the Mach numbers of one to five. This can be seen in Figure 9 below.



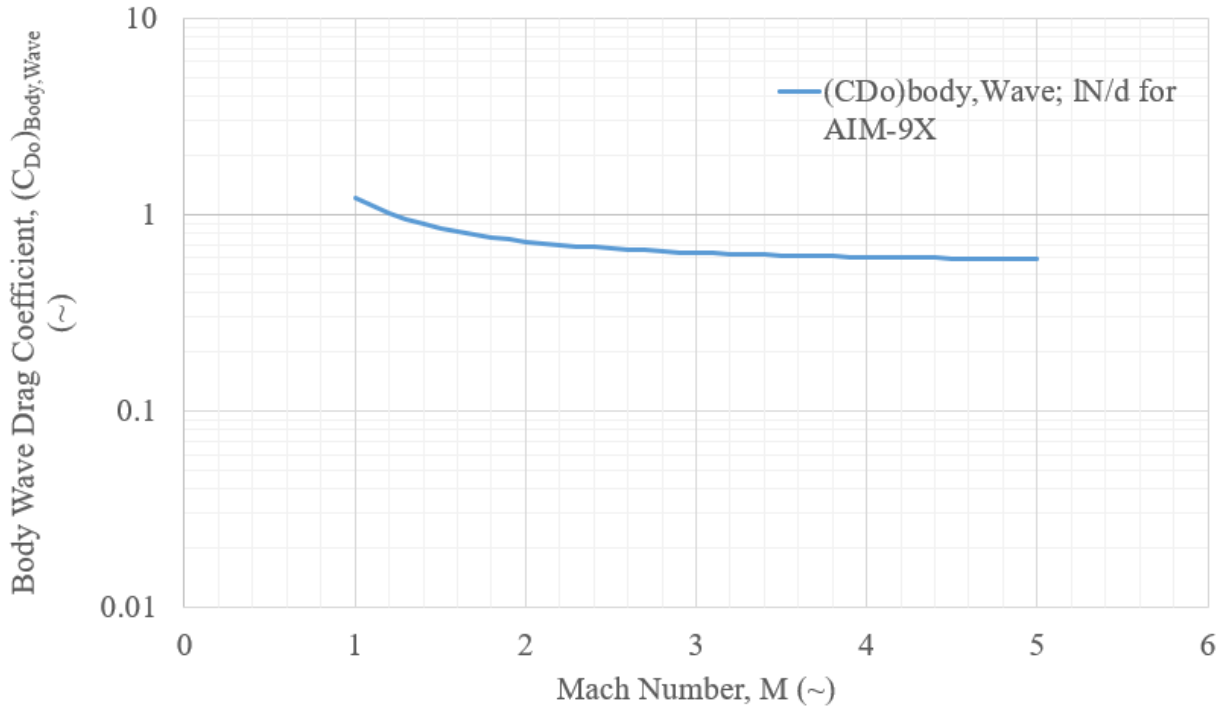


Figure 9: CDo Body, Wave for AIM-9X Block II

This plot was then overlaid with Figure 8 to produce Figure 10.

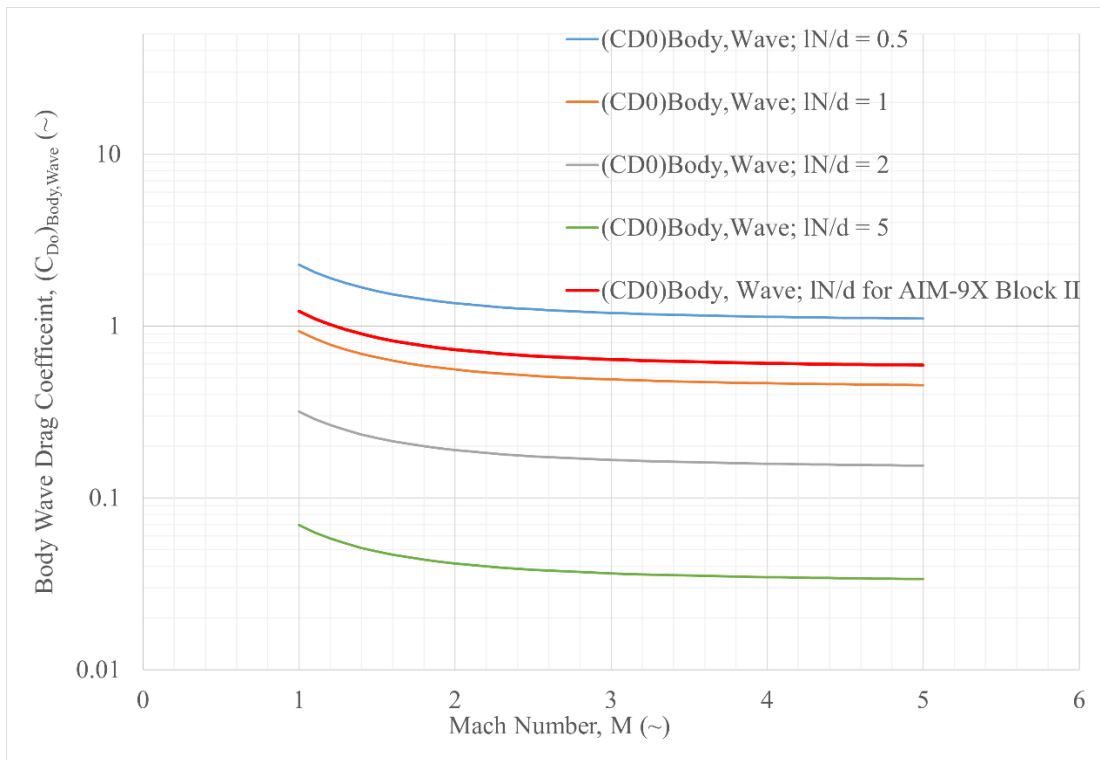


Figure 10: CDo Body, Wave (Fleaman and AIM-9X Block II)



The AIM-9X Block II does have a high body wave drag coefficient. This makes sense because the AIM-9X Block II has a low nose fineness ratio. This is because this missile's seeker is in a hemisphere in the nose. This decreases the nose length and increases the diameter.

4.5 Boattail Effect

This section recreates Figure 2.11 from Ref.10, shown below in Figure 11, which demonstrates the effect that boattail has on drag. It shows that a higher boattail angle reduces the drag on the missile but only for a subsonic Mach number. The drag is highest in the transonic region and gradually decreases as the Mach number increases. A large boattail angle can cause flow separation in the supersonic and hypersonic regions which increases the drag on the missile. This is one of the reasons that the AIM-9X Block II does not have a boattail. The other reason for not having boattail is that decreasing the nozzle diameter would not result in increasing the speed of the missile. Since the AIM-9X Block II is a supersonic missile, maximizing speed is a desirable characteristic.

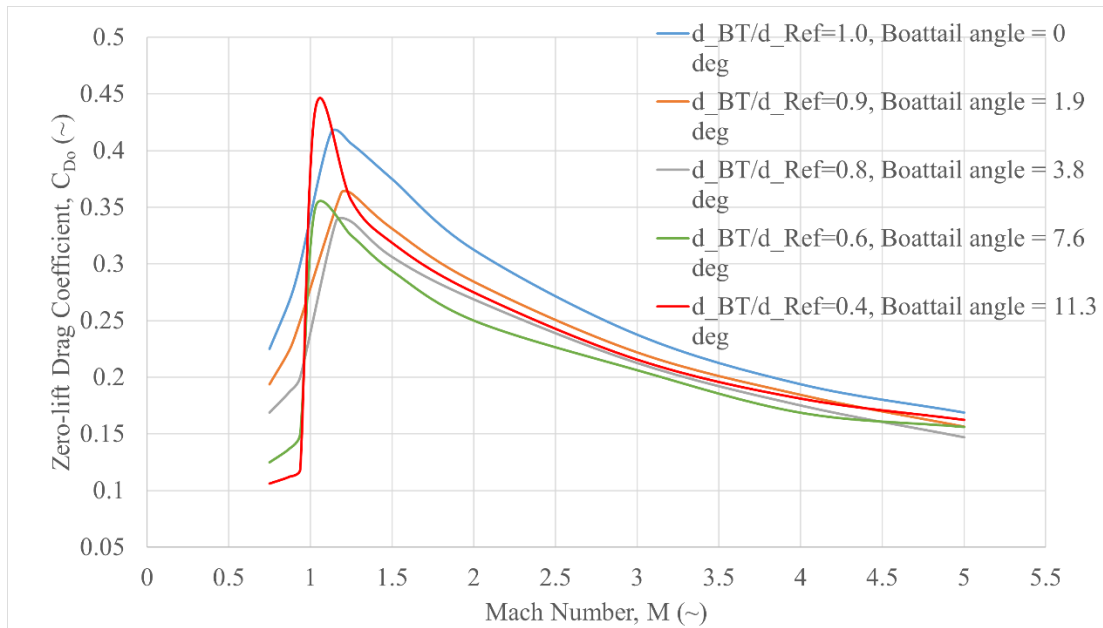


Figure 11: Boattail Effect on Zero-Lift Drag Coefficient vs. Mach Number (Fleeman)

4.6 Body Normal Force to Aspect Ratio

Figure 2.12 from Ref. 10 can be recreated quite simply by using Equation 14. With this figure, a good relationship can be seen between the aspect ratio of the missile and the normal



force coefficient. At small angles of attack this normal force coefficient can be said to be roughly equivalent to the coefficient of lift. The equation for the normal force coefficient can be seen below in Figure 12:

$$|C_N| = \left[\frac{a}{b} \cos^2(\phi) + \frac{b}{a} \sin^2(\phi) \right] \left[\left| \sin(2\alpha) \cos\left(\frac{\alpha}{2}\right) \right| + 1.3 * \frac{l}{d} \sin^2\alpha \right] \quad (14)$$

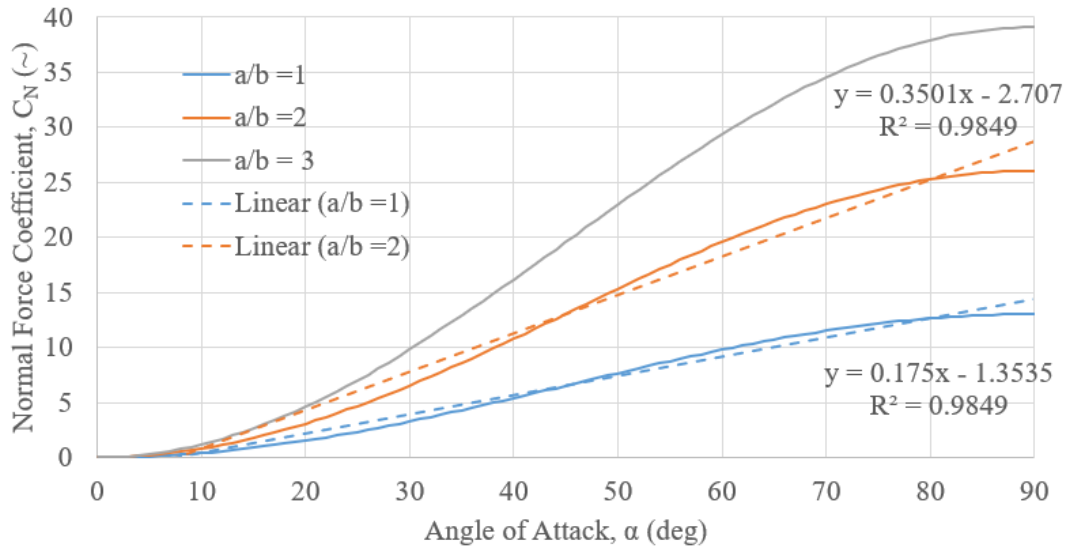


Figure 12: Normal Force Coefficient vs. Angle of Attack (Fleeman)

4.7 Relate Body Lift-to-Drag Ratio with Aspect Ratio, Fineness Ratio and Angle of Attack

This section recreates Figure 2.13 from Ref. 10. This was done using Equation 15 from Ref. 10.

$$\frac{L}{D} = \frac{C_L}{C_D} = \frac{C_N * \cos(\alpha) - C_{D_0} * \sin(\alpha)}{C_N * \sin(\alpha) + C_{D_0} * \cos(\alpha)} \quad (15)$$

Since the angle of attack is assumed to be low, C_L is assumed to be approximately C_N . C_N was calculated with Equation 16 below.

$$C_N = \left[\frac{a}{b} \cos^2(\phi) + \frac{b}{a} \sin^2(\phi) \right] * \left[\left| \sin(2 * \alpha) * \cos\left(\frac{\alpha}{2}\right) \right| + 1.3 * \frac{l}{d} * \sin^2(\alpha) \right] \quad (16)$$

Using the above equations, Figure 2.13 of Ref. 10 was recreated in Figure 13 with the following conditions:



- High drag, low fineness body:
 - $a/b = 1$
 - $l/d = 10$
 - $C_{D0} = 0.5$
- High fineness low drag
 - $a/b = 1$
 - $l/d = 20$
 - $C_{D0} = 0.2$
- Low drag nose
 - $a/b = 1$
 - $l/d = 10$
 - $C_{D0} = 0.2$
- Lifting body, high fineness, low drag
 - $a/b = 2$
 - $\phi = 0$ deg
 - $l/d = 20$
 - $C_{D0} = 0.2$

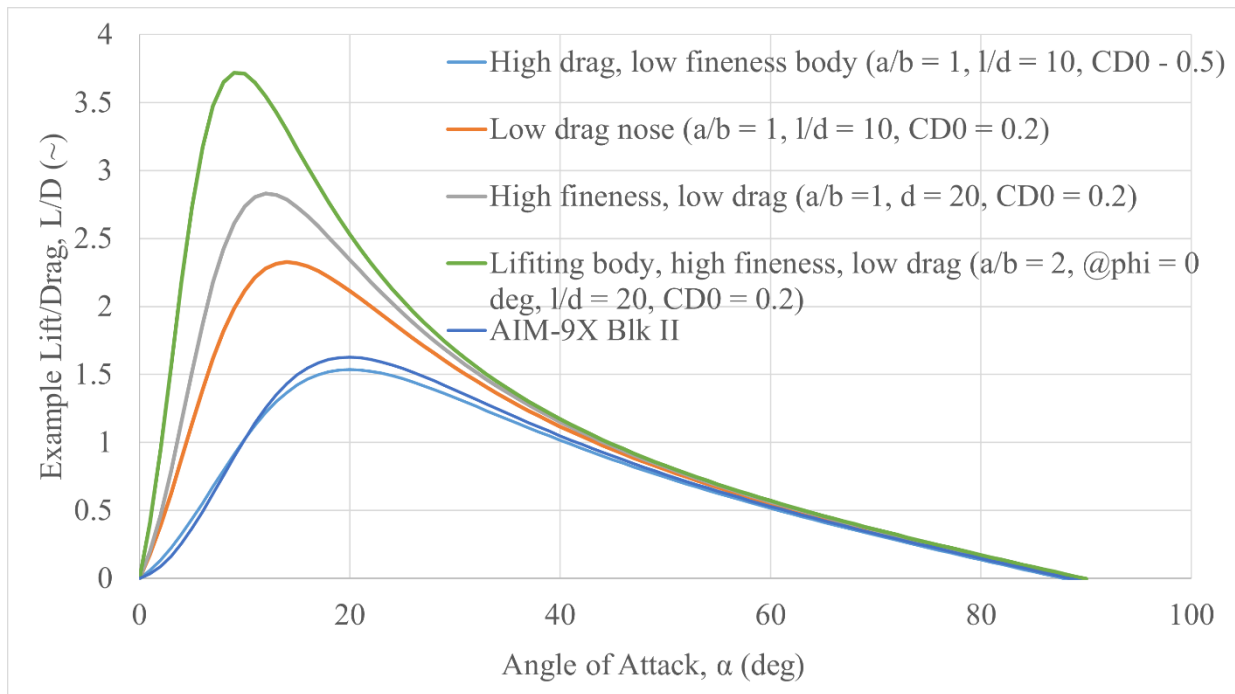


Figure 13: L/D vs. Angle of Attack (Fleeman)

After creating the figure above, Equation 15 and Equation 16 were used to make a similar plot for the AIM-9X Block II. This plot was created with the following properties:

- $a/b = 1$
- $l = 9.92$ ft
- $d = 0.42$ ft
- $C_{D0} = 0.865$



It should be noted that the zero-lift drag coefficient was chosen from Figure 6 with the assumption that the missile is flying under power at an altitude of 20,000 feet and at Mach 2.5. The result was Figure 14.

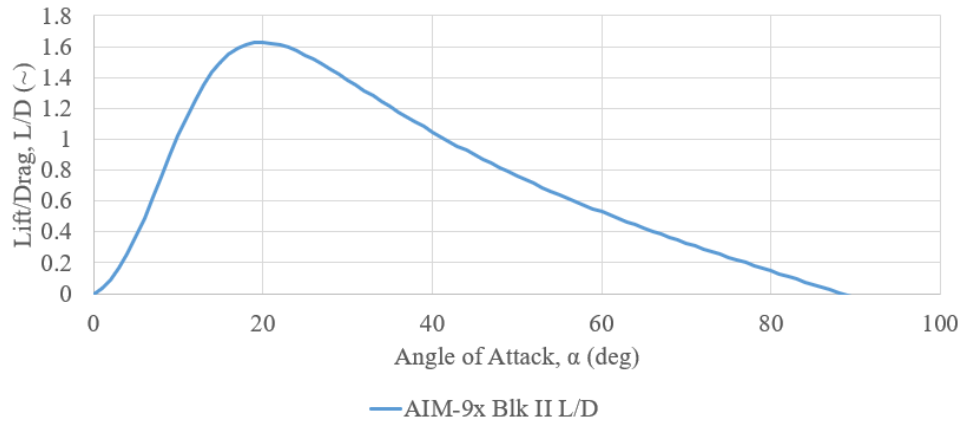


Figure 14: AIM-9X Block II L/D

When Figure 13 and Figure 14 are overlaid, Figure 15 results.

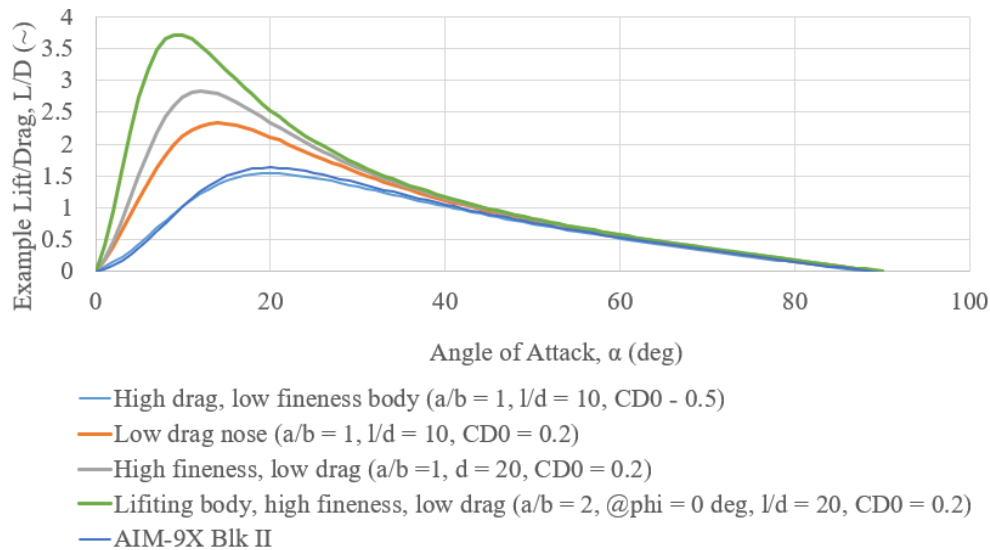


Figure 15: Fleeman Fig. 2.13 and AIM-9X Block II

It should be noted that the L/D for the AIM-9X Blk II is low. This makes sense as its C_{D0} is very high, even though its l/d is greater than 20.

4.8 Relate Body Lift-to-Drag Ratio with Dynamic Pressure

Within this section, Figure 2.14 from Ref. 10 will be recreated using values and relationships for the AIM-9X. Figure 16 below shows the recreation of the relationship between



lift to drag ratio and dynamic pressure. This relationship was made according to the other relationships found in the following sections.

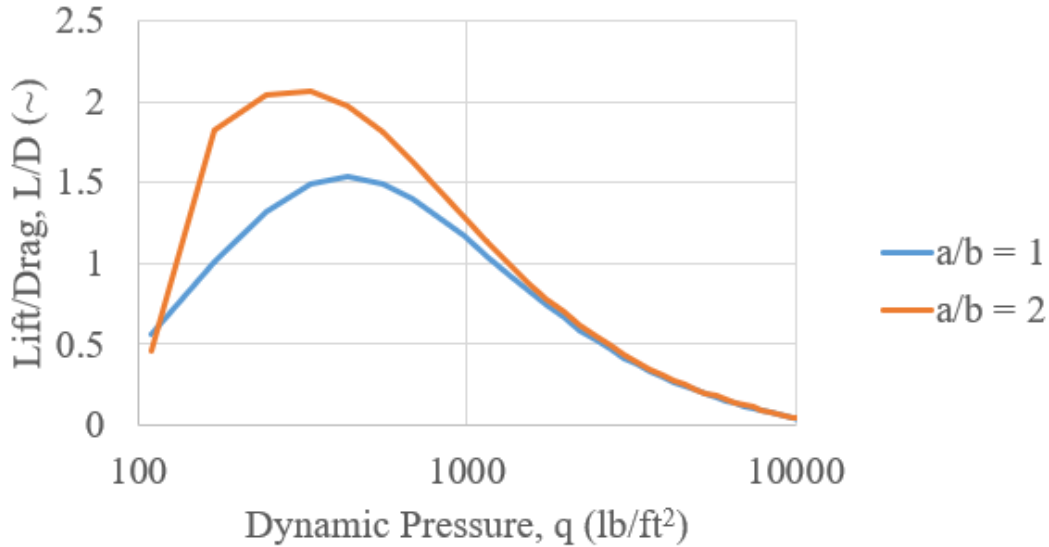


Figure 16: L/D vs. Dynamic Pressure (Fleeman)

4.8.1 Lift Coefficient to Stay Airborne

Within this section, the coefficient of lift required to stay airborne will be found at different Mach number and at different altitudes. For this, it will be assumed that the missile is in steady, level, 1g flight. Because of this assumption, lift is equal to weight. To model the missile accurately without the change of mass that occurs from burning fuel, it was assumed that the weight of the missile is the missile weight at half fuel. This was done as shown in Appendix B and resulted in a weight of 129.1 lbs being used within this section. Finally, the speed of sound at sea level, 10,000ft, 20,000ft, and 30,000ft can be found using Equation 1. Next, the velocity and then the dynamic pressure of the missile can be found at Mach 1.5, 2, 3, and 4 using Equation 2 and Equation 3. Finally, because it was assumed that lift is equal to weight, the coefficient of lift was found using Equation 17 shown below:

$$L = W = qSc_L \Rightarrow c_L = \frac{W}{qS} \quad (17)$$

This equation can then be used to find the coefficient of lift required to sustain steady, level flight at the various altitudes and Mach numbers. The results from this are shown below in Figure 17.



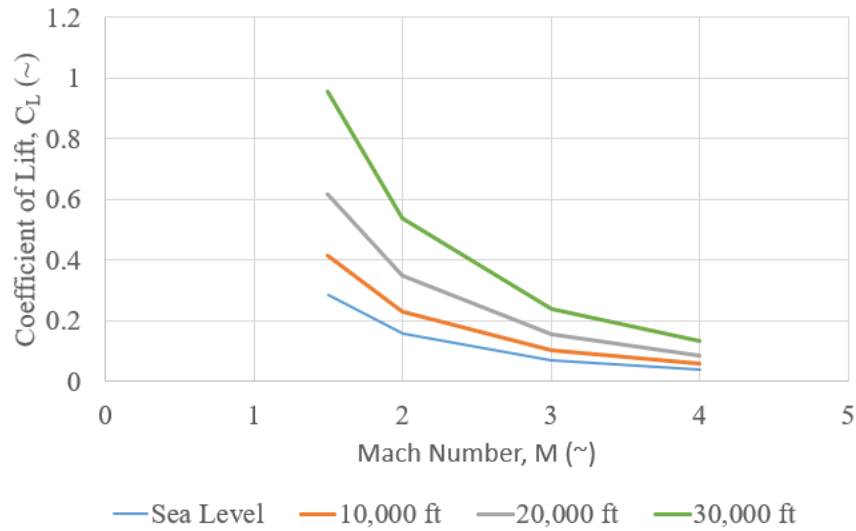


Figure 17: Coefficient of Lift vs. Mach Number at Different Altitudes

4.8.2 Angle of Attack to Stay Airborne

Within this section, the relationships used to generate Figure 17 above will be analyzed to find a relationship between the angle of attack required to sustain steady, level flight and Mach number. To do this, a linear approximation of the C_n - α graph was used for an aspect ratio of one. Only the aspect ratio of one was used because this is the aspect ratio of the AIM-9X. After finding the linear approximation for this, the coefficient of determination, the R^2 value, was found to be 0.985. The authors deemed this a close enough approximation, thus this linear approximation was used. Finally, the coefficients of lift found in Section 4.8.1 can be used alongside the inverse of the equation seen in Figure 12, Equation 18, to find the required angle of attack.

$$\alpha = \frac{C_L + 1.3535}{0.175 \left(\frac{1}{deg} \right)} \tag{18}$$

With Equation 18, Figure 18 was generated:



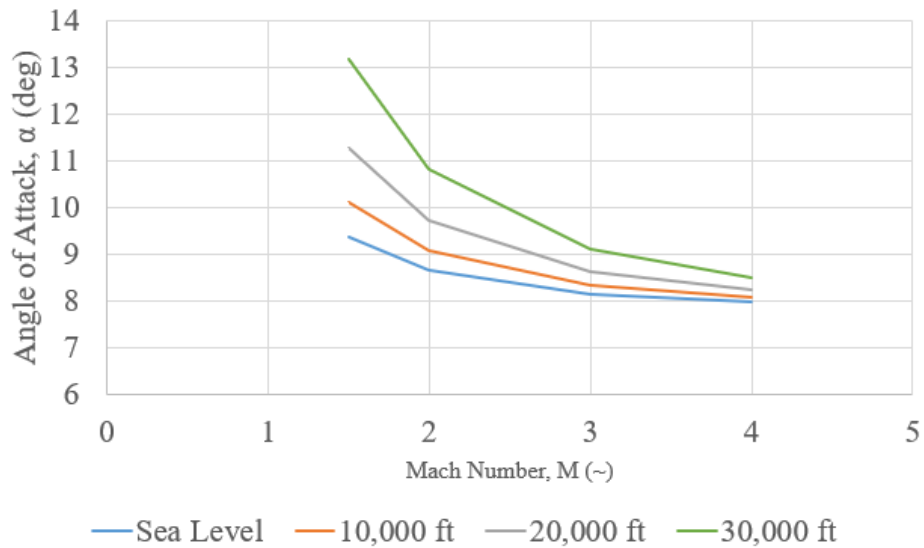


Figure 18: Angle of Attack vs. Mach Number at Different Altitudes

4.8.3 L/D vs. Mach Number

With the angles of attack found in Section 4.8.2, the lift to drag ratio of the missile was found for the same flight conditions. This was done using Equation 15 from Ref. 10. The results from this can be seen below in Figure 19.

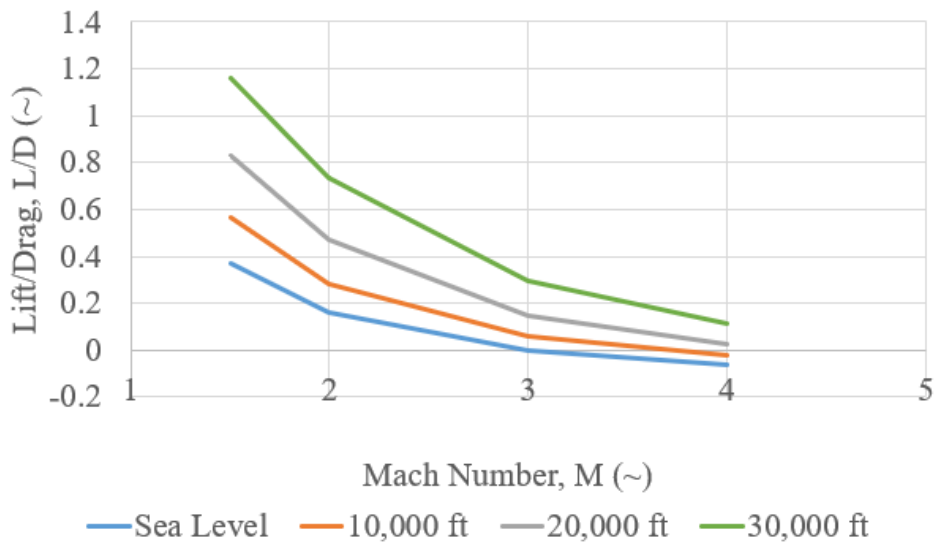


Figure 19: L/D vs. Mach Number at Different Altitudes



4.9 L/D Comparison

This section shows the AIM-9X Block II tradeoff of low observables and $(L/D)_{max}$ versus volumetric efficiency compared to other aircraft, per Fleeman Figure 2.15 (Ref. 10). Fleeman Figure 2.15 is a function of total planform area, total fuselage volume, and $(L/D)_{max}$. The calculations for total planform area and body volume were found using an image from Ref. 15 and was found to be 0.88. The full calculation is in Appendix C. The $(L/D)_{max}$ value used for this figure was found from Figure 19 at 30,000 ft and at Mach 1.5 and was found to be 1.16.

Figure 20 below displays Fleeman Figure 2.15 with the addition of where the AIM-9X Block II variant lies compared to other aircraft, shown by the red dot. Note with the addition of the AIM-9X Block II, Figure 20 is no longer to scale.

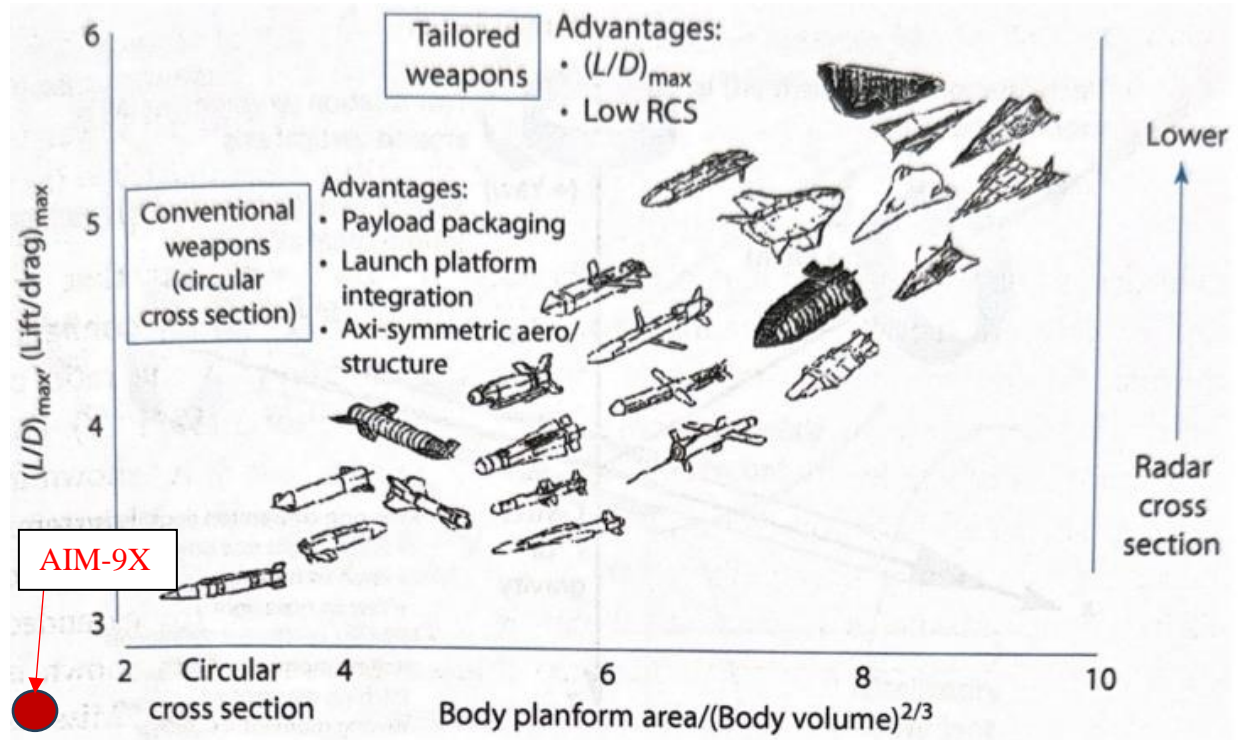


Figure 20: AIM-9X Block II Max L/D vs. Body Design (Fleeman)

The AIM-9X Block II variant has a small cross section, long fuselage body, and short lifting surfaces. These attributes combine to give a small ratio of planform area to body volume. The $(L/D)_{max}$ on the AIM-9X Block II is low since it is a short range, air to air missile that is driven dominantly by engine power rather than lifting devices.



5 Body Aerodynamic Center Prediction

This section will predict the change of aerodynamic center with respect to angle of attack. First, Figure 2.18 from Ref. 10 is recreated directly as shown in, then the calculation is repeated with the values for the AIM-9X as shown in Figure 21. To find the length of body to length of nose ratio, Figure C.1 in Appendix C was used. With this, the aerodynamic center's shift due to angle of attack can be seen which can help with planform sizing for stability characteristics.

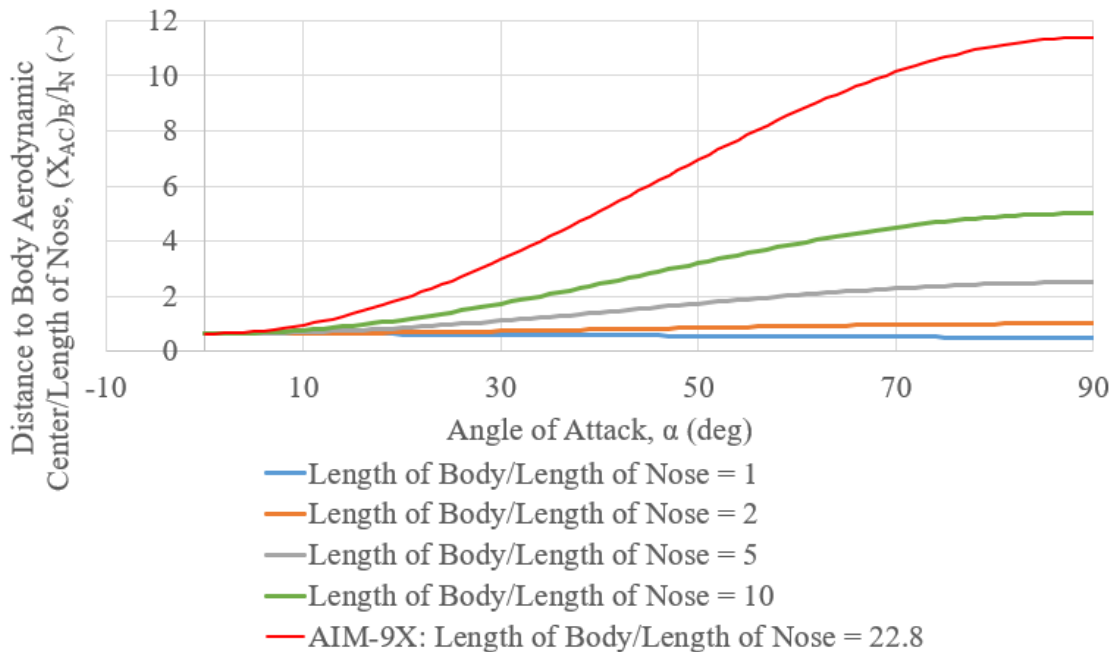


Figure 21: Aerodynamic Center Shift Due to Angle of Attack Normalized with Length of Nose

This figure was created using Equation 19 below:

$$\frac{X_{ACB}}{l_N} = 0.63(1 - \sin^2\alpha) + 0.5\left(\frac{l_B}{l_N}\right)\sin^2\alpha \quad (19)$$



6 Flare Stabilizer Effects

This section covers the effects of a flare stabilizer. To characterize the effect of utilizing a flare stabilizer on the ac, the rear fins of the AIM-9X are replaced with a body flare. As instructed, a flare with diameter 10% greater than that of the missile is added, a flare to diameter ratio of 1.1. The resulting geometry is shown below in Equations 20-22.

$$d_F = 1.1 * d_m = 1.1 * 0.42ft = 0.462ft \quad (20)$$

$$l_F = \frac{\frac{1}{2} * (0.462ft - 0.42ft)}{\tan(10^\circ)} = 0.12ft \quad (21)$$

$$x_F = 9.92ft - 0.12ft = 9.8ft \quad (22)$$

Utilizing this calculated geometry and the equations presented in Fleeman, we can estimate the location of the flare AC, the normal force coefficient of the flare due to angle of attack, as well as the total missile AC in Equations 23 and 24.

$$(x_{ac})_F = x_F + \frac{0.33l_F \left[\left(2 \frac{d_F}{d} \right) + 1 \right]}{\frac{d_F}{d} + 1} \quad (23)$$

$$(x_{ac})_F = 9.8ft + 0.33(0.12ft)[2(1.1) + 1]/(1.1 + 1)$$

$$(x_{ac})_F = 9.86ft$$

$$(C_{N\alpha})_F = 2 \left(\left(\frac{d_F}{d} \right)^2 - 1 \right) \quad (24)$$

$$(C_{N\alpha})_F = 2(1.1^2 - 1)$$

$$(C_{N\alpha})_F = 0.42rad^{-1}$$



Utilizing component build up methods, we can estimate the total missile AC using the following equation, assuming the normal force coefficient due to angle of attach of the body is 2 per radian,

$$X_{ac} = \frac{x_{AC_B} + \frac{(C_{N\alpha})_F}{(C_{N\alpha})_B} * \frac{d_F}{d} * x_{AC_F}}{1 + \frac{(C_{N\alpha})_F}{(C_{N\alpha})_B} * \frac{d_F}{d}} \quad (25)$$

Equation 25 can be plotted for a range of α , based upon the work to estimate the AC of the body from the previous section. It is important to note that the AC location in the previous section is ac location divided by nose length, we must multiply the found value from Section 5 by the nose length of 0.348 ft to use it in the above equation, then divide the result by 0.348 ft for the plot. The resultant plot is shown below in Figure 22.

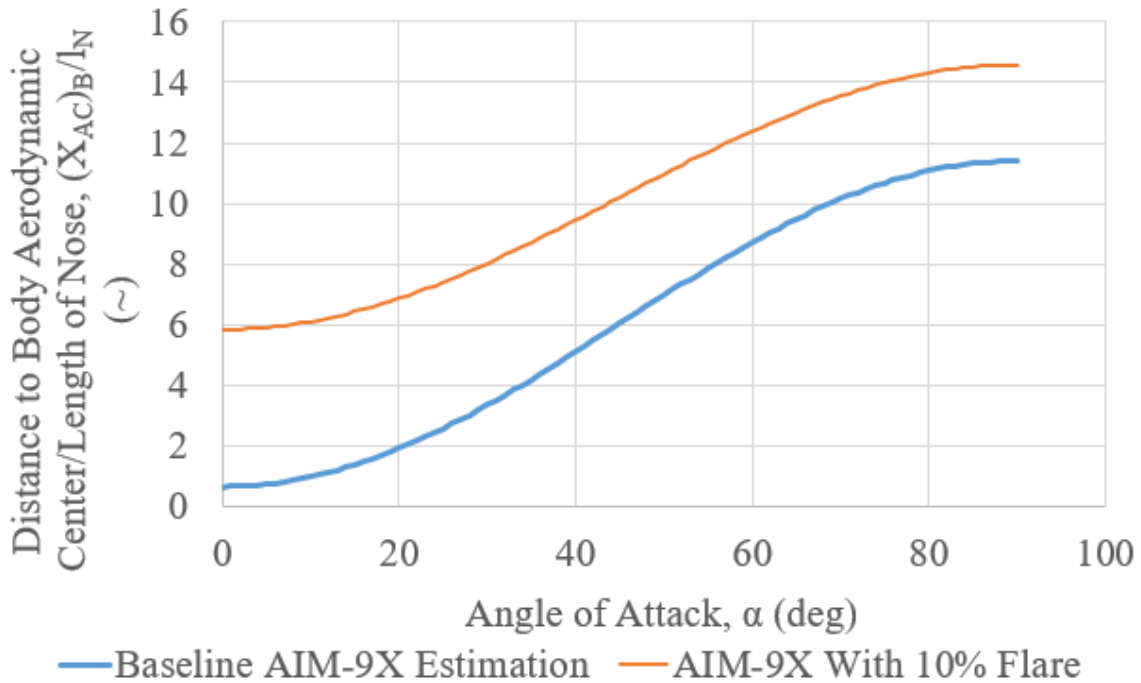


Figure 22: Distance to AC_{body} /Length of the Nose vs. Angle of Attack



We can see that by adding the tail flare into the estimation of missile AC significantly moves the AC back, and the AC is behind the nose at $\alpha = 0$. A more useful plot may be one that shows AC location normalized against body length, as the AC shifts significantly farther with the tail flare. This plot was generated and is shown in Figure 23.

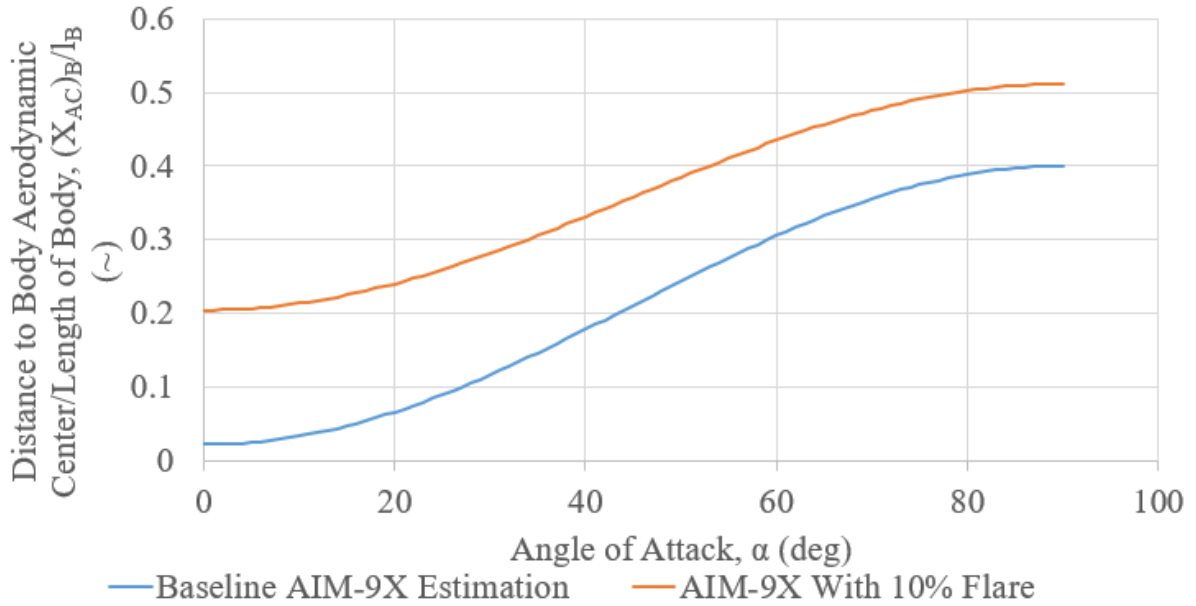


Figure 23: Distance to AC_{body} /Length of the Body vs. Angle of Attack



7 Normal Force Prediction for Surfaces

This section covers the non-dimensional normal force coefficient slope with angle of attack ($dC_N/d\alpha$) for the baseline missile from Fig. 2.25 from Section 2.14 of Ref. 10 as well as the prediction for the AIM-9X Block II canards and tail. It also presents the prediction of normal force coefficients for the wing of the baseline missile in Fig. 2.26 from Section 2.14 of Ref. 10, and the canard, tail and total normal force coefficients for the AIM-9X Block II.

7.1 Non-dimensional C_N Slope with Angle of Attack

For the baseline missile, the normal force coefficient slope with angle of attack was found using Equation 26 for linear wing theory, shown below.

$$\frac{dC_N}{d\alpha} = \left[\frac{4}{\sqrt{M^2 - 1}} \right] \left[\frac{S_{Surface}}{S_{Ref}} \right], \alpha' < 10 \text{ deg}, M > \sqrt{\left\{ 1 + \left[\frac{8}{(\pi A)^2} \right] \right\}} \quad (26)$$

If slender wing theory was used then Equation 27, below was used.

$$\frac{dC_N}{d\alpha} = \left(\frac{\pi A}{2} \right) \left(\frac{S_{Surface}}{S_{Ref}} \right), \alpha' < 10 \text{ deg}, M < \sqrt{\left\{ 1 + \left[\frac{8}{(\pi A)^2} \right] \right\}} \quad (27)$$

It should be noted that the aspect ratio, reference area and surface area, in the case of the baseline missile the surface was the wing, used in the equations above were given in Ref. 10. To figure out which wing theory to use the limiting Mach number at each aspect ratio was found. It was found using Equation 28 below.

$$M < \sqrt{\left\{ 1 + \left[\frac{8}{(\pi A)^2} \right] \right\}} \quad (28)$$



Each of the four aspect ratios used to create Fig. 2.25 from Ref. 10 and the Mach number that limits the use of slender wing theory are shown below in Table 1.

Table 3: Aspect Ratio and Slender Wing Theory Mach Number Limit

Aspect Ratio, A (~)	Mach Number Limit for Slender Wing Theory
0.5	5.19
1	2.74
2	1.62
3	1.31

Knowing the limit to which slender wing theory can be used to calculate the non-dimensional normal force coefficient slope with angle of attack, Equation 26 and Equation 27 were used to calculate $dC_N/d\alpha$ in Excel for each aspect ratio in the table above for the baseline missile, recreating Fig. 2.25 from Ref. 10. The recreation of the figure is shown in Figure 24 below.

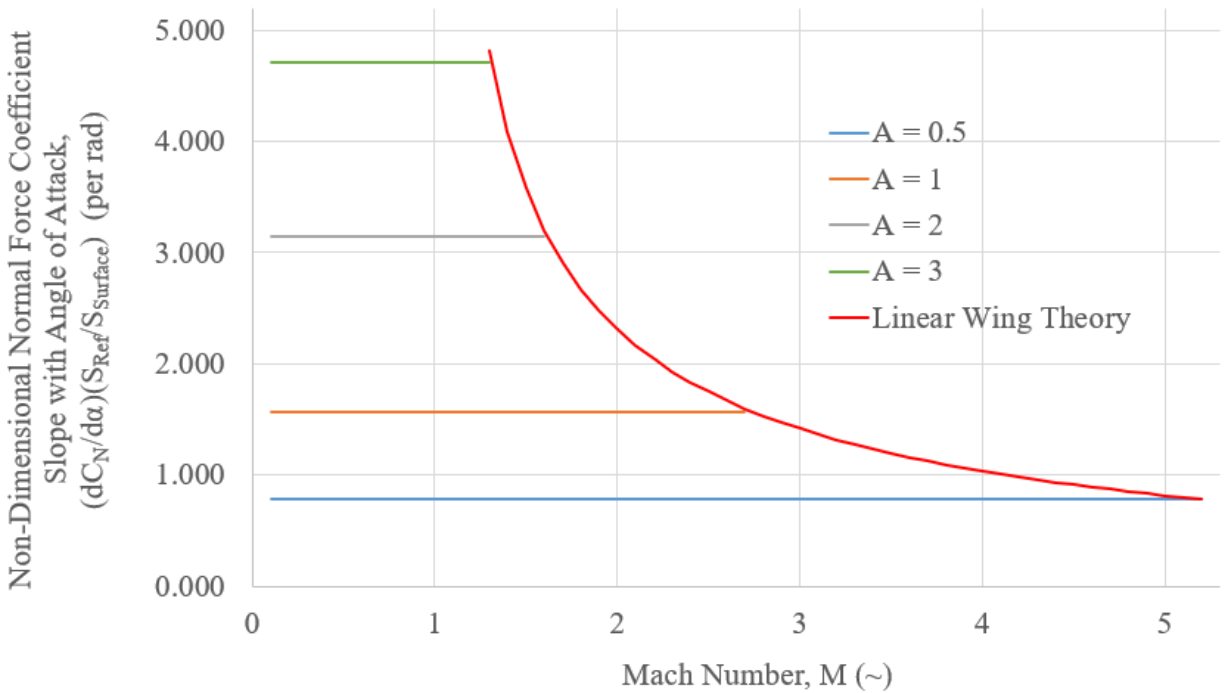


Figure 24: Non-Dimensional Normal Force Coefficient Slope with Angle of Attack vs. Mach Number

Using the figure in Appendix D, the characteristics needed to calculate the aspect ratio, reference area and surface area for the canard and tail of the AIM-9X Block II were found. The aspect ratio, reference area, and surface area were then calculated in Appendix D. The non-dimensional normal force coefficient slope with angle of attack was then calculated for the canard and tail. To find the limit to which slender wing theory holds, Equation 28 again was used. The table of the Mach number that limits slender wing theory for each control surface aspect ratio is shown below in Table 4.

Table 4: Canard and Tail Aspect Ratios and Limiting Mach Number

Aspect Ratio, A (~)	Mach Number Limit for Slender Wing Theory
1.75 (canard)	1.77
1.78 (tail)	1.75

Knowing the limits to which slender wing theory can be used to calculate the non-dimensional normal force coefficient slope with angle of attack, Equation 26 and Equation 27



were again used to calculate $dC_N/d\alpha$ for the canard of the AIM-9X Block II and the result was overlaid with Fig. 2.25 from Ref. 10. This can be shown in Figure 25 below.

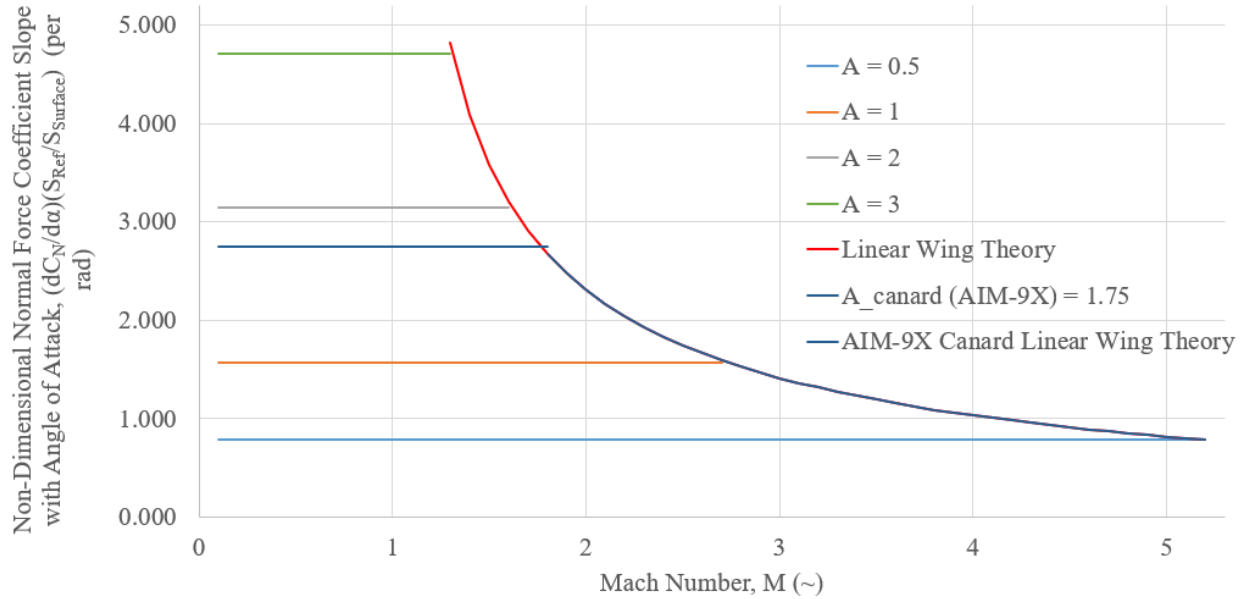


Figure 25: Non-Dimensional Normal Force Coefficient Slope with Angle of Attack vs. Mach Number Overlaid with AIM-9X Canard

The non-dimensional normal force coefficient slope with angle of attack was also calculated for the tail of the AIM-9X Block II, using Equation 26 and Equation 27, and overlaid with Fig. 2.25 from Ref. 10. The resulting figure is shown below in Figure 26.



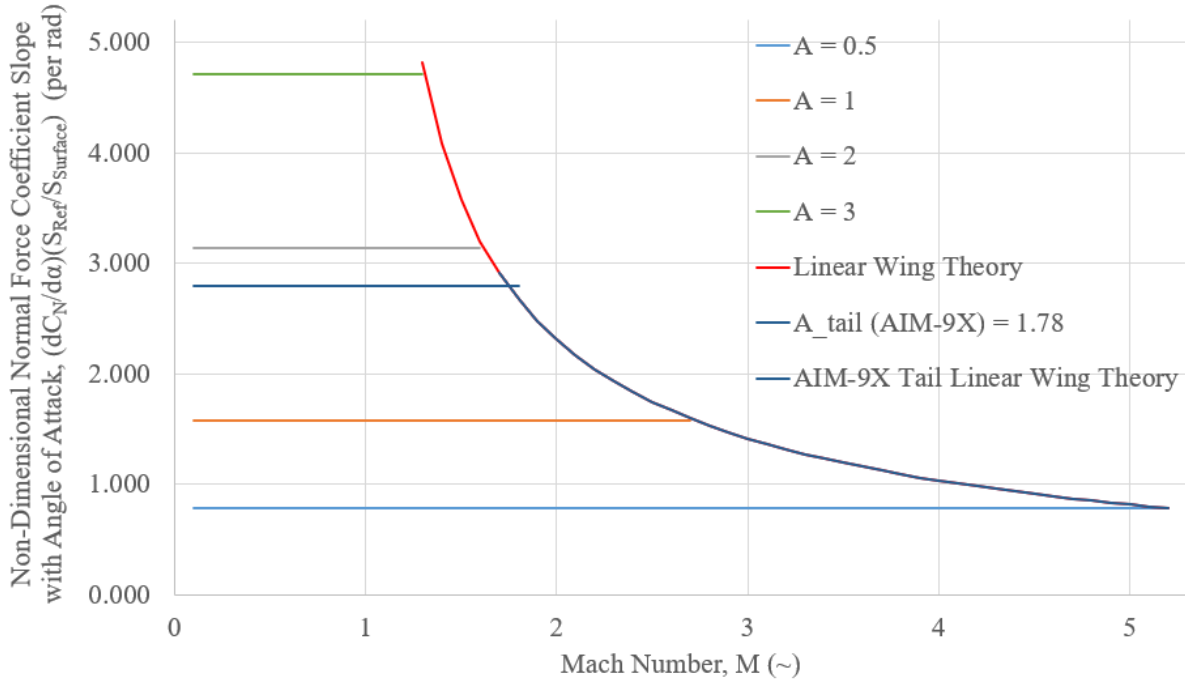


Figure 26: Non-Dimensional Normal Force Coefficient Slope with Angle of Attack vs. Mach Number Overlayed with Tail

In the use of linear wing theory, the non-dimensional normal force coefficient slope with angle of attack is independent of aspect ratio. This means that for the canard and tail at an engagement speed of Mach 2.5, which uses linear wing theory because the Mach number is above the Mach number which limits slender wing theory, the surface normal force coefficient is the same. Examining the above figures, the non-dimensional normal force coefficient slope with angle of attack of the tail and the canard of the AIM-9X Block II at Mach 2.5 is approximately 1.75.

7.2 Normal Force Coefficient Prediction of Surfaces

The normal force coefficient for a surface was calculated using Equation 29 if linear wing theory, i.e., the Mach number was greater than the Mach number calculated from Equation 28, and Newtonian impact theory were used.

$$|C_{N_{Surface}}| = \left(\frac{4|\sin\alpha' \cos\alpha'|}{\sqrt{M^2 - 1}} + 2\sin^2\alpha' \right) \left(\frac{S_{Surface}}{S_{Ref}} \right), M > \sqrt{\left\{ 1 + \left[\frac{8}{(\pi A)^2} \right] \right\}} \quad (29)$$



The other method the normal force coefficient for a surface was calculated was using Equation 30. This method was used if slender wing theory, i.e., the Mach number was less than the Mach number calculated from Equation 28, and Newtonian impact theory were used.

$$|C_{N_{Surface}}| = \left[\left(\frac{\pi A}{2} \right) |\sin \alpha' \cos \alpha'| + 2 \sin^2 \alpha' \right] \left(\frac{S_{Surface}}{S_{Ref}} \right), M < \sqrt{1 + \left[\frac{8}{(\pi A)^2} \right]} \quad (30)$$

For the baseline missile, the aspect ratio, reference area and wing surface area were again given in Ref. 10. The wing normal force coefficient was analyzed for three different Mach numbers (1.35, 2 and 5) at effective angles of attack from one degree to 90 degrees. Using Equation 29 and Equation 30, Fig. 2.26 from Ref. 10 was recreated. This figure is shown below in Figure 27.

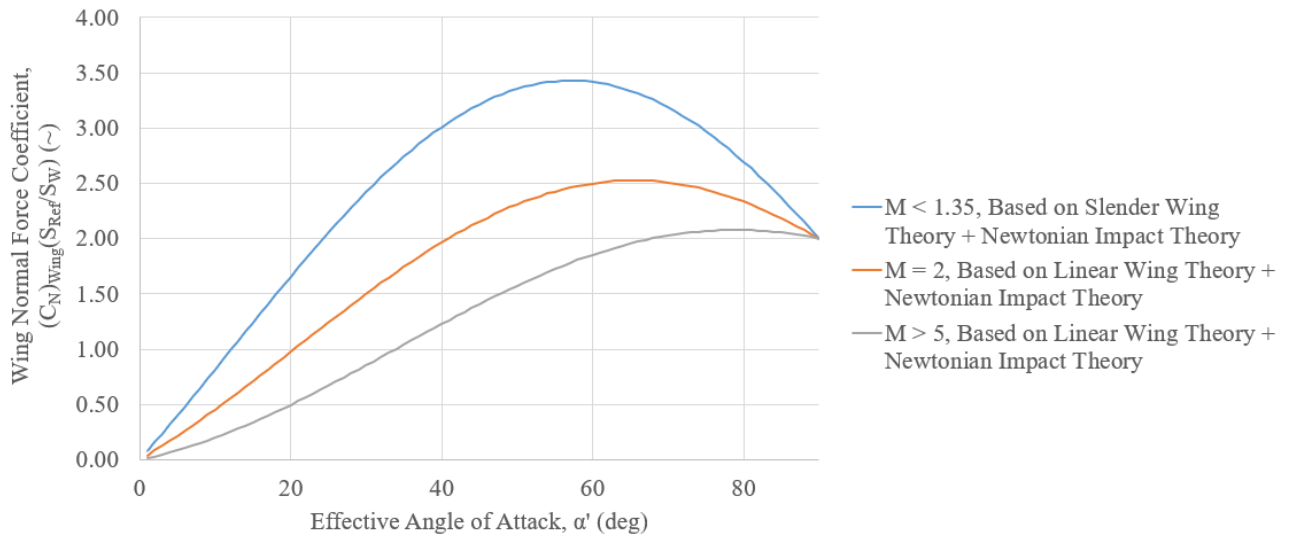


Figure 27: Wing Normal Force Coefficient vs. Effective Angle of Attack

The normal force for the canard and tail of the AIM-9X Block II were then analyzed for the same three Mach numbers and range of effective angle of attack. The aspect ratio, reference area and surface area for the canard and tail were calculated in Appendix D. The canard normal force coefficient for the AIM-9X Block II was then calculated using Equation 29 and Equation 30. The resulting normal force coefficient at various effective angles of attack was overlaid with the recreation of Fig. 2.26 from Ref. 10 in Figure 28 below.



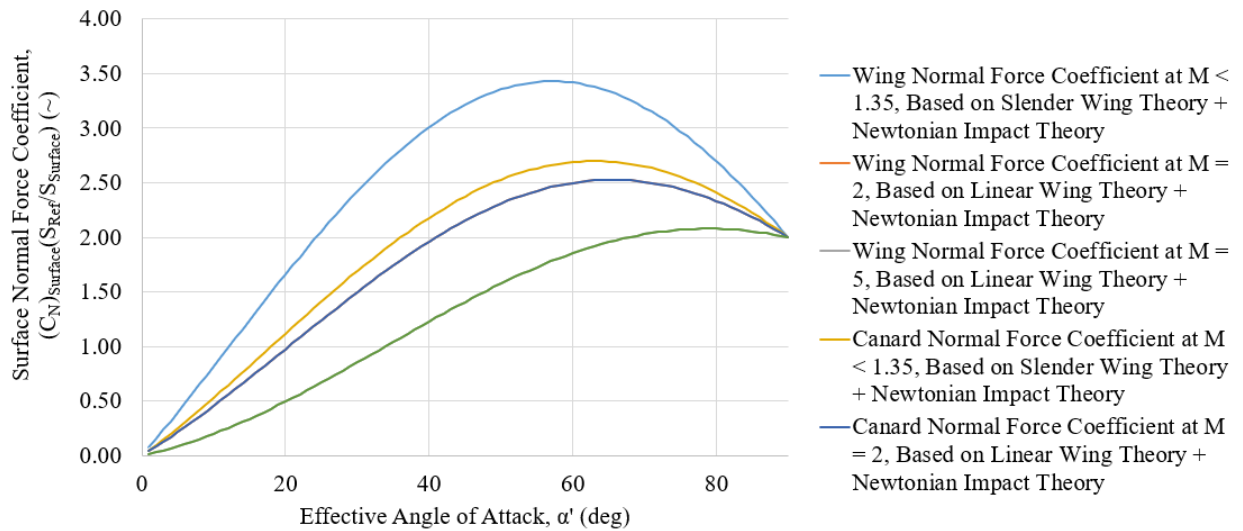


Figure 28: Surface Normal Force Coefficient vs. Effective Angle of Attack Overlaid with Canard of AIM-9X Block II

For Mach numbers where linear wing theory and Newtonian impact theory must be used the normal force coefficient for the canard is the same for that of the baseline missile from Ref. 10. This is again because Equation 29 is independent of aspect ratio. When slender wing theory and Newtonian impact theory was used, the normal force coefficient for the canard of the AIM-9X Block II was less than the baseline missile from Ref. 10.

The tail normal force coefficient for the AIM-9X Block II was also calculated using Equation 29 and Equation 30. The resulting normal coefficient at various angles of attack was overlaid with the recreation of Fig. 2.26 from Ref. 10 in Figure 29 below.



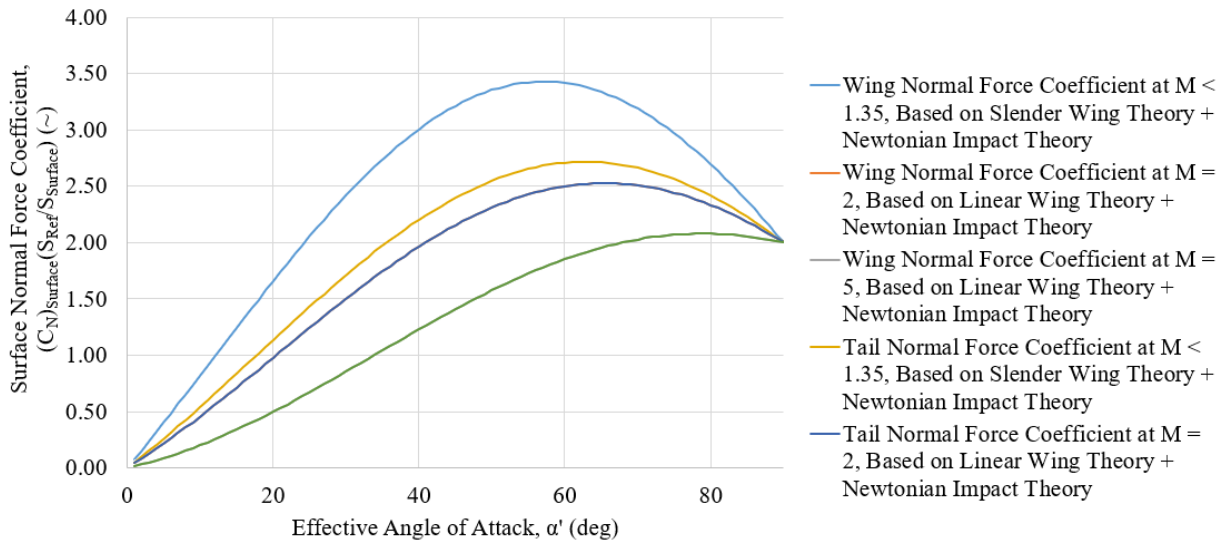


Figure 29: Surface Normal Force Coefficient vs. Effective Angle of Attack Overlaid with Tail of AIM-9X Block II

Again, for Mach numbers where linear wing theory and Newtonian impact theory must be used the normal force coefficient for the tail is again the same as the baseline missile. When slender wing theory and Newtonian impact theory was used, the normal force coefficient for the tail of the AIM-9X Block II was less than the baseline missile from Ref. 10, but about the same as the canard. This is because the tail and canard aspect ratios of the AIM-9X Block II are very similar. The normal force coefficient for the tail above the limit of slender wing theory and Newtonian impact theory is still the same as the baseline missile, since the equation is independent of the aspect ratio.

The total normal force coefficient for the AIM-9X Block II was also graphed against the local angle of attack. For this graph the canard was deflected five degrees upward and the tail was deflected two degrees down. The Mach number was a normal engagement speed of Mach 2.5. First the normal force coefficient for the body was calculated using Equation 31, where l/d is the fineness ratio, calculated prior in this report.

$$(C_N)_B = \sin(2\alpha) \cos\left(\frac{\alpha}{2}\right) + 1.3 \left(\frac{l}{d}\right) \sin^2 \alpha \quad (31)$$



The total normal force coefficient is the sum of the normal force coefficients of the control surfaces and the body. The equation for total normal force coefficient is shown below in Equation 32.

$$C_N = (C_N)_C + (C_N)_T + (C_N)_B \quad (32)$$

The normal force coefficients of the canard and tail were found by multiplying Equation 29 by the ratio of surface area to reference area. These normal force coefficients were found for angles of attack of one to 90 degrees. The total normal force coefficient of the AIM-9X Block II is plotted against local angle of attack below, in Figure 29. The dot below is the total normal force coefficient for a canard deflection of five degrees up and a tail deflection of two degrees down. The local angle of attack is 9.4 degrees, which is the same angle of attack assumed in the example in Ref. 10. The Mach number is the normal engagement speed of the AIM-9X Block II of Mach 2.5.

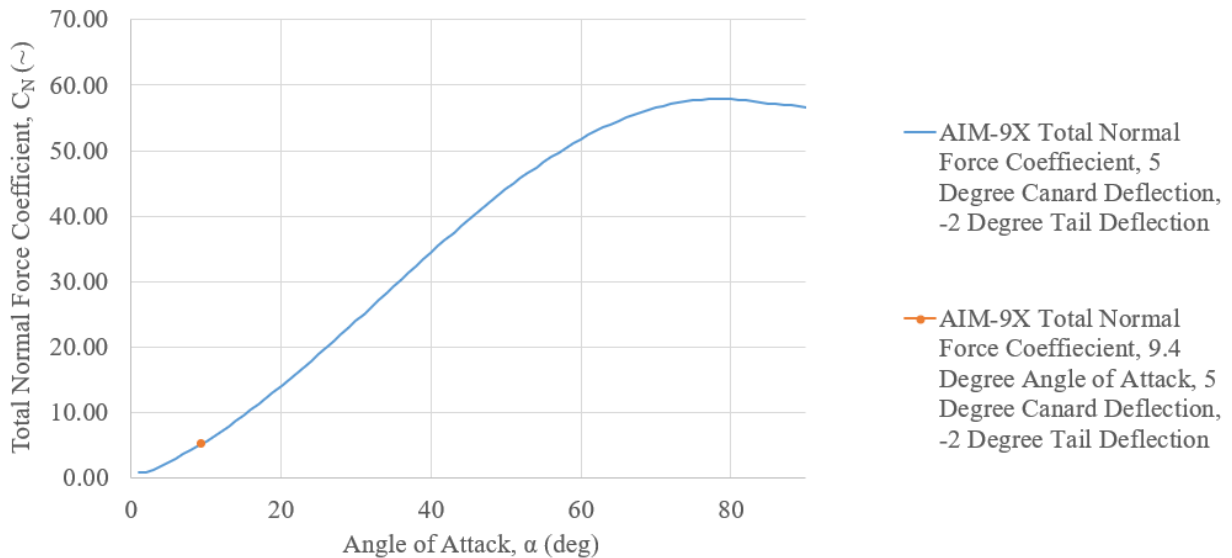


Figure 30: Total Normal Force Coefficient of the AIM-9X Block II vs. Local Angle of Attack

The total normal force coefficient of the AIM-9X Block II is 5.26 for a local angle of attack of 9.4 degrees, canard deflection of five degrees up and tail deflection of two degrees down at an engagement speed of Mach 2.5.



8 Aerodynamic Center Prediction for Planar Surfaces

This section predicts the change in aerodynamic centers of the AIM-9X front and aft planforms as Mach number increases. To predict the change in aerodynamic center, aspect ratio (AR) is needed for both the front and aft lifting surfaces. The baseline equation for the prediction of change is a function of AR and M, and can be seen below in Equation 33, per Ref. 10.

$$\frac{X_{AC}}{C_{mac}} = \frac{\left[A(M^2 - 1)^{\frac{1}{2}} - 0.67 \right]}{\left[2A(M^2 - 1)^{\frac{1}{2}} - 1 \right]} \quad (33)$$

This equation is only valid for Mach numbers greater than 2. For Mach numbers less than or around 0.7, the aerodynamic center is assumed to be at 25% of the mean geometric chord. Figure 31 below shows the diagram in change of aerodynamic center as Mach number increases from Fleeman’s text, Ref. 10.

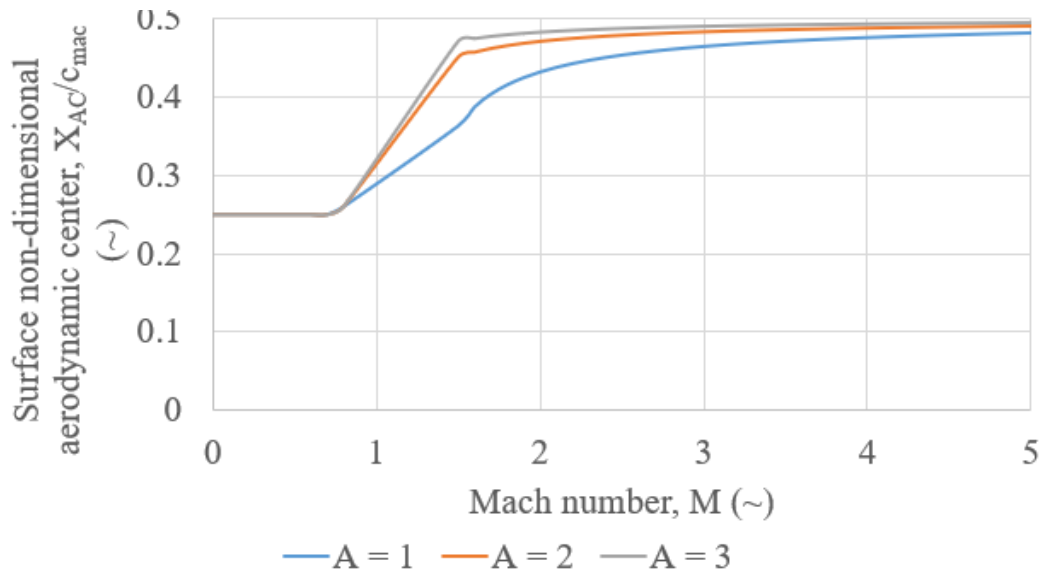


Figure 31: AC of Planar Surfaces vs. Mach Number (Fleeman)

It should be noted that due to the nature of the transonic region and the equations given, the area between Mach 0.8 and Mach 1.5 was approximated using Excel. To create the figure above for the AIM-9X, the aspect ratios of the front and aft planforms were calculated in Appendix D. For the front planform the aspect ratio was found to be 1.75 and the aft planform



was found to be 1.78. Figure 32 shows the AC shift of the front planform as Mach number increases.

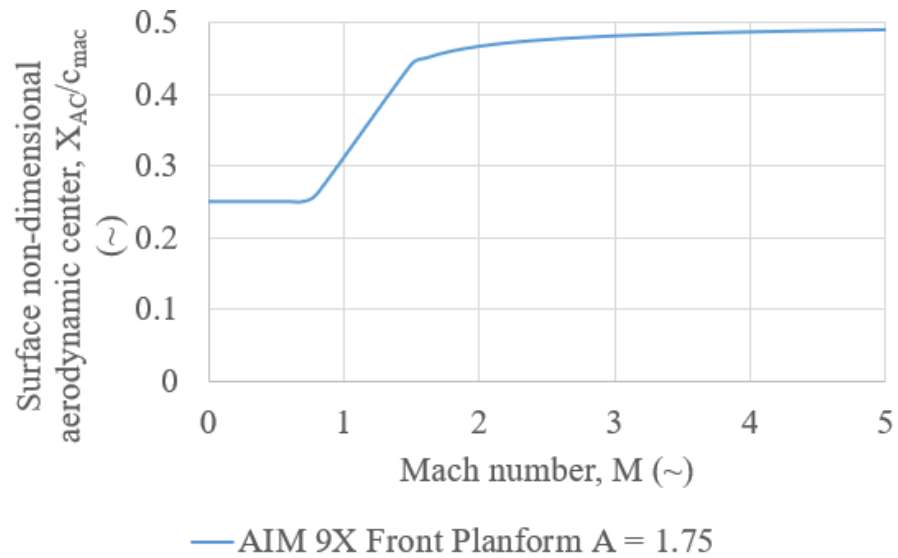


Figure 32: AC of Front Planform vs. Mach Number (AIM-9X)

Figure 33 shows the same graph, but with the aft planform aspect ratio.

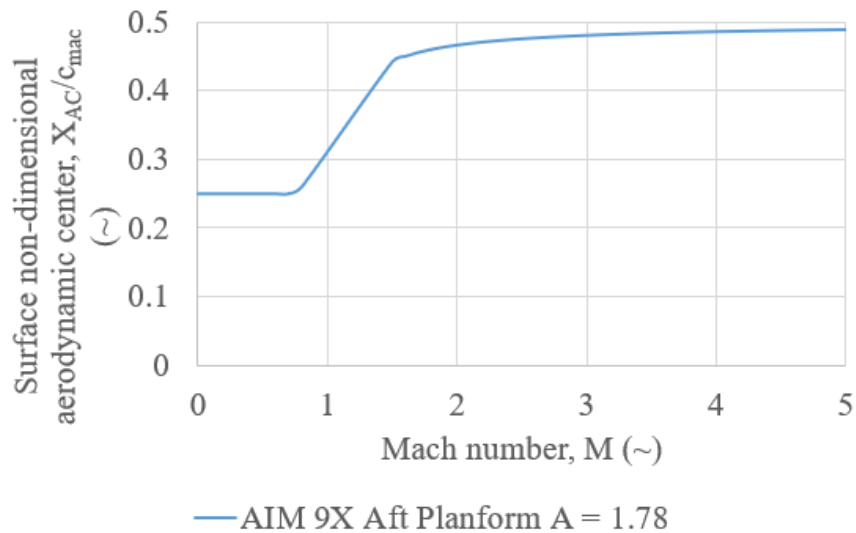


Figure 33: AC of Aft Planform vs. Mach Number (AIM-9X)



It should be noted that the aspect ratios of the front and aft planforms are very similar. This means that the AC shift is approximately the same. These were then overlayed shown in Figure 34.

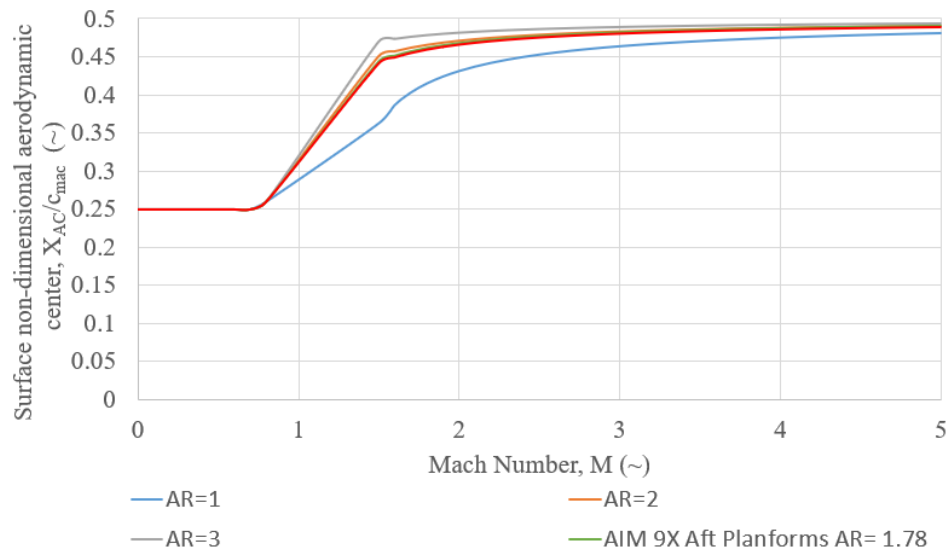


Figure 34: AC of Planar Surfaces vs. Mach Number

It should be noted that as Mach number increases, the AC moves back; however, it does not reach 50% of the mac. After inspecting Figure 34, the AC moves approximately 47% of the mac.



9 Hinge Moment Prediction

This section covers the hinge moment (HM) prediction for the baseline missile in Section 2.16 from Ref. 10 and for the AIM-9X Block II

9.1 Hinge Moment Prediction for Fleeman Missile

To predict the HM, figure 2.28 from Ref 10 was recreated in Excel. To recreate this figure, Ref. 10 uses the following missile geometry.

- $S_W = 2.55 \text{ ft}^2$
- $S_{Ref} = 0.349 \text{ ft}^2$
- $A_W = 2.82$
- $c_{mac} = 13.3 \text{ in}$
- $x_{HL} = 0.25$

To predict HM, the following equation was used.

$$HM = N_{Surface} * (x_{AC} - x_{HL})_{Surface} \quad (34)$$

It should be noted that $N_{Surface}$ must be calculated. This was done with Equation 35.

$$N_{Surface} = C_{N_{Surface}} * q * S_{Ref} \quad (35)$$

Also, x_{AC} and x_{HL} are normalized with respect to c_{mac} . Thus, Equation 34 is multiplied by c_{mac} . Since x_{AC} moves back at transonic and supersonic speeds, the x_{AC} needs to be found at each of the following Mach numbers:

- $M = 0.8$
- $M = 1.35$
- $M = 2$
- $M = 5$



To do this, figure 2.27 from Ref. 10 was recreated with Equation 33. This figure can be seen below in Figure 35.

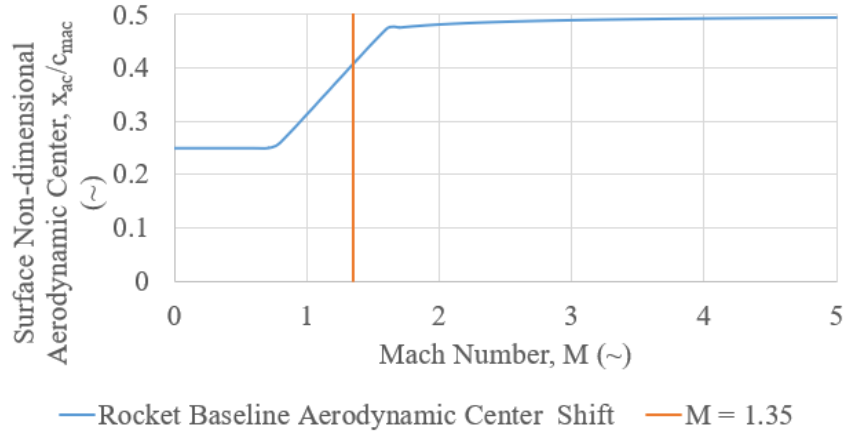


Figure 35: Aerodynamic Center of Fleeman's Example Rocket Shifts with Mach Number

Using Figure 35, as well as Equation 33, the following x_{AC} values were found.

- $x_{ac} = 0.26$ (when $M = 0.8$)
- $x_{ac} = 0.4$ (when $M = 1.35$)
- $x_{ac} = 0.48$ (when $M = 2$)
- $x_{ac} = 0.49$ (when $M = 5$)

It should be noted that since $x_{HL} = 0.25$, x_{ac} was assumed to shift back. If this was not done, the hinge line moment at $M = 0.8$, would be zero. Inspection of figure 2.28 in Ref. 10 shows that this moment is not zero. Thus, x_{ac} was assumed to be 0.26. After x_{ac} was calculated, $C_{N_{Surface}}$ was calculated using the same M values as above and the Equations 28, 29, and 30. Once this was done, $N_{Surface}$ was calculated using Equation 38 and the following dynamic pressures:

- $q = 436 \text{ psf}$ ($M = 0.8$)
- $q = 1242 \text{ psf}$ ($M = 1.35$)
- $q = 2725 \text{ psf}$ ($M = 2$)
- $q = 17,031 \text{ psf}$ ($M = 5$)



It should be noted that this dynamic pressure is at an altitude of 20,000 feet. After calculating $N_{Surface}$, HM was calculated using Equation 34. After this, Figure 2.28 from Ref. 10 was recreated using Excel and is shown below in Figure 36.

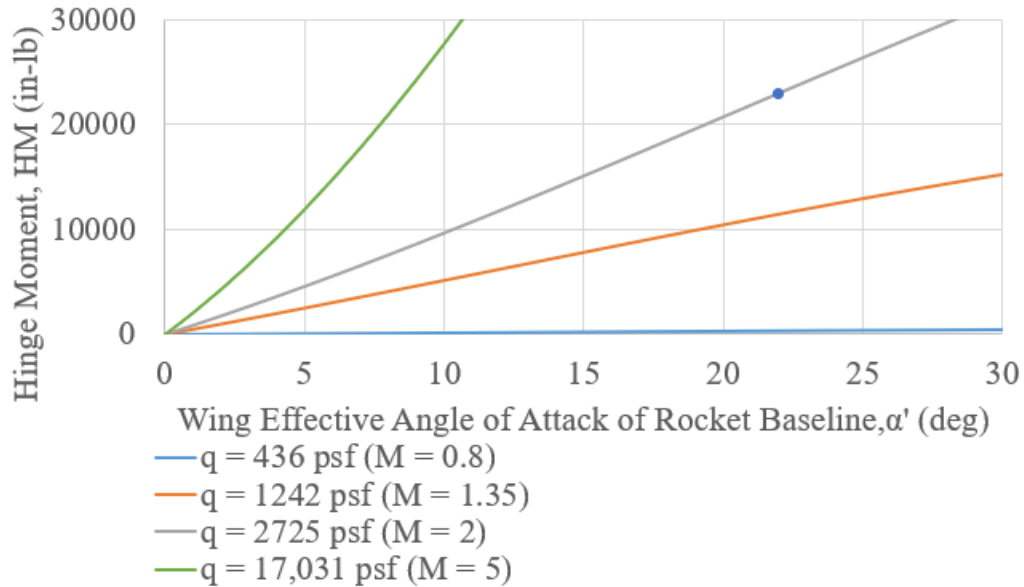


Figure 36: Figure 2.28 from Ref. 10 Recreated in Excel

Additionally, the baseline missile from Ref. 10 was added to this graph to confirm its validity. This was done using the geometry described above, when α' was 22 deg, when M was 2, and Equations 34 and 35. It yielded a HM of 23,000 lbf-in (2,600 N-m). It can be seen as the blue dot on Figure 36.

9.2 Hinge Moment Prediction for AIM-9X Block II

To predict the HM for the AIM-9X Block II, the tail surface was used. Even though the AIM-9X Block II does have canards on the front, these are fixed. Since these are fixed, no HM was calculated for the canards. To predict the HM for the tail, several salient characteristics were determined with Appendix D and Table 1. They can be seen below:



- $S_T = 92.39 \text{ in}^2$
- $S_{Ref} = 9.975 \text{ in}^2$
- $A_T = 1.778$
- $c_{mac} = 3.203 \text{ in}$
- $x_{HL} = 0.44$

Additionally, Equation 28 was used to calculate the limiting Mach number for slender wing theory for the AIM-9X Block II. This was found to be 1.75. C_{N_T} was then calculated at the same Mach numbers as Section 9.1 and Equations 29 and 30. Similarly, N_T was calculated using the same dynamic pressures as Section 9.1 and Equation 34. To predict HM, the following x_{AC} values were calculated using Equation 33 and estimated using Figure 33:

- $x_{AC} = 0.26$
- $x_{AC} = 0.41$
- $x_{AC} = 0.47$
- $x_{AC} = 0.49$

Lastly, HM was predicted using the x_{AC} values listed above, N_T , x_{HL} of the AIM-9X Block II, and the c_{mac} listed above. Figure 37 was then created in Excel.

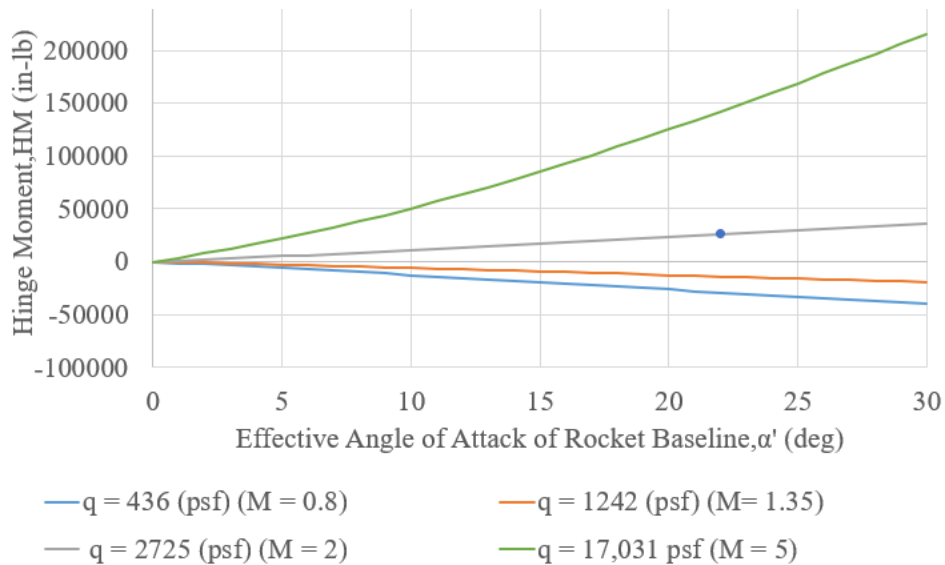


Figure 37: HM Prediction for the AIM-9X Block II at Different Mach Numbers and Dynamic Pressures



Additionally, the HM was calculated at an α' of 22 deg and a Mach number of 2. This yielded a HM of 26,200 lbf-in (2,960 N-m). This graph is very different from Figure 36. However, this makes sense as the hinge line location was much further back. This caused a negative hinge moment at Mach numbers below two. However, this makes sense for the AIM-9X Block II's mission. Since the AIM-9X Block II is a short to medium range missile, it needs to be fast and highly maneuverable at high speeds. To achieve this, the designers moved the hinge line further back along c_{mac} . This reduces the required hinge moment. However, this means that the missile is unstable at subsonic and low supersonic speeds. Upon inspecting Figure 33, the AIM-9X Block II tail's x_{ac} was determined to be the same as its x_{HL} when $M = 1.5$, approximately. This means that the missile is unstable below that Mach number. However, this is irrelevant for its mission, as it will not be operating below those speeds.



10 Planar Surface Drag Prediction

This section will discuss and predict the planar surface drag of the baseline missile from Section 2.17 of Ref. 10 and of the AIM-9X Block II.

10.1 Zero Lift Drag Coefficient Increase due to Increasing Planform Area

This section shows how the zero lift drag coefficient changes with respect to the ratio of surface area to reference area. The equation for this section was used from Ref. 10 and can be seen below.

$$(C_{D0})_{Surface,Friction} = n_{surface} \left[0.0133 \left(\frac{M}{qC_{mac}} \right)^{0.2} \right] \left(\frac{nS_{Surface}}{S_{Ref}} \right) \quad (36)$$

Below in Figure 38, Figure 2.29 from Ref. 10, shows the trend of how the zero lift drag increases linearly with an increase of the ratio of surface area to reference area.

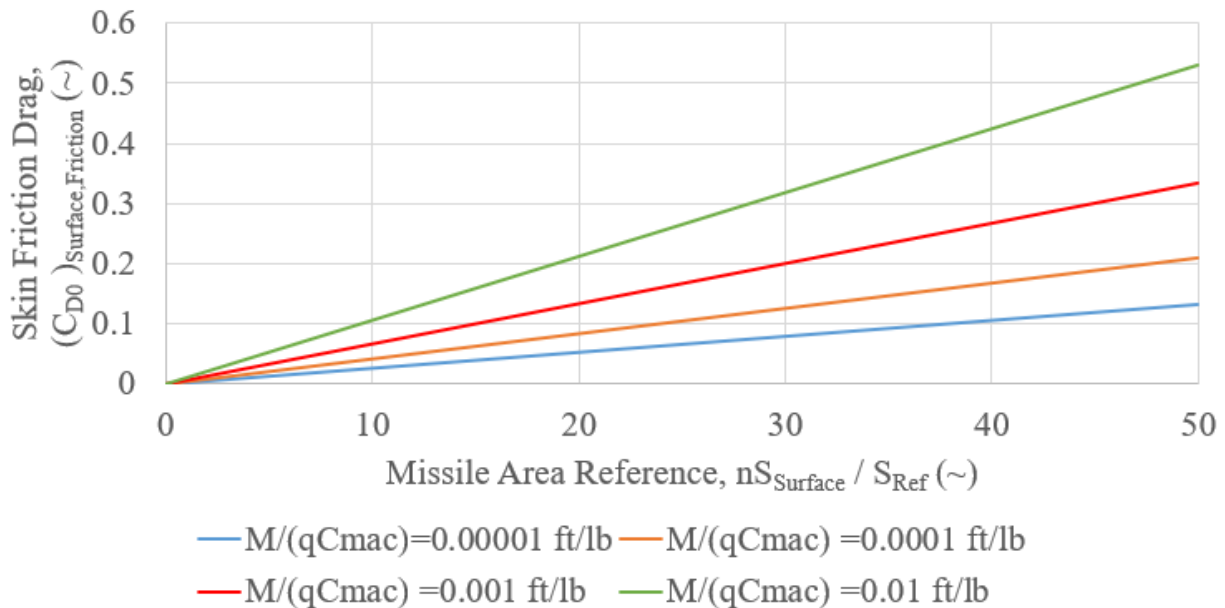


Figure 38: Skin Friction Drag vs. Missile Area Reference (Fleeman)

Since this equation is a function of surface area to reference area, the Mach number for the AIM-9X calculation was assumed to be 2.5. The altitude was assumed to be 20,000 ft, therefore the density was found using Ref. 11. The AIM-9X has 4 surfaces that were used for



analysis, and the surface and reference area were found from Appendix C. The calculation for finding the $\frac{M}{qC_{mac}}$ and the missile area reference values for the AIM-9X can be found in Appendix D. Below in Figure 39, the AIM-9X zero lift drag coefficient can be seen using the math from Appendix D.

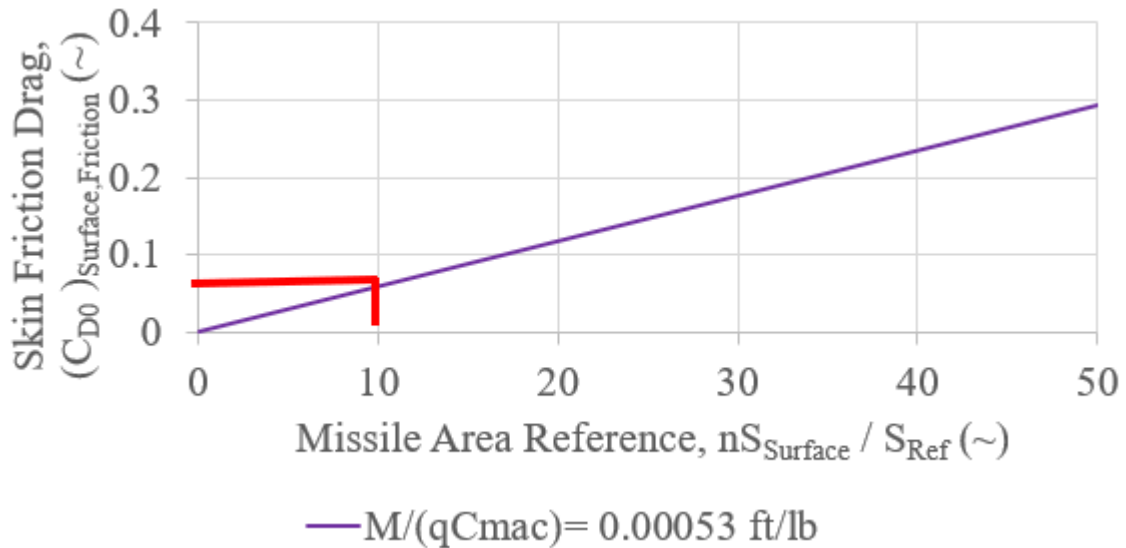


Figure 39: AIM 9X Zero Lift Drag from Planform Characteristics

Below in Figure 40, the AIM-9X zero Lift Drag trend in Figure 39 is compared to the reference missiles in Figure 38.

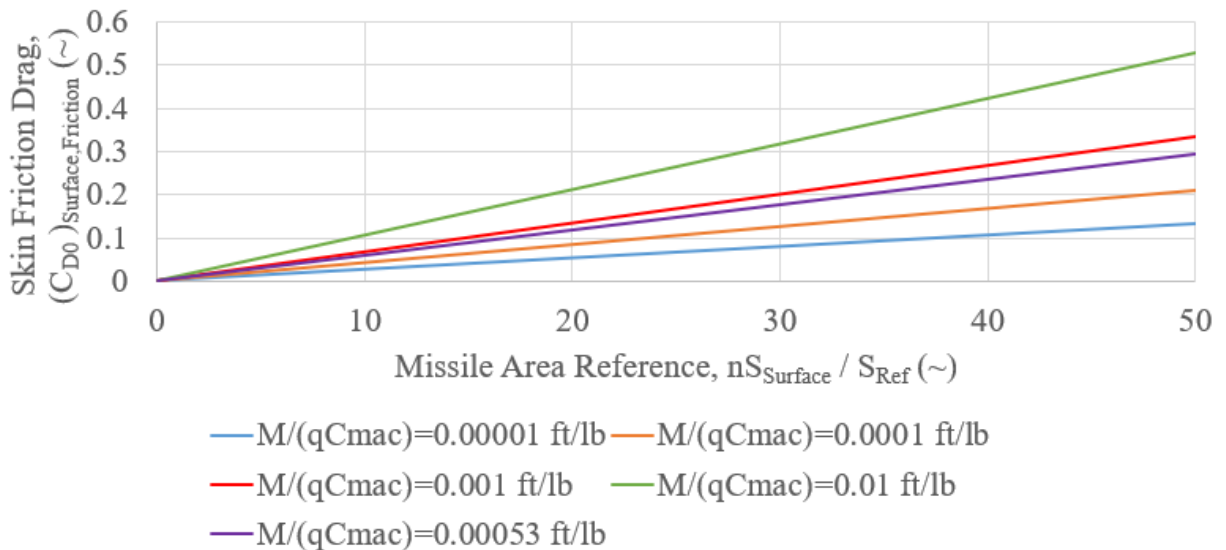


Figure 40: AIM 9X Zero Lift Drag Compared to Reference Missiles



10.2 Supersonic Drag of Planar Surfaces of AIM-9X

This section discusses the supersonic drag of planar surfaces for the baseline missile in Section 2.17 from Ref. 10 and for the AIM-9X Block II. From the Fleeman textbook (Ref. 10) Figure 2.30 was recreated using Equation 37 and Equation 38 below.

$$(C_{Do})_{Surface,Wave} = n_{Surface} \left(\frac{1.429}{(M_{\Lambda LE})^2} \right) \left\{ (1.2M_{\Lambda LE}^2)^{3.5} \left(\frac{2.4}{2.8M_{\Lambda LE}^2 - 0.4} \right)^{2.5} - 1 \right\} \left(\frac{\sin^2 \delta_{LE} \cos \Lambda_{LE} t_{mac} b}{S_{Ref}} \right) \quad (37)$$

$$M_{\Lambda LE} = M \cos \Lambda_{LE} \quad (38)$$

Figure 41 below shows the supersonic shock wave drag of the baseline missile with different leading edge section angles. This figure shows that the wave drag becomes smaller with a smaller leading edge section angle.

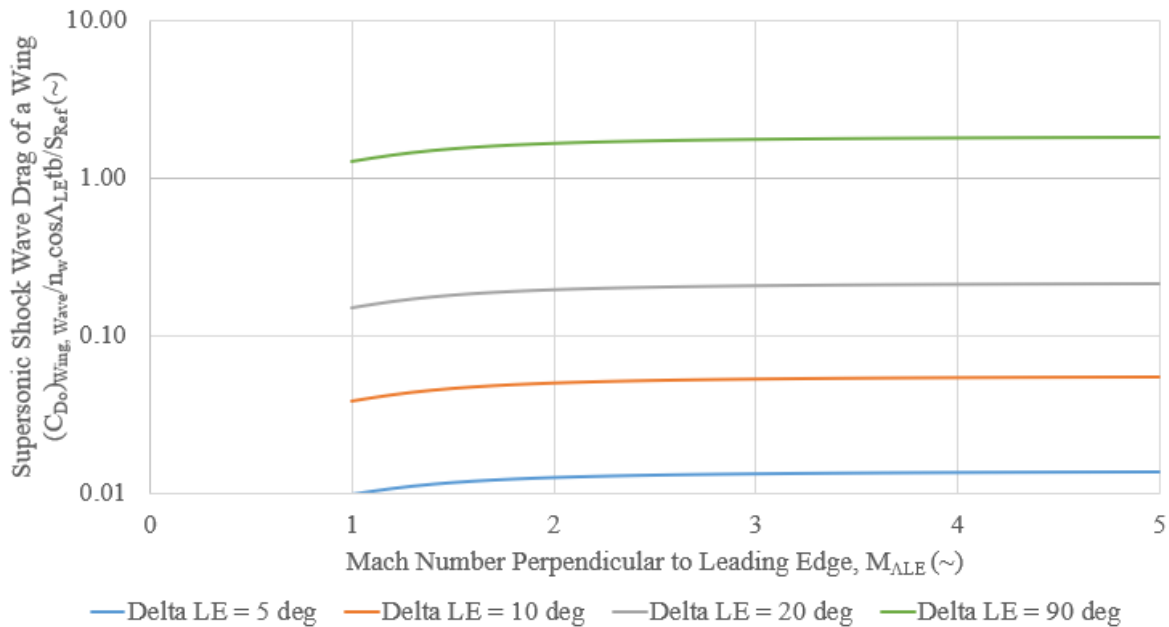


Figure 41: Planar Surface Wave Drag vs Mach Number Perpendicular to Leading Edge (Fleeman)

To calculate the planar surface wave drag of the AIM-9X, the span, sweep angle, thickness at the mean aerodynamic chord, and the leading edge section angle of the tail and



canard are needed. These necessary planar surface geometry values for the AIM-9X and their calculations were found using the figure in Appendix D. Using these values and Equation 37, the relationship between the wave drag of the planar surfaces on the AIM-9X and Mach number was plotted and is shown below in Figure 42:

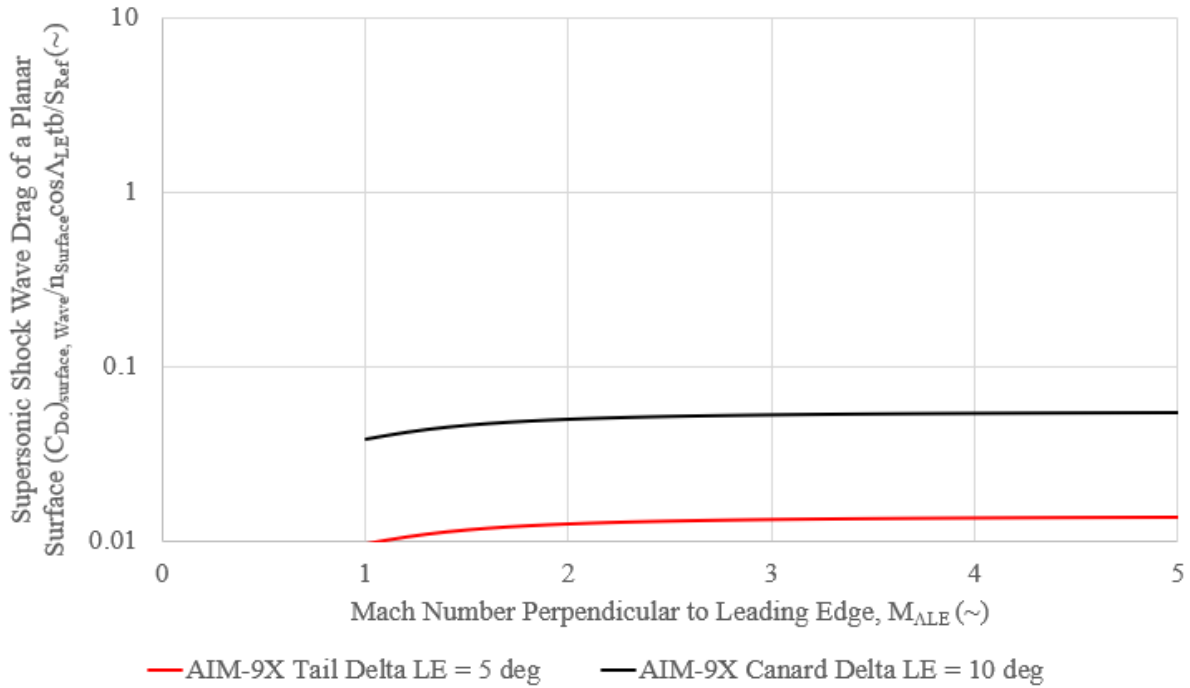


Figure 42: Planar Surface Wave Drag vs. Mach Number Perpendicular to Leading Edge (AIM-9X)

In Figure 43 below the AIM-9X planar surface wave drag is compared to the baseline missile planar surface wave drag from Ref. 10.



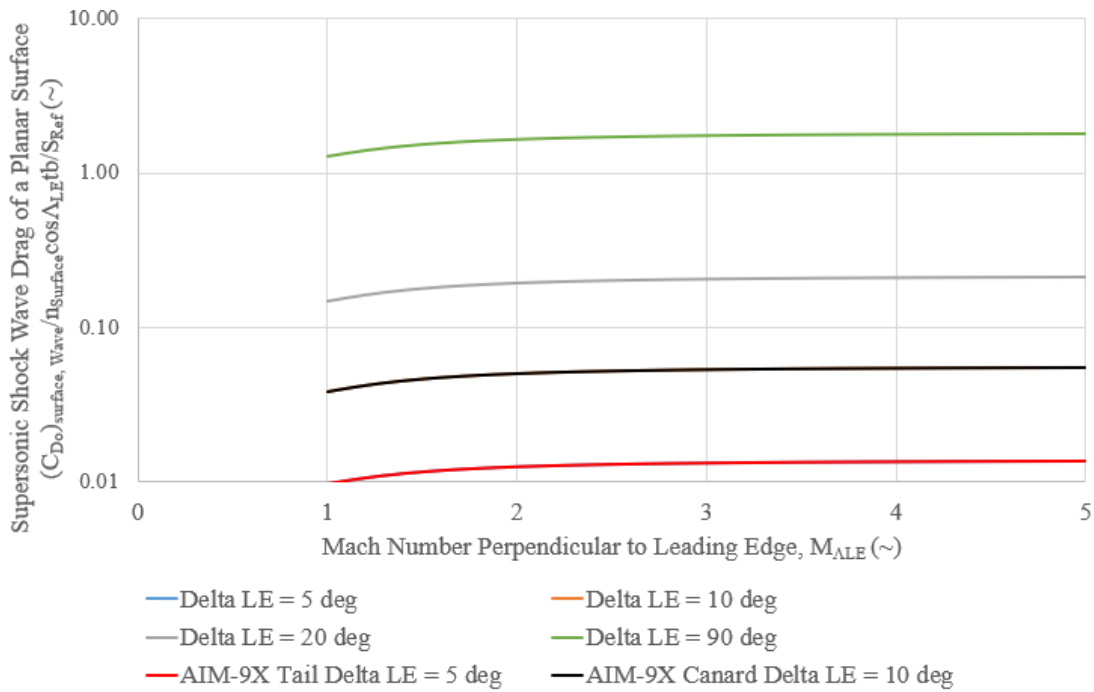


Figure 43: Planar Surface Wave Drag vs. Mach Number Perpendicular to Leading Edge (Fleeman and AIM-9X)

10.3 L/D of AIM 9X with Respect to Local Angle of Attack

This section discusses the L/D of the AIM 9X with respect to local angle of attack, α' . The equation for lift over drag, L/D, was used from Ref. 10 and can be seen below.

$$\frac{L}{D} = \frac{(C_N \cos(\alpha) - C_{D0} \sin(\alpha))}{(C_N \sin(\alpha) + C_{D0} \cos(\alpha))} \tag{39}$$

Since the airfoil used on the AIM 9X is thin, an assumption was made that $\alpha = \alpha'$. The zero lift drag coefficient, C_{D0} , was found in Section in 10.1 and was assumed constant at 0.11 (\sim). The normal force coefficient, C_N , was not assumed constant, but rather a function of α' , and the equation for C_N can be seen below, per Ref. 10.



$$C_N = \left\{ \frac{\pi A}{2} [\sin(\alpha') \cos(\alpha')] + 2 \sin^2(\alpha') \right\} \quad (40)$$

Using these equations, the L/D of the AIM 9X can be found. Below in Figure 44, Figure 2.31 from Ref. 10 was recreated. This figure shows the trend of L/D as α' increases.

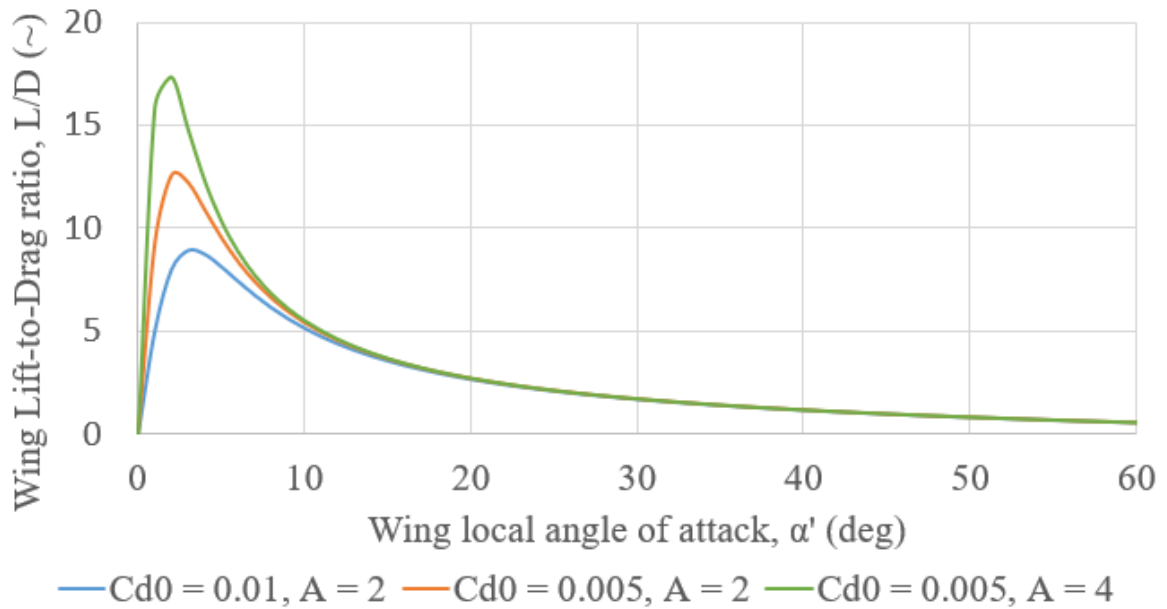


Figure 44: Lift to Drag Ratio vs. Local Angle of Attack (Fleeman)

Now using the zero lift drag coefficient, C_{D0} , of 0.11 (~) and the aspect ratio, A, of the tail of 1.78 (~), Figure 44 can be recreated for the AIM-9X missile and is seen below in Figure 45.



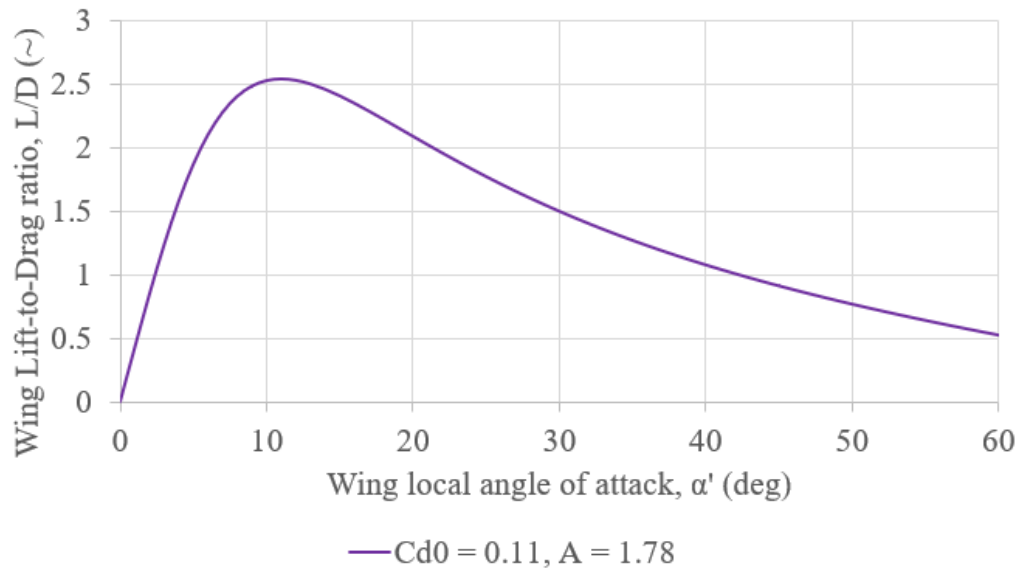


Figure 45: AIM 9X Lift to Drag Ratio vs. Local Angle of Attack

Figure 45 shows the L/D of the AIM 9X is roughly 75% smaller than that of the reference missiles found in Figure 44. This makes sense as the AIM 9X is an air-to-air missile that is designed for performance and not for high lift. Since the range on the AIM 9X is only 20 miles, high L/D is not the most important design parameter. Figure 46 below shows the AIM-9X L/D vs α' compared to the reference missiles.

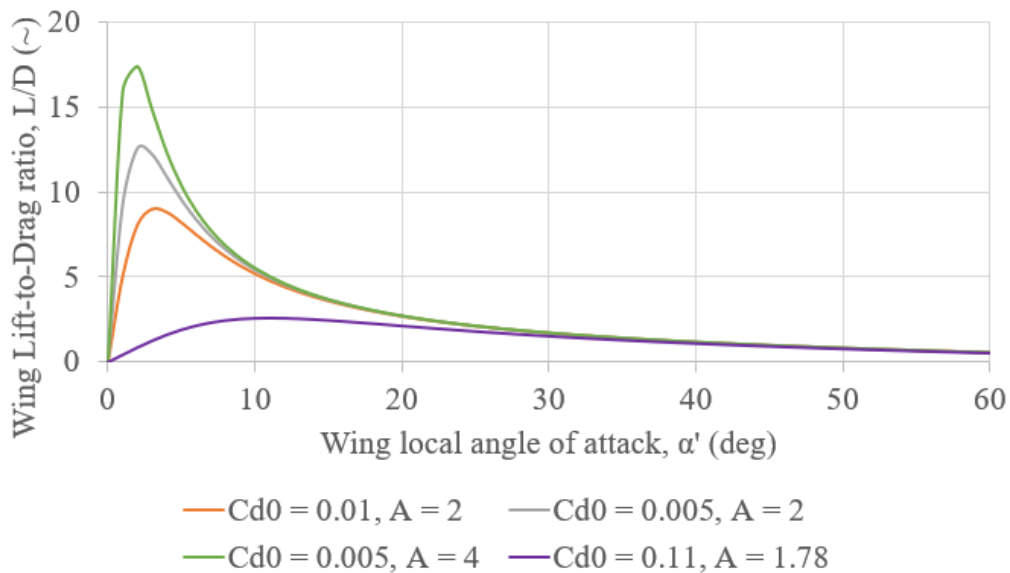


Figure 46: AIM 9X Lift to Drag Ratio vs. Local Angle of Attack Compared to Baseline Missiles



11 Surface Planform Geometry and Planform Alternatives

This section will outline the design of alternative planforms that could be used on the AIM-9X as seen in section 2.19 in Ref. 10. This section will specifically focus on the conceptual design of a lattice fin tail to replace the current traditional fin on the AIM-9. Lattice fins are used on several missiles and are especially desirable on tube-launched missiles due to their ability to be folded against the body of the missile for more compact storage and ease of transportation. This does come with the disadvantage of high drag at high subsonic, transonic, and low supersonic speeds, however.

When designing a grid fin for the RAIDER AIM-9, the authors chose a relatively large t/h ratio to account for the high g 's that the missile will need to pull to maintain its high off boresight capabilities. For the design, the authors chose a cell height of 0.75 inches and a cell wall thickness of 0.06 inches. This gives a t/h ratio of 0.08. This conceptual geometry can be seen below in Figure 47:

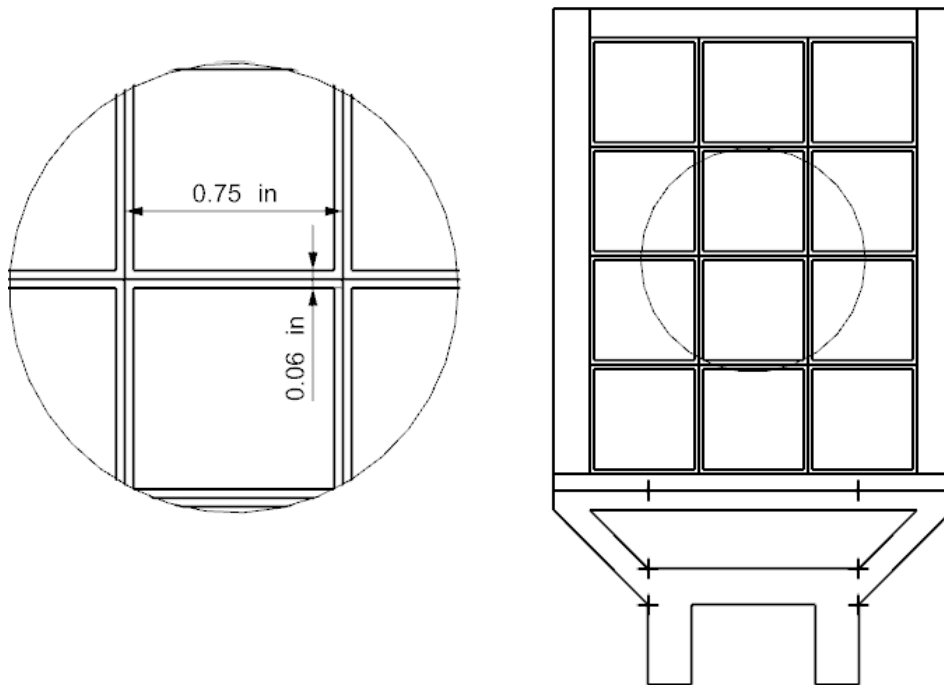


Figure 47: RAIDER AIM-9 Grid Fin with Detailed View

The comparison of this grid fin design to Figure 2.42 in Ref. 10 can be seen below in

Figure 48:

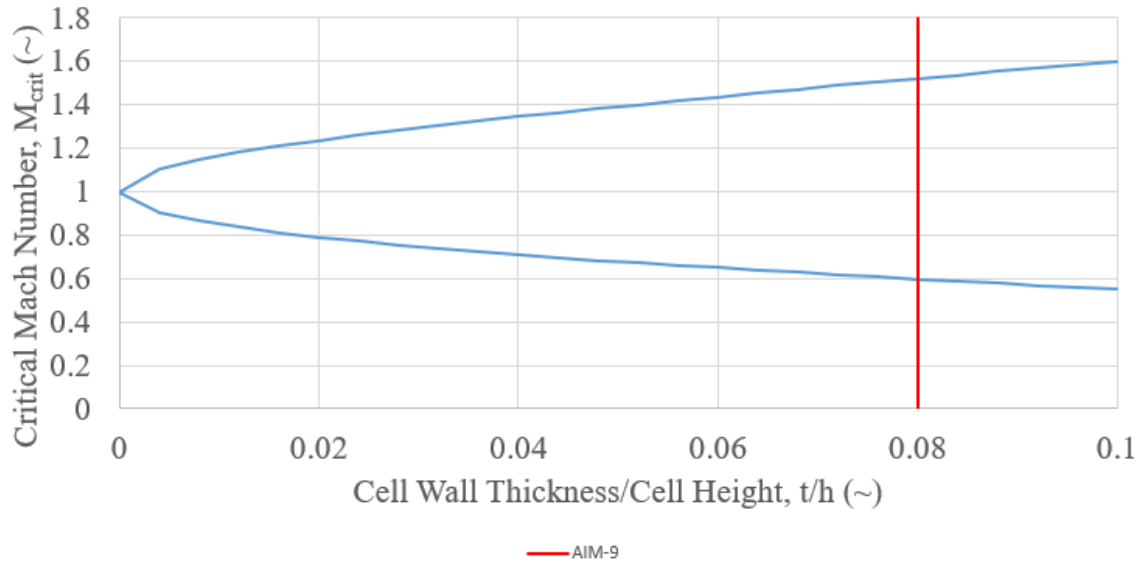


Figure 48: Critical Mach Number vs. Cell Geometry with AIM-9 RAIDER Grid Fin Geometry

As seen above, this grid fin geometry results in critical Mach numbers of roughly 0.6 and 1.5. Because of the top speed of the AIM-9 being around Mach 2.5, this may be unfavorable as much of the flight could be within the region of the critical Mach numbers, resulting in high drag and reduced performance of the RAIDER AIM-9X.

12 Tail Area Sizing

This section will estimate the required tail area for stability given a specified static margin. From (Ref. 10), Equation 41 is presented to find static margin for a specified tail area.

$$\frac{X_{AC} - X_{CG}}{d} = \left\{ -(C_{N\alpha})_B \frac{(X_{cg} - (X_{AC})_B)}{d} + (C_{N\alpha})_W \frac{(X_{cg} - (X_{AC})_W)}{d} \left(\frac{S_W}{S_{ref}} \right) + \left((C_{N\alpha})_T * \frac{(X_{CG} - (X_{AC})_T)}{d} \right) \left(\frac{S_T}{S_{ref}} \right) \right\} / \left\{ (C_{N\alpha})_B + (C_{N\alpha})_W \left(\frac{S_W}{S_{ref}} \right) + (C_{N\alpha})_T \left(\frac{S_T}{S_{ref}} \right) \right\} \quad (41)$$

Rearranging this equation, simplifying using the assumptions presented that $X_{AC}=X_{CG}$ and normalizing with l instead of d , gives Equation 42.

$$\frac{S_T}{S_{ref}} = \frac{\left((C_{N\alpha})_B \frac{(X_{cg} - (X_{AC})_B)}{l} \right) - (C_{N\alpha})_W \frac{(X_{cg} - (X_{AC})_W)}{l} \left(\frac{S_W}{S_{ref}} \right)}{(C_{N\alpha})_T \frac{(X_{CG} - (X_{AC})_T)}{l}} \quad (42)$$

Knowing that the static margin is defined as Equation 43, we can further reduce Equation 42 into Equation 44 that will be used to re-create Figure 2.60 from Fleeman 2.60.

$$SM = \frac{(X_{cg} - (X_{AC})_W)}{l} \left(\frac{S_W}{S_{ref}} \right) \quad (43)$$

$$\frac{S_T}{S_{ref}} = \frac{\left((C_{N\alpha})_B \frac{(X_{cg} - (X_{AC})_B)}{l} \right) - (C_{N\alpha})_W * SM}{(C_{N\alpha})_T \frac{(X_{CG} - (X_{AC})_T)}{l}} \quad (44)$$

The result of plotting Equation 44 for the baseline missile is shown in Figure 49.



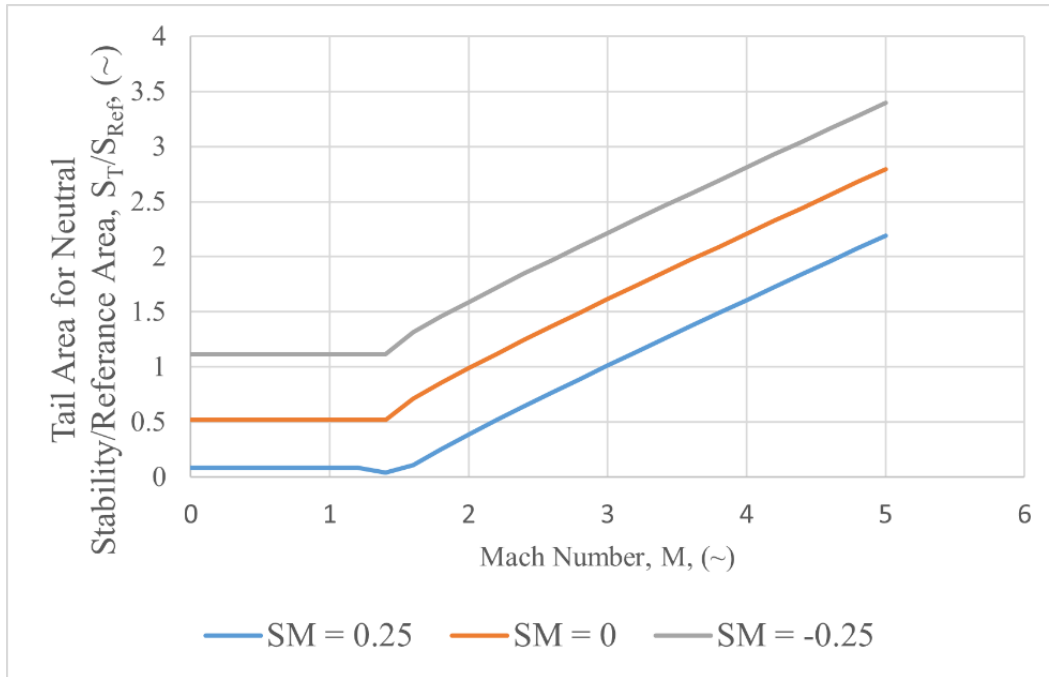


Figure 49: Tail Area for Stability Given SM, Baseline Missile

Equation 44 will be utilized to generate a similar plot for the AIM-9X assuming a full and empty fuel load that will shift the CG location of the missile. CG locations were estimated using a CAD model and finding COM with and without the fuel present in the model. The AC location of the tail was assumed to be consistent with the findings in Section 8. The results of these calculations are shown below in Figure 50 Figure 51.



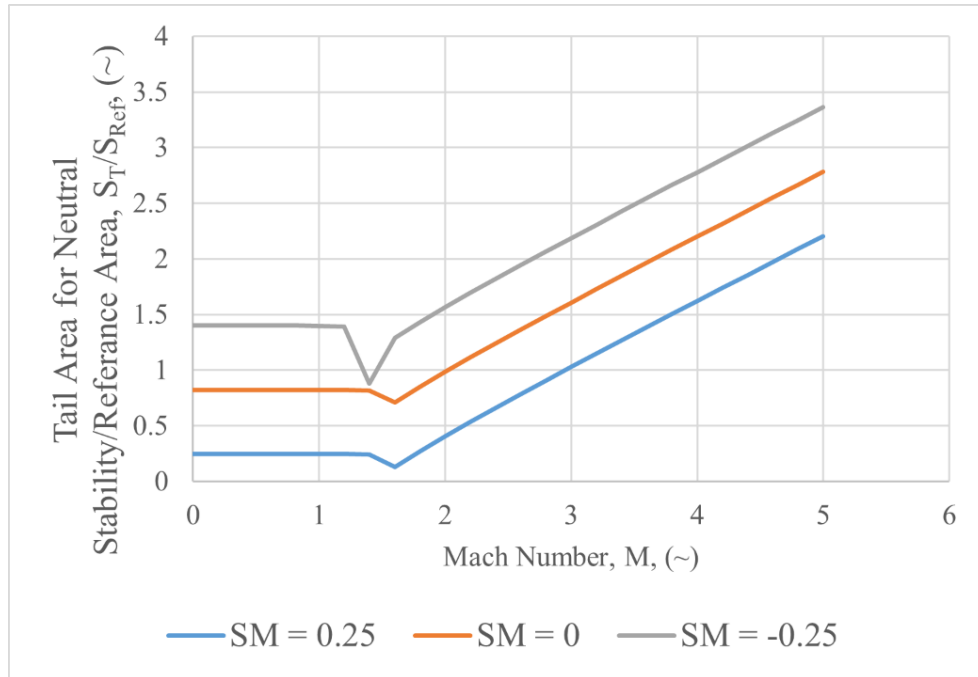


Figure 50: Tail Area for Stability Given SM, AIM-9X Full Fuel

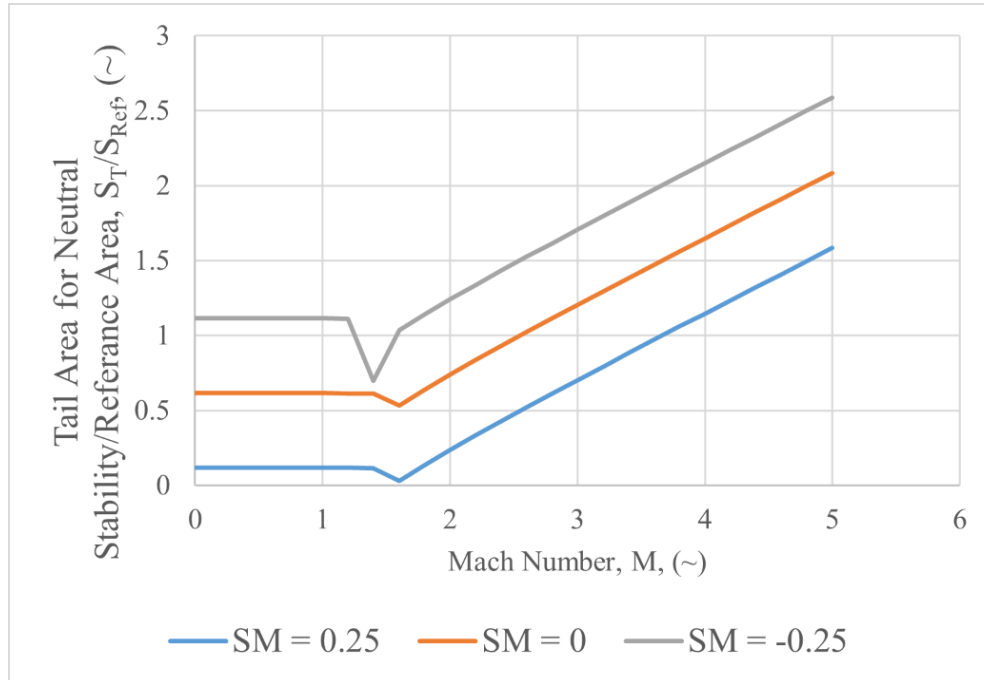


Figure 51: Tail Area for Stability Given SM, AIM-9X Empty Fuel



13 Aerodynamic Configuration Buildup

This section covers the aerodynamic buildup of the AIM-9X Block II. The total normal force coefficient and its components will be presented.

13.1 Normal Force Coefficient Build Up

The total normal force coefficient is calculated using Equation 32 from Section 7.2. The total normal force coefficient and the contributions from the canard, tail, and body of the AIM-9X Block II can be seen below in Figure 52:

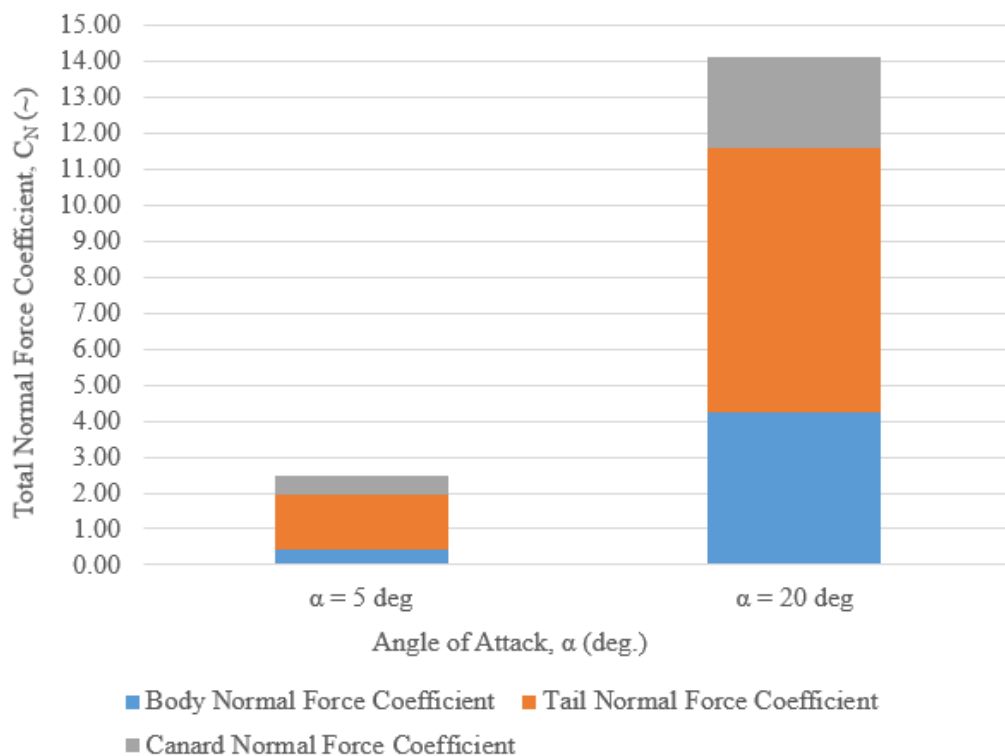


Figure 52: AIM-9X Block II Normal Force Coefficient Build Up

It can be seen above that the total normal force coefficient at a higher angle of attack (20 degrees) is much greater than at a low angle of attack (5 degrees). The total normal force coefficient at five degrees angle of attack is about 2.5 and the normal force coefficient at 20 degrees angle of attack is about 14. In both cases, the biggest contribution comes from the tail of the missile. The tail is 60% of the total normal force at a low angle of attack and about 50% at a high angle of attack. This makes sense and the canards and body cross section are relatively small compared to the tail.



14 Reverse Engineering of Baseline System

This section covers the reverse engineering of the AIM-9X Block II missile.

14.1 Baseline Missile Data

The baseline missile data used for the reverse engineering is displayed below in Table 5.

Table 5: Reverse Engineering Baseline Missile Data (Ref. 1, Ref. 6, Ref. 19)

Length	9.92 ft (3.02 m)
Canard Span	0.62 ft (0.19 m)
Finspan	1.16 ft (0.35 m)
Diameter	0.42 ft (0.13 m)
Weight	191 lbs (86.6 kg)
Speed	Mach 2.5
Range	20 mi (32.2 km)
Propulsion	Mk 36 Rocket Engine
Warhead	21 lbs (9.4 kg) WDU-17/B annular blast fragmentation
Max. Thrust	4,000 lbf

This data will be used in the subsequent sections to reverse engineer other characteristics about the AIM-9X Block II.

14.2 Design Mission Profile

The mission profile has been constructed from the baseline data found and summarized in Section 14.1. The mission profile is shown in Figure 53 below.

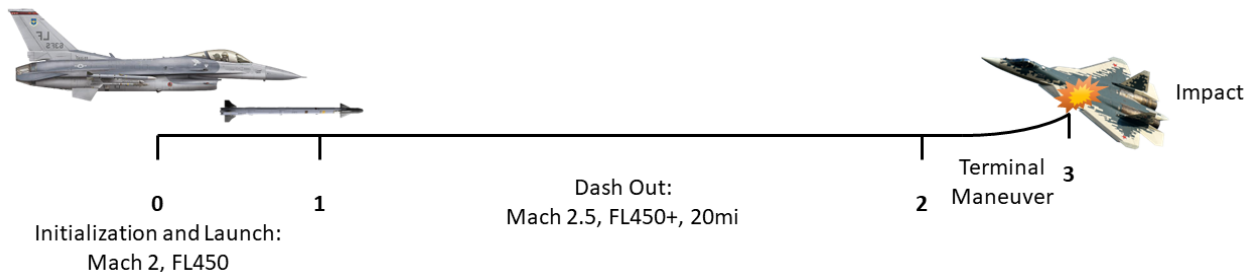


Figure 53: AIM-9X Mission Profile (Ref. 20, Ref. 21)

14.3 Payload Range Diagram

The payload range diagram for the AIM-9X Block II is shown below in Figure 54.

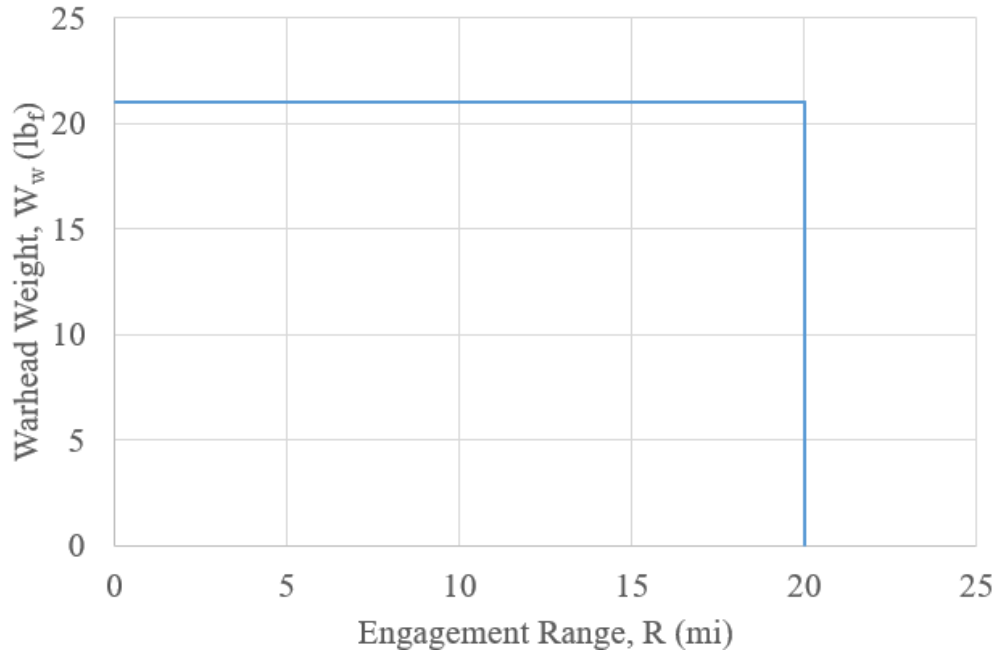


Figure 54: Payload Range Diagram

The payload for the AIM-9X Block II is 21 pounds for its entire range profile. There is only one payload used and it is used independent of engagement range.

14.4 Propellant Weight

To estimate the propellant weight, the calculation in Appendix B was updated to reflect a new given density, ρ_{new} , of 0.058 lb/in³. The density ratio used to update the calculation can be shown below in Equation 45, where ρ_{old} is the original assumed density of 0.1 lb/in³.

$$\sigma = \frac{\rho_{new}}{\rho_{old}} \quad (45)$$

The new weight of the propellant, $W_{fuel,new}$, can be found by Equation 46 below, where W_{fuel} was the calculated fuel in Appendix B.

$$W_{fuel,new} = W_{fuel} * \sigma = 123.7 \text{ lbs} * \frac{.058 \frac{\text{lb}}{\text{in}^3}}{.1 \frac{\text{lb}}{\text{in}^3}} = 71.75 \text{ lbs} \quad (46)$$



14.5 Approximation of I_{sp} and Thrust Specific Fuel Consumption (TSFC)

An estimate of I_{sp} was provided to the authors at 265s. TSFC can be calculated using Equation 47 as shown below from Ref. 22.

$$TSFC = \frac{\dot{W}_f}{T} = \frac{1}{I_{sp}} \quad (47)$$

$$TSFC = \frac{1}{265s} * \frac{3600s}{hr} = 13.6 \frac{lbf}{lbf-hr} \quad (48)$$

14.6 Estimation of Time of Flight

Time of flight (TOF) can be estimated using TSFC and the known motor thrust. The equation to estimate TOF with the engine at max thrust is shown below in Equation 49 and Equation 50 from Ref. 22.

$$TOF = \frac{\Delta W_f}{T * TSFC} \quad (49)$$

$$TOF = \frac{71.75lbf}{4,000lbf * 13.6 \frac{lbf}{lbf-hr}} * \frac{3600s}{1hr} = 4.75s \quad (50)$$

Estimated TOF is shown to be 4.75s.

14.7 Mission Profile with Derived Values

To construct an updated mission profile, additional values were to be calculated. The time to accelerate from the launch velocity to the dash velocity was calculated as shown in Equation 51 using an assumed launch velocity of Mach 2.0.

$$\Delta t = \frac{\Delta V}{a} = \frac{V_{dash} - V_{launch}}{T/m} = \frac{2420ft/s - 1936ft/s}{\left(\frac{4,000lbf}{191lb/32.2ft/s}\right)} = 0.72s \quad (51)$$

Range was then calculated for the acceleration phase as shown in Equation 52.

$$Range_{accel} = V_{avg} * t_{accel} = \frac{2420 + 1936}{2} * 0.72s = 1563ft = 0.30mi \quad (52)$$

Dash range was found simply by subtracting the acceleration range from the known total range of the AIM-9X. Time of flight during the dash phase was calculated as shown in Equation 53.



$$TOF_{dash} = \frac{Range_{dash}}{V_{dash}} = \frac{19.7mi * 5280ft/mi}{2420ft/s} = 43.0s \quad (53)$$

The remaining fuel weight during the dash phase was calculated as shown in Equation 54.

$$W_{f_{dash}} = W_f - \left(t_{accel} * \frac{W_f}{TOF} \right) = 71.75lbf - \left(0.72s * \frac{71.75lbf}{4.75s} \right) = 61lbf \quad (54)$$

The thrust required in the dash was calculated as shown in Equation 55.

$$T_{dash} = I_{sp} * \frac{W_{f_{dash}}}{TOF_{dash}} = 265s * \frac{61lbf}{43s} = 376lbf \quad (55)$$

The results of all these calculations are summarized in the updated mission profile, shown in Figure 55.

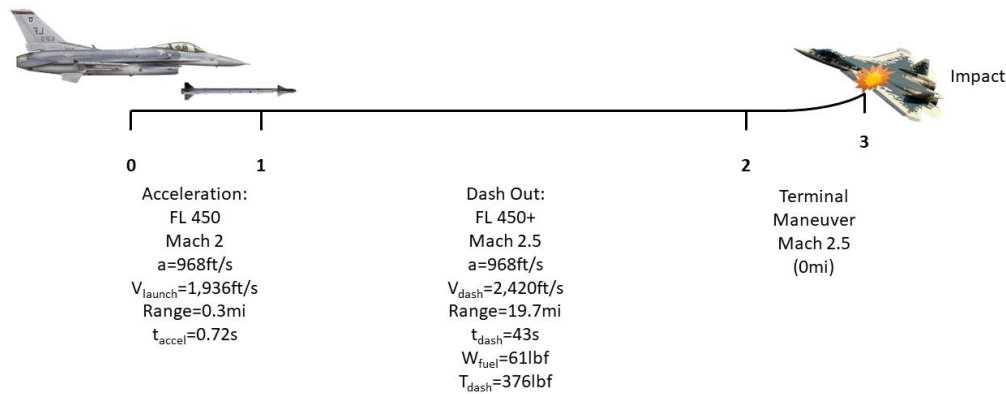


Figure 55: Updated Mission Profile

14.8 Mission L/D

L/D for the dash segment is estimated assuming that wave drag dominates, and that the thrust will be equal to the drag during this phase of flight. We assume that the weight during the dash phase is the weight of the full fuel load missile minus the average. The resultant calculation is shown in Equation 56.

$$\frac{L}{D} = \frac{W_{missile} - (W_f - W_{f_{dash}})}{T_{dash}} = \frac{191lb - (71.75lbf - 61lbf)}{376lbf} = 0.48 \quad (56)$$

14.9 Empty Weight Ratio

Empty weight ratio was calculated using Equation 57.



$$\frac{W_e}{W_{launch}} = \frac{(W_{launch} - W_{warhead} - W_{propellant})}{W_{launch}} = \frac{191 - 21 - 71.75}{191} = 51\% \quad (57)$$

14.10 Lift and Drag Expressions with Mach

To plot the lift and drag expressions with respect to Mach number, C_{D_0} was found using Equation 58 taken from Ref. 22.

$$C_{D_0}(\alpha, M) = C_{D_{o,body}}(\alpha, M) + C_{D_{o,surface,friction}}(\alpha, M) + C_{D_{o,surface,wave}} \quad (58)$$

In the equation above, $C_{D_{o,body}}(\alpha, M)$, $C_{D_{o,surface,friction}}(\alpha, M)$ and $C_{D_{o,surface,wave}}(\alpha, M)$ were calculated using Equation 7, Equation 36 and Equation 37 respectively. The density and other atmospheric data used to calculate the dynamic pressure used in the previous equations was taken from Ref. 11 at an altitude of 45,000 ft. The Mach number for Equation 7, Equation 36 and Equation 37 was assumed to be 2.5. The normal force coefficient was calculated using Equation 59 below taken from Ref. 22.

$$C_N(\alpha, M) = C_{N_{body}}(\alpha, M) + C_{N_{canard}}(\alpha, M) + C_{N_{tail}}(\alpha, M) \quad (59)$$

In the equation above $C_{N_{body}}(\alpha, M)$ was calculated using Equation 14 and $C_{N_{canard}}(\alpha, M)$ and $C_{N_{tail}}(\alpha, M)$ were calculated by taking the $dC_N/d\alpha$ of the surface found from Equation 26 and multiplying it by the angle of attack. Now with C_{D_0} and the normal force coefficient, the coefficient of drag was found using Equation 60 below from Ref. 10.

$$C_D = C_N \sin(\alpha) + C_{D_0} \cos(\alpha) \quad (60)$$

The axial force coefficient, C_A , was found using Equation 61 taken from Ref. 22.

$$C_A(\alpha, M) = \frac{C_D(\alpha, M) - C_N(\alpha, M) \sin(\alpha)}{\cos(\alpha)} \quad (61)$$

Then the coefficient of lift, C_L , was found using Equation 62 taken from Ref. 22.

$$C_L(\alpha, M) = C_N(\alpha, M) \cos(\alpha) - \left(\frac{C_D(\alpha, M) - C_N(\alpha, M) \sin(\alpha)}{\cos(\alpha)} \right) \sin(\alpha) \quad (62)$$

The lift-to-drag ratio, L/D , was found via Equation 63.

$$\frac{L}{D} = \frac{C_L}{C_D} \quad (63)$$

Knowing the expressions for C_N , C_A , C_L , C_D and L/D , their trends can be plotted for a certain Mach number and angle of attack range. The first relevant Mach number was Mach 2.5,



as was assumed above, and the range for the angle of attack was from zero to 12 degrees. The trends for the coefficients and L/D for these conditions can be seen below in Figure 56.

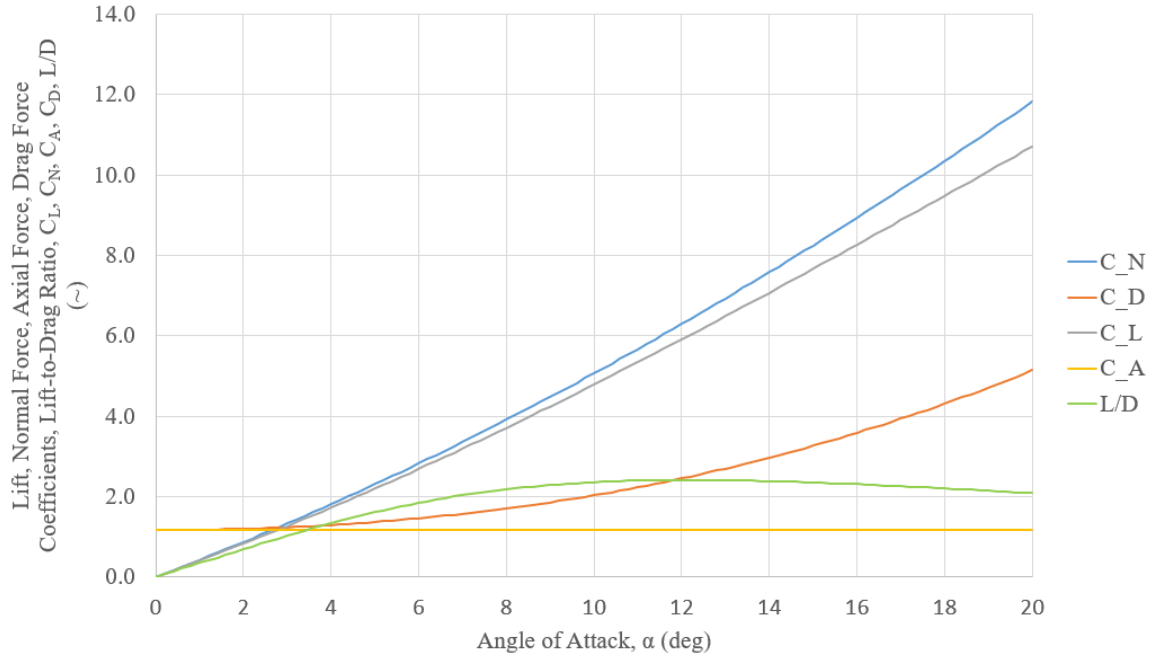


Figure 56: C_L , C_N , C_A , C_D , L/D vs. Angle of Attack at Mach 2.5

The trends of these coefficients and ratios can be plotted for other relevant Mach numbers. Figure 57 below shows these trends at Mach 2 for an angle of attack range of zero to 12 degrees.



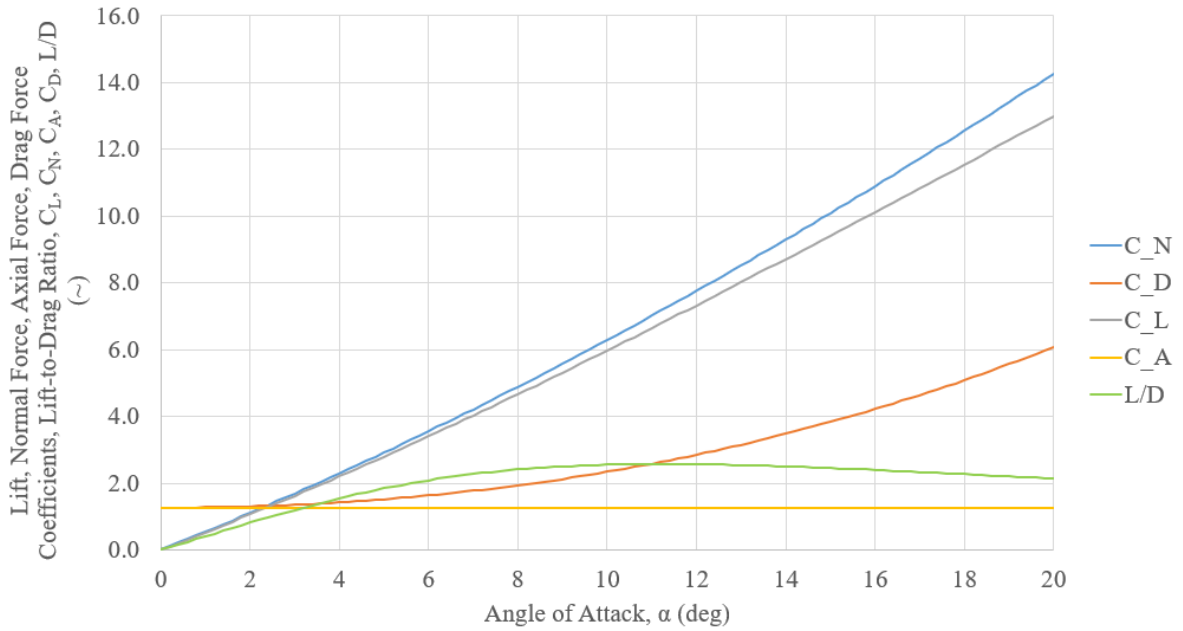


Figure 57: C_L , C_N , C_A , C_D , L/D vs. Angle of Attack at Mach 2

Figure 58 below shows these trends at Mach 3 for an angle of attack range of zero to 12 degrees.

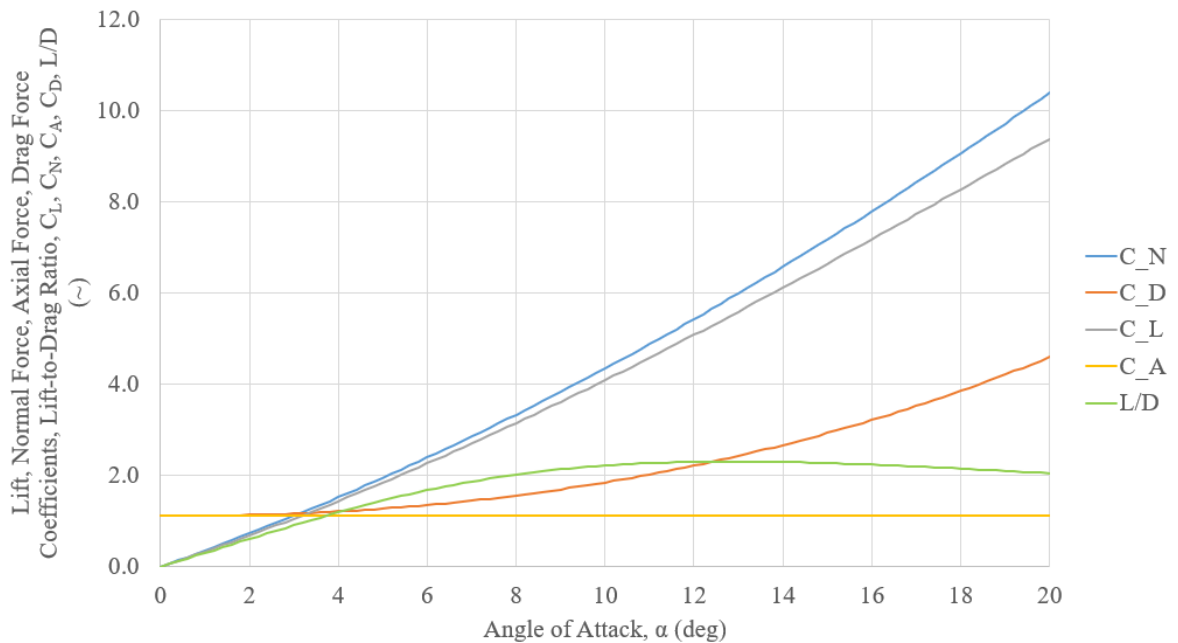


Figure 58: C_L , C_N , C_A , C_D , L/D vs. Angle of Attack at Mach 3



Figure 59 below shows these trends at Mach 3.5 for an angle of attack range of zero to 12 degrees.

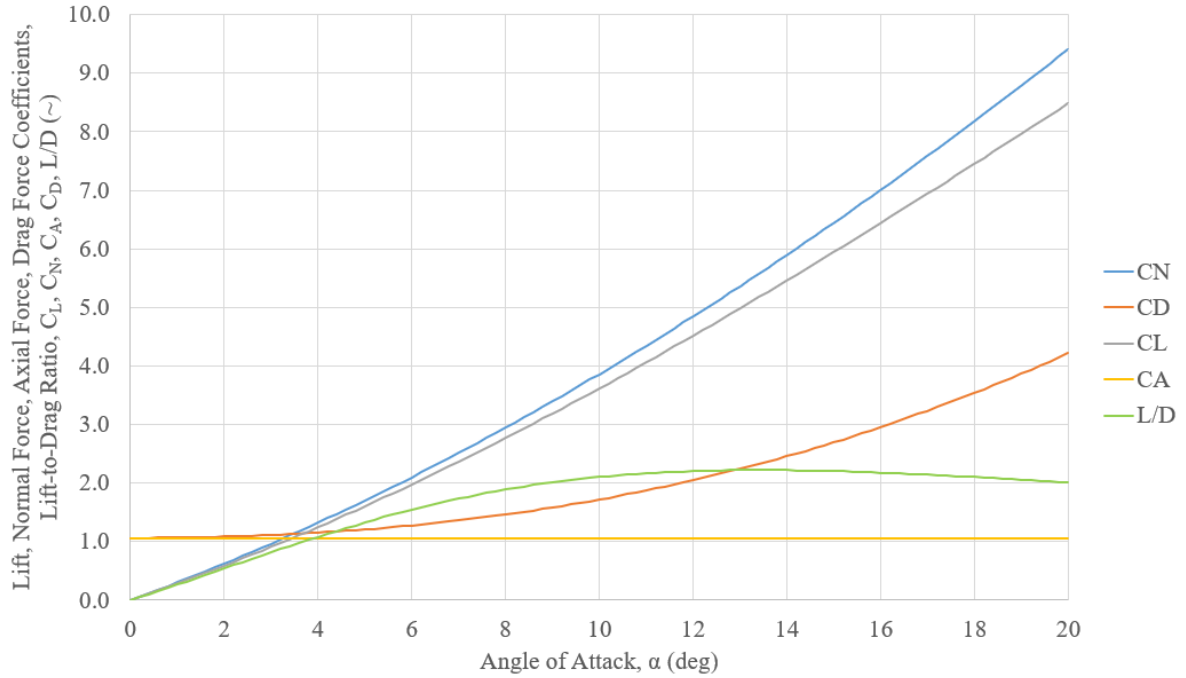


Figure 59: CL, CN, CA, CD, L/D vs. Angle of Attack at Mach 3.5

Figure 60 below shows these trends at Mach 4 for an angle of attack range of zero to 12 degrees.



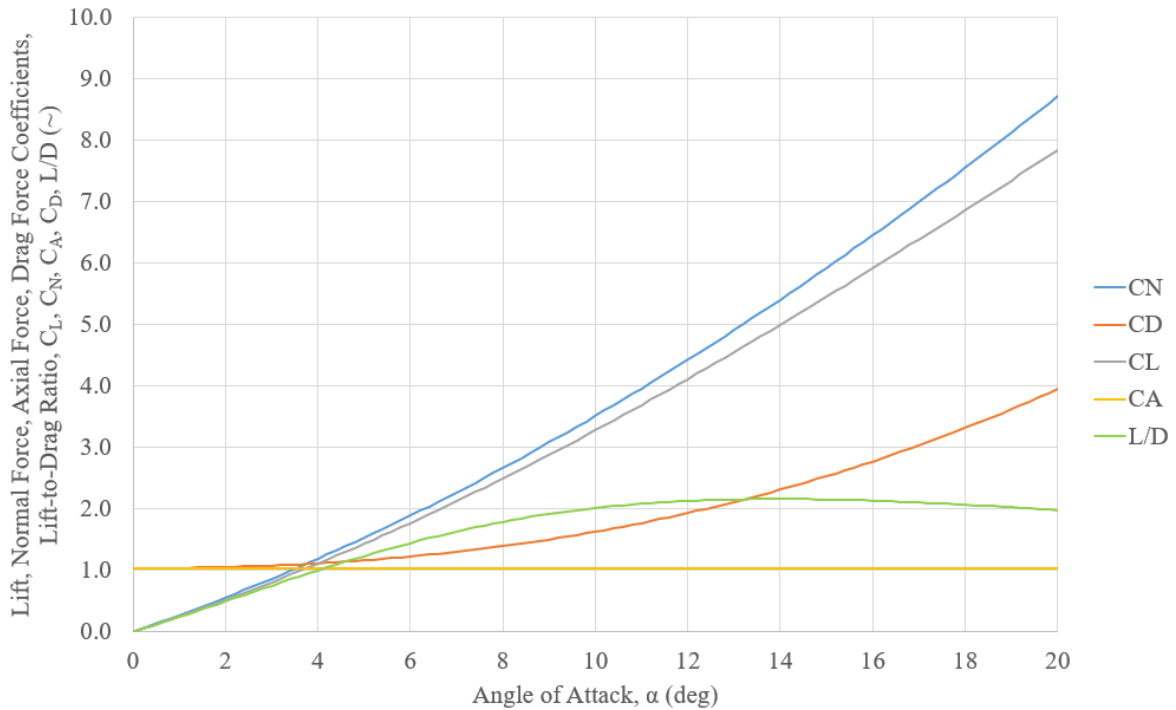


Figure 60: C_L , C_N , C_A , C_D , L/D vs. Angle of Attack at Mach 4

With the above trends of the various coefficients and L/D ratio, the cruise Mach number and angle of attack can be found for the previously calculated L/D_{cruise} of the AIM-9X. Since the cruise Mach number is already known to be 2.5, Figure 56 will be used to find the other coefficients at the previously calculated L/D_{cruise} .

14.11 Mach and Alpha at L/D Cruise

The cruise Mach was already known and has been assumed prior to be Mach 2.5. To find the cruise angle of attack Figure 56 was examined. Knowing the previously calculated L/D of 0.48 from Section 14.8, the angle of attack corresponding to an L/D of 0.48 on Figure 56 would be the cruise angle of attack. Looking at Figure 56, the cruise angle of attack for an L/D of 0.48 is 1.4 degrees.

14.12 $C_{L_{\text{cruise}}}$, L/D_{cruise} , and α_{cruise}

Using Figure 56 from Section 14.10, the $C_{L_{\text{cruise}}}$ at a cruise Mach of 2.5 and a cruise angle of attack of 1.4 degrees is found to be 0.57. The L/D_{cruise} was already found to be 0.48 and from Section 14.11, as previously stated, the cruise angle of attack was found to be 1.4 degrees.



14.13 Cruise Mid-Point Air Density

To find the mid-point air density at cruise altitude, a couple assumptions were made. The first is using 50% of the fuel weight since the missile is in cruise. The other assumption is that the temperature is constant at high altitudes in the troposphere. The temperature was assumed constant at 389.99 degrees Rankine. This temperature was used, using Equation 1 to find the speed of sound at high altitudes of the troposphere. The constant high-altitude speed of sound value was then multiplied by the assumed cruise Mach number of 2.5 to yield the velocity at high altitudes. Equation 64 shows the cruise density equation and calculation. Note that takeoff and fuel weight, $C_{Lcruise}$, and S_{ref} have all been found previously.

$$\rho_{cruise} = \frac{2(W_{TO} - 0.5W_F)}{V^2 C_{Lcruise} S_{ref}} = \frac{2(191 \text{ lbf} - 0.5(71.75 \text{ lbf}))}{\left(2420 \frac{\text{ft}}{\text{s}}\right)^2 * 0.57 * 0.349 \text{ ft}^2} = 2.66 \times 10^{-4} \frac{\text{slug}}{\text{ft}^3} \quad (64)$$

At this density, the altitude is 56,500 ft, per Ref. 11.

14.14 Mission Profile with Mid-Point Cruise Detail

With the mid-point cruise altitude known, the mission profile was updated. The updated mission profile is shown below in Figure 61.



Figure 61: Mission Profile Updated with Mid-Point Cruise Altitude

It was found that with the mid-point cruise altitude of 56,500 ft the flight level (FL) for the mission profile changed to FL 565. This did not influence any of the other mission profile parameters as the temperature at high altitudes in the troposphere is assumed to be constant.



15 Proverse Engineering of RAIDER

This section covers the proverse engineering of the new RAIDER AIM-9 missile.

15.1 Baseline Aerodynamic and Inertial Information

The baseline missile data used for the proverse engineering is displayed below in Table 6.

Table 6: Baseline AIM-9X Block II Aerodynamic and Inertial Information

Range	20 mi (32.2 km)
Max. Axial Acceleration	124 gs
Speed	Mach 2.5
Range	20 mi (32.2 km)
Cruise Angle of Attack	1.4 deg
Warhead	21 lbs (9.4 kg) WDU-17/B annular blast fragmentation
Propulsion	Mk 36 Rocket Engine
Max. Thrust	4,000 lbf
Cruise L/D	0.48

15.2 Proposed Changes

To improve the current design of the AIM-9, the authors propose implementing a RAIDER design featuring a rocket engine to accelerate to cruise speed, a ramjet to power the missile after cruise speeds have been reached, and inflatable ducts on the side of the missile to divert the ram air around all internal components as well as increase the lift-to-drag ratio. With the addition of these ducts, the aspect ratio will also increase which will increase the lift-to-drag ratio. The new RAIDER AIM-9 will also implement folding canard surfaces and tail surfaces. This will allow for the new missile to be tube launched as well. To complete the resizing of the new RAIDER AIM-9, an aspect ratio of the missile fuselage of 2 will be assumed.

15.3 New Size Solution

An estimate of I_{sp} of 1,100s was used by the authors when completing the required calculations for a ramjet. TSFC can be calculated using Equation 61 as shown below.



$$TSFC = \frac{\dot{W}_f}{T} = \frac{1}{I_{sp}} \quad (61)$$

$$TSFC = \frac{1}{1100s} * \frac{3600s}{hr} = 3.27 \frac{lb_f}{lb_f - hr} \quad (62)$$

The above equations and their results will be used in later subsections.

15.3.1 RAIDER Performance at AIM-9X Form Factor

First, the performance of the RAIDER AIM-9 will be found if the missile has the same form factor as that of the AIM-9X. To complete this, Figure 56 through Figure 60 had to be recreated using Equation 58 through Equation 63. The trends of the coefficients and L/D at Mach 2 can be seen below in Figure 62.

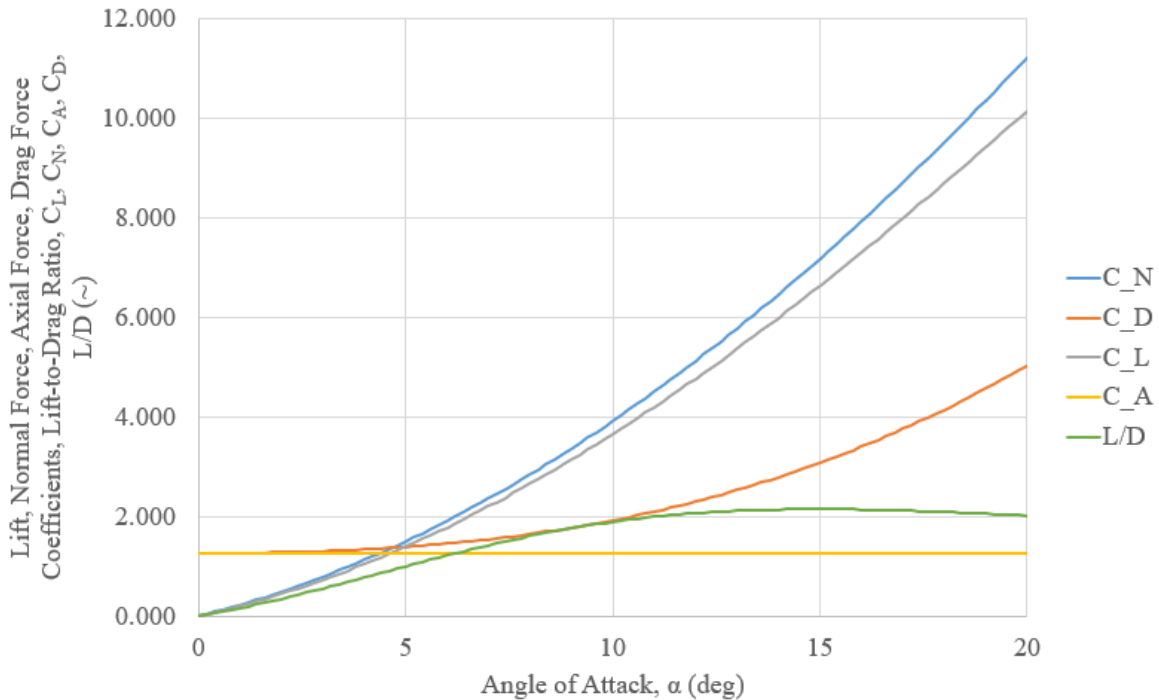


Figure 62: C_L , C_N , C_A , C_D , L/D vs. Angle of Attack at Mach 2 for RAIDER Variant

The trends of the coefficients and L/D at Mach 2.5 can be seen below in Figure 63.



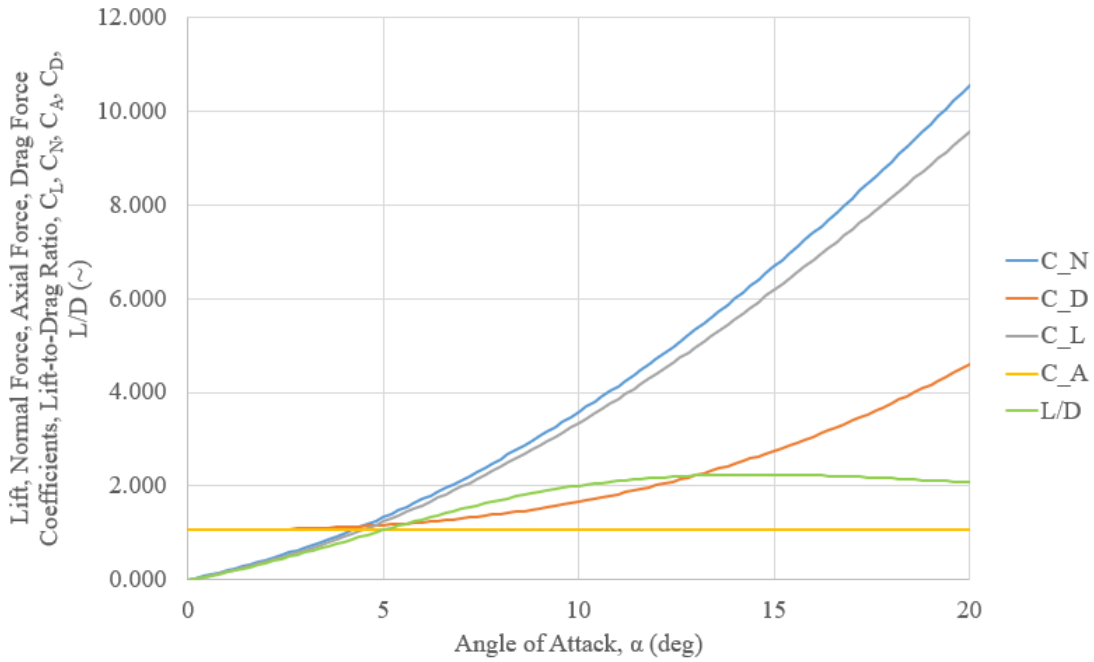


Figure 63: C_L , C_N , C_A , C_D , L/D vs. Angle of Attack at Mach 2.5 for RAIDER Variant

The trends of the coefficients and L/D at Mach 3 can be seen below in Figure 64.

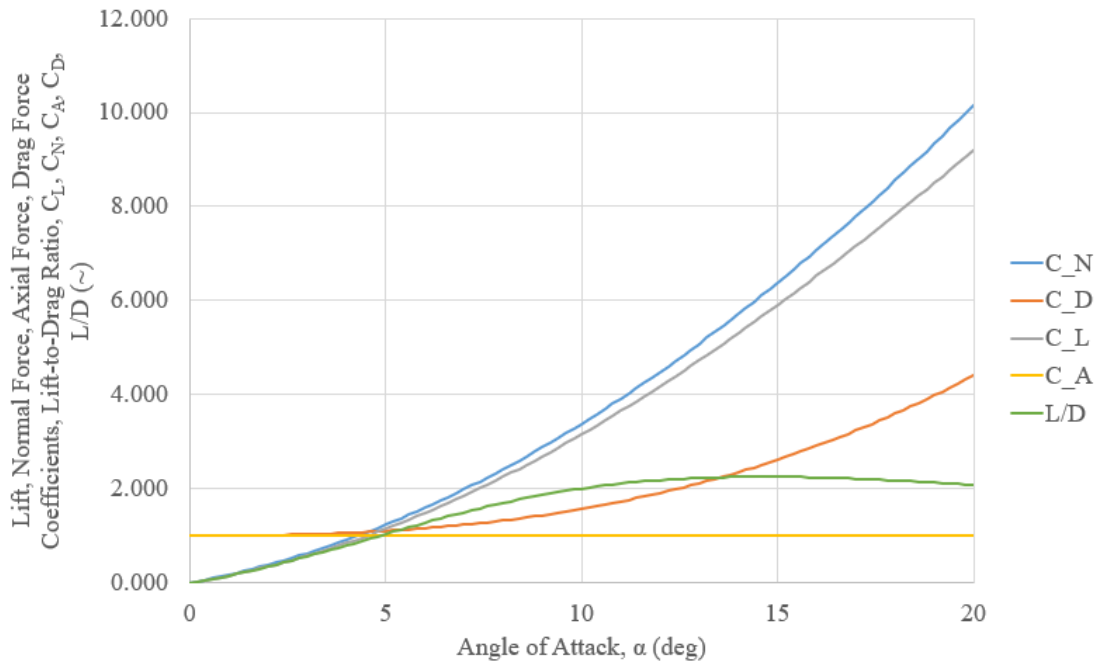


Figure 64: C_L , C_N , C_A , C_D , L/D vs. Angle of Attack at Mach 3 for RAIDER Variant

The trends of the coefficients and L/D at Mach 3.5 can be seen below in Figure 65.



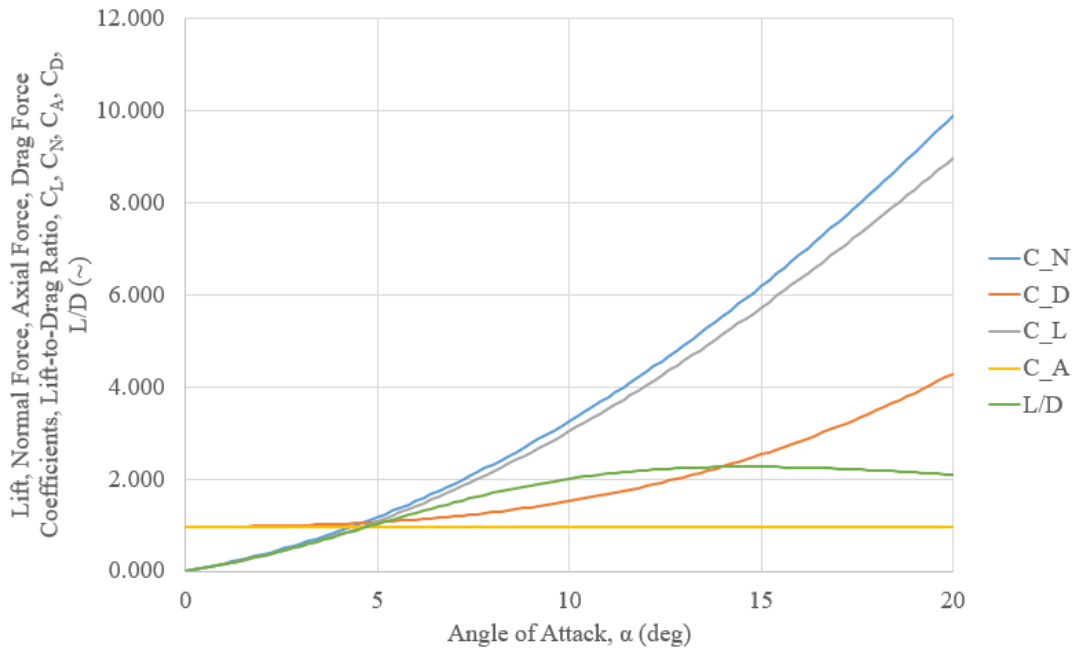


Figure 65: C_L , C_N , C_A , C_D , L/D vs. Angle of Attack at Mach 3.5 for RAIDER Variant

The trends of the coefficients and L/D at Mach 2 can be seen below in Figure 66.

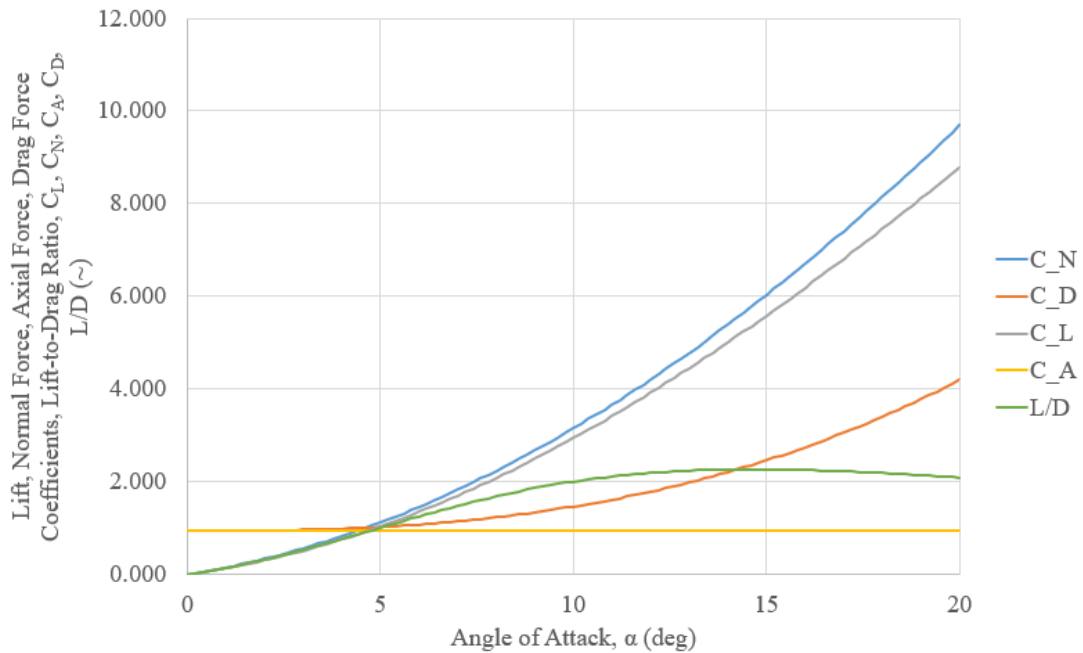


Figure 66: C_L , C_N , C_A , C_D , L/D vs. Angle of Attack at Mach 4 for RAIDER Variant



With these figures, the performance of the RAIDER can be found as seen below assuming the same weights of each component as the AIM-9X Block II. It should also be noted that the team chose to design to a cruise angle of attack of 8 degrees. While the maximum lift-to-drag ratio occurs at a larger angle, the team chose to design to 8 degrees to ensure high performance of the ramjet that is utilized on the RAIDER. As seen in Figure 63, the lift-to-drag ratio of the RAIDER AIM-9 at Mach 2.5 and an angle of attack of 8 degrees is 1.71. With this, the performance can be calculated following the following steps as shown in Equation 63 through Equation 73 below.

$$V_{RAIDER} = \frac{\pi d^2 L}{4} = \frac{\pi * 5.04^2 * 119}{4} = 2,375 \text{ in}^3 \quad (63)$$

With this complete volume of the RAIDER AIM-9, the volume of everything within the missile can be found as seen in Appendix B.

$$V_{rocket \text{ fuel}} = 906 \text{ in}^3 = \frac{W_{rocket \text{ fuel}}}{\rho_{rocket \text{ fuel}}} = \frac{10.75 \text{ lbf}}{0.058 \frac{\text{lbf}}{\text{in}^3}} = 185 \text{ in}^3 \quad (64)$$

$$V_{payload} = 906 \text{ in}^3 \quad (65)$$

$$V_{jet \text{ fuel}} = V_{RAIDER} - V_{payload} - V_{rocket \text{ fuel}} = 1,284 \text{ in}^3 \quad (66)$$

$$W_{jet \text{ fuel}} = V_{jet \text{ fuel}} * \rho_{jet \text{ fuel}} = 1,284 \text{ in}^3 * 0.029 \frac{\text{lbf}}{\text{in}^3} = 37.2 \text{ lbf} \quad (67)$$

$$W_{payload} = W_{AIM-9X} - W_{warhead} - W_{fuel} = 191 - 21 - 71.75 = 98.25 \text{ lbf} \quad (68)$$

$$W_{RAIDER} = W_{rocket \text{ fuel}} + W_{jet \text{ fuel}} + W_{warhead} + W_{payload} = 167 \text{ lbf} \quad (69)$$

With the final weight of the RAIDER variant AIM-9 and the lift-to-drag ratio, the thrust required from the missile can be found using the assumption of steady, level, 1 g flight as seen below in Equation 70 and Equation 71.

$$L = W = 167 \text{ lbf} \quad (70)$$

$$T = D = \frac{L}{\frac{L}{D}} = \frac{167}{1.71} = 97.9 \text{ lbf} \quad (71)$$

Finally, the TOF and the range can be found using Equation 72 and Equation 73 below.



$$TOF = I_{sp} * \frac{W_{jet\ fuel}}{T} = 1,100\ s * \frac{37.2\ lbf}{97.6\ lbf} = 418\ s \quad (72)$$

$$Range = TOF * V_{cruise} = 418s * 2420 \frac{ft}{s} = 1,012,609\ ft = 192\ mi \quad (73)$$

15.3.2 Iterating for Same Performance and Smaller Size

To resize the RAIDER AIM-9, an iterative process will be used. This was done by selecting a factor to scale each linear dimension of the missile, solving for the performance of the RAIDER, and resizing if needed until the performance of the RAIDER is the same as the AIM-9X Block II. To complete this, Figure 56 through Figure 60 had to be recreated using Equation 58 through Equation 63. The trends for the coefficients and L/D at Mach 2 can be seen below in Figure 67.

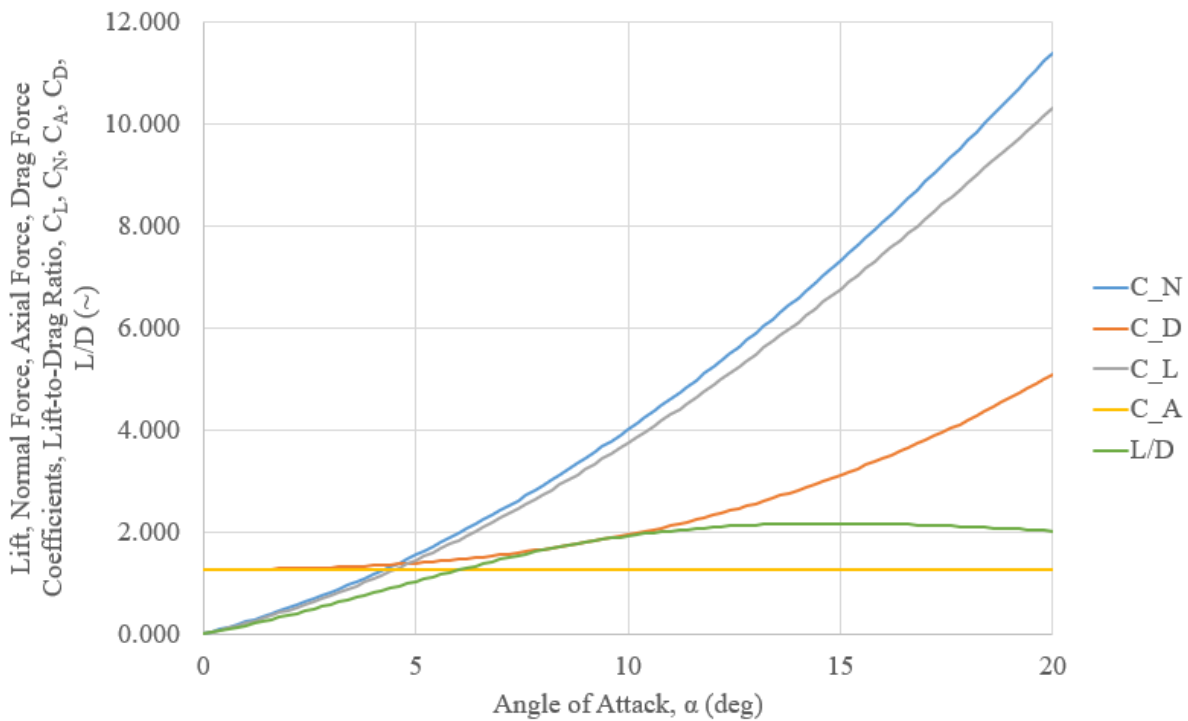


Figure 67: CL, CN, CA, CD, L/D vs. Angle of Attack at Mach 2 for Resized RAIDER Variant

The trends for the coefficients and L/D at Mach 2.5 can be seen in Figure 68 below.



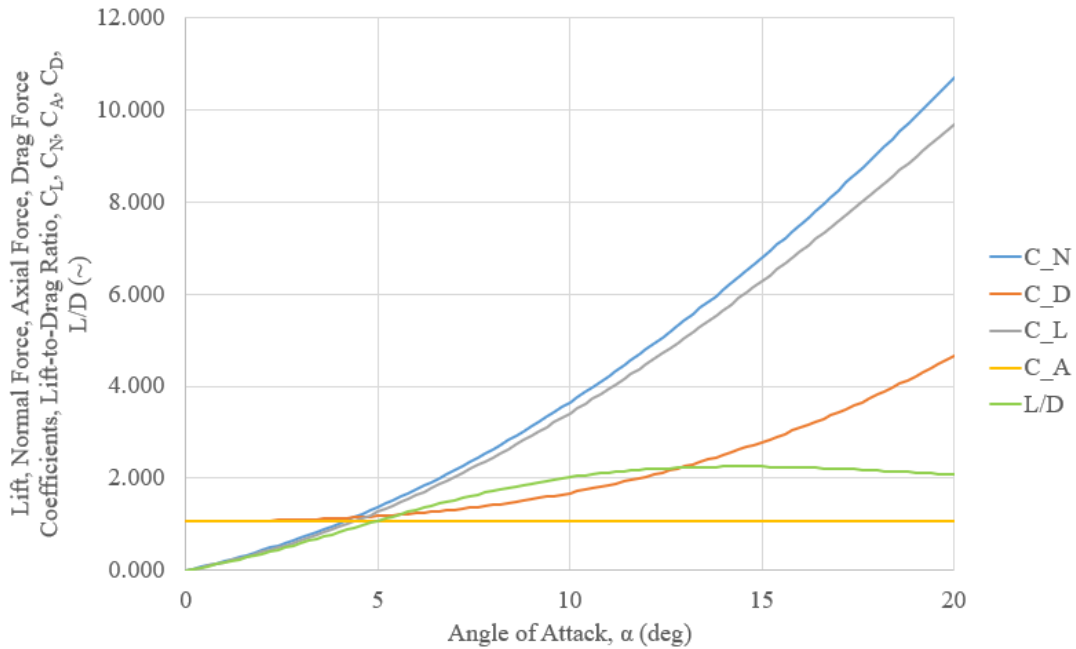


Figure 68: C_L , C_N , C_A , C_D , L/D vs. Angle of Attack at Mach 2.5 for Resized RAIDER Variant

The trends for the coefficients and L/D at Mach 3 can be seen below in Figure 69.

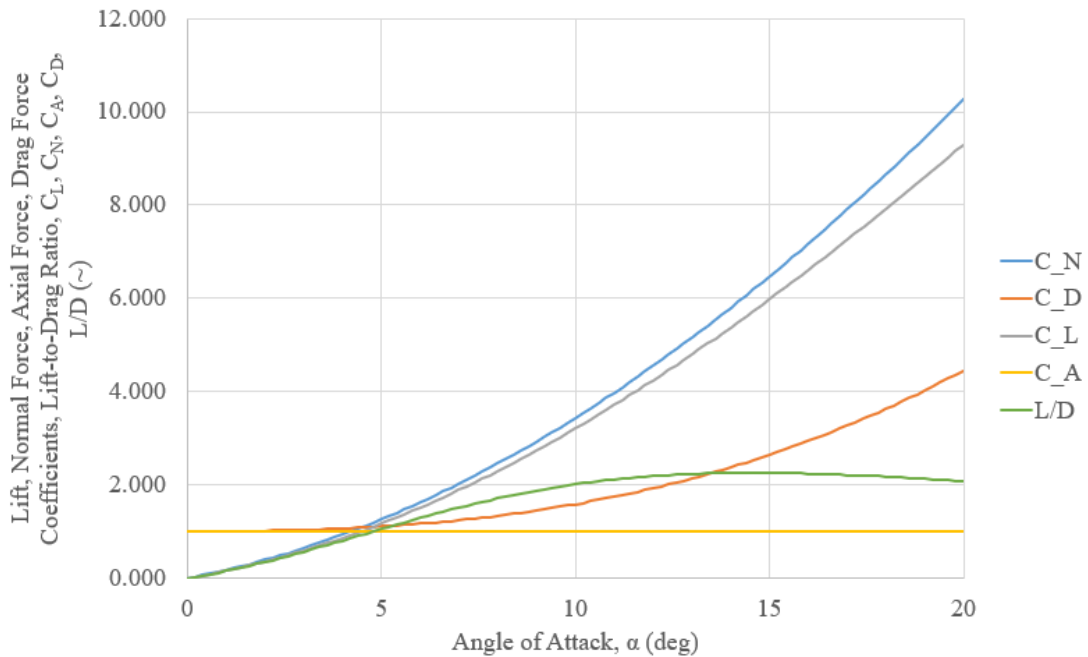


Figure 69: C_L , C_N , C_A , C_D , L/D vs. Angle of Attack at Mach 3 for Resized RAIDER Variant



The trends for the coefficients and L/D at Mach 3.5 can be seen below in Figure 70.

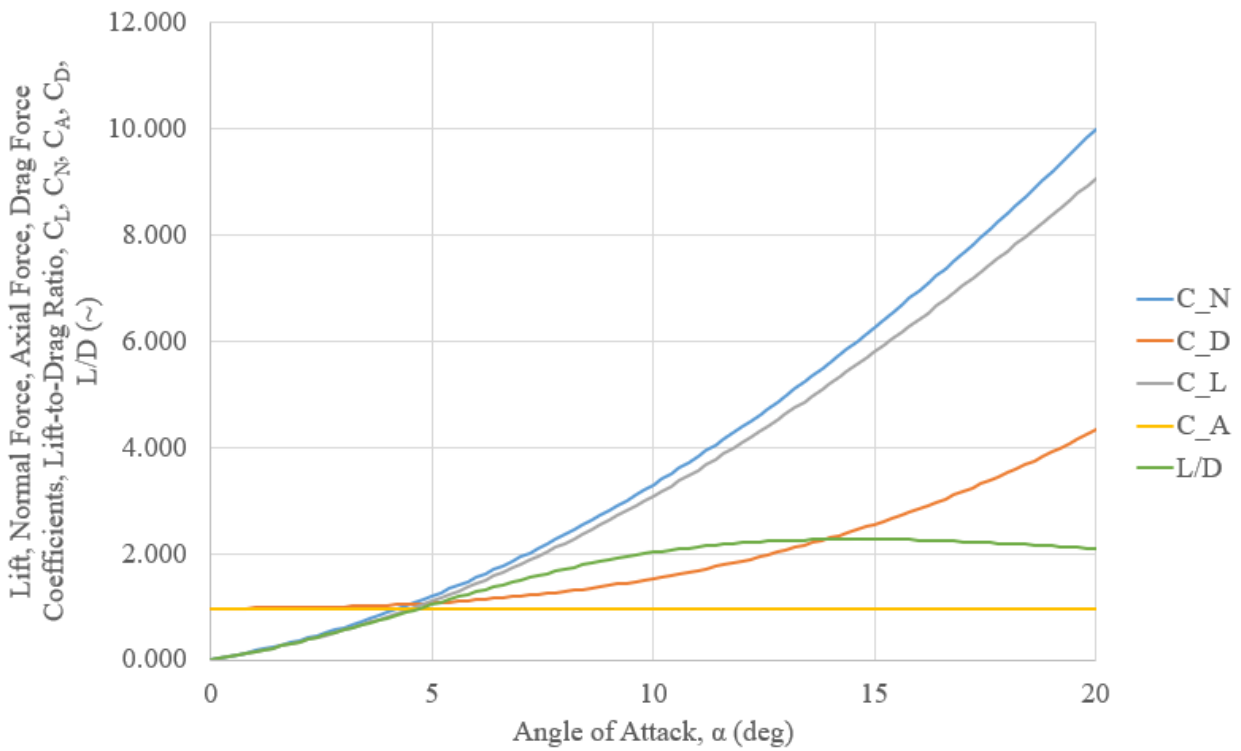


Figure 70: C_L , C_N , C_A , C_D , L/D vs. Angle of Attack at Mach 3.5 for Resized RAIDER Variant

The trends for the coefficients and L/D at Mach 4 can be seen below in Figure 71.



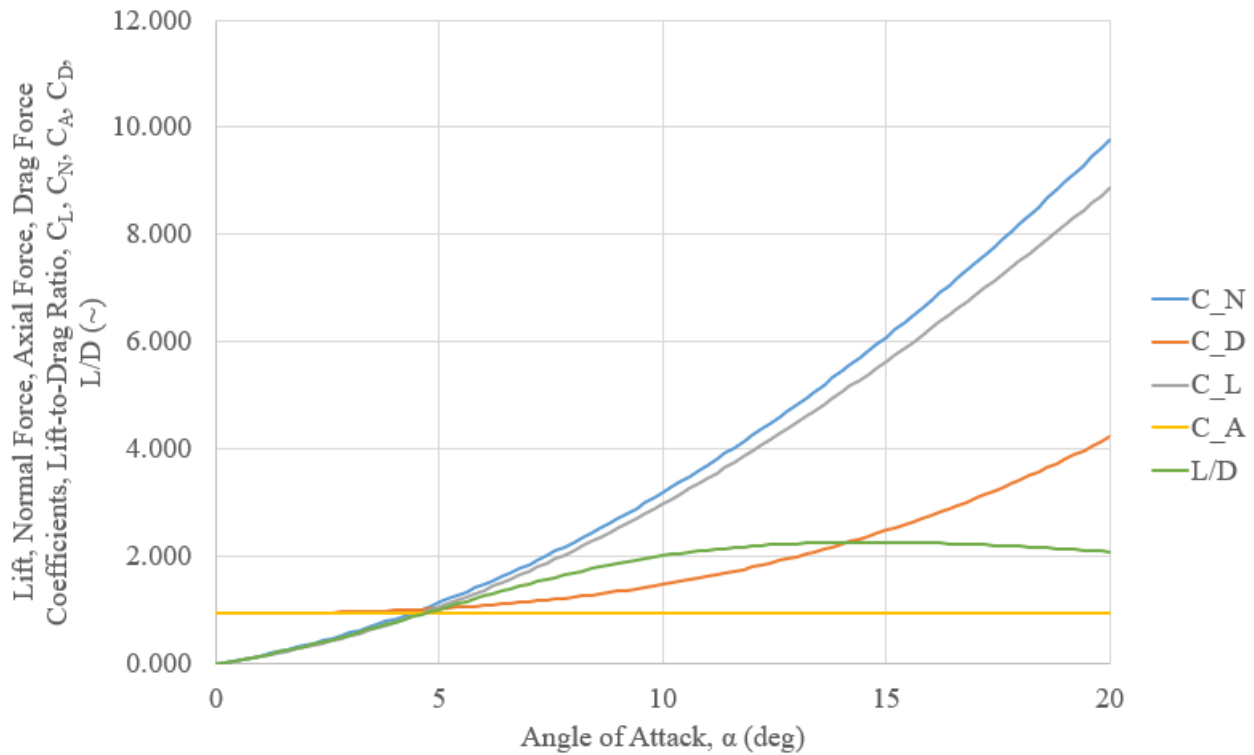


Figure 71: C_L , C_N , C_A , C_D , L/D vs. Angle of Attack at Mach 4 for Resized RAIDER Variant

When comparing Figure 56 through Figure 60 with Figure 67 through Figure 71, it can be seen that the lift-to-drag ratio increases due to the increase in missile fuselage aspect ratio. Because the same performance as seen in Table 6 is desired from the new RAIDER AIM-9, the size will be iteratively changed until the range is the same as the AIM-9X Block II, which is 20 miles. When resizing and redesigning, it was imperative that the warhead stayed the same size as seen in Table 5. With this information, several volumetric and weight constraints could be solved for as seen in Equations 74 through Equation 79. Within these equations, several assumptions will be made including the assumption that the weight of the form and electronics payload would scale down proportionally with the volume scale and the weight of the rocket fuel used to accelerate to dash velocity is constant. It should be noted that all equations shown below are for a linear geometric scale of 66.9% of the size of the AIM-9X.

$$V_{RAIDER_{new}} = V_{RAIDER} * 0.669^3 = 711 \text{ in}^3 \quad (74)$$



With this complete volume of the RAIDER AIM-9, the volume of everything within the missile can be found as seen in Appendix B and are shown below in Table 7 for ease of reference.

Table 7: RAIDER AIM-9 Component Volumes

Warhead Volume (in³):	185
Rocket Fuel Volume (in³):	291
Volume of Electronics Package (in³):	615

$$V_{electronics_{new}} = V_{electronics} * 0.669^3 = 184 \text{ in}^3 \quad (75)$$

$$V_{jet \text{ fuel}_{new}} = V_{RAIDER_{new}} - V_{warhead} - V_{rocket \text{ fuel}} - V_{electronics_{new}} = 51 \text{ in}^3 \quad (76)$$

$$W_{jet \text{ fuel}_{new}} = V_{jet \text{ fuel}_{new}} * \rho_{jet \text{ fuel}} = 51 \text{ in}^3 * 0.029 \frac{\text{lb}}{\text{in}^3} = 1.47 \text{ lbf} \quad (77)$$

$$W_{payload_{new}} = W_{payload} * 0.669^3 = 98.25 * 0.669^3 = 29.4 \text{ lbf} \quad (78)$$

$$W_{RAIDER_{new}} = W_{rocket \text{ fuel}} + W_{jet \text{ fuel}_{new}} + W_{warhead} + W_{payload_{new}} = 62.6 \text{ lbf} \quad (79)$$

With the final weight of the resized RAIDER variant AIM-9, the performance can be calculated. To do this, the authors will, once again, design to a cruise angle of attack of 8 degrees. From Figure 68, this results in a lift-to-drag ratio of 1.74. With this, the thrust required from the missile can be found using the assumption of steady, level, 1 g flight as seen below in Equation 80 and Equation 81.

$$L = W = 62.6 \text{ lbf} \quad (80)$$

$$T = D = \frac{L}{\frac{L}{D}} = \frac{62.7}{1.74} = 36.1 \text{ lbf} \quad (81)$$

Finally, the TOF and the range can be found using Equation 82 and Equation 83 below.

$$TOF = I_{sp} * \frac{W_{jet \text{ fuel}}}{T} = 1,100 \text{ s} * \frac{1.47 \text{ lbf}}{36.1 \text{ lbf}} = 45 \text{ s} \quad (82)$$

$$Range = TOF * V_{cruise} = 45 \text{ s} * 2420 \frac{\text{ft}}{\text{s}} = 108,825 \text{ ft} = 20.6 \text{ mi} \quad (83)$$

With this, it can be seen that after resizing the linear dimensions of the AIM-9X to just 66.9% of their original values for the RAIDER AIM-9, the performance is able to remain constant.



16 Model CAD and Physical Model Preparation

Both a physical and CAD model of the newly proposed configuration AIM-9X will be produced to facilitate the attendance of the Air Armament Symposium. This section will cover the considerations made to construct the models.

16.1 CAD Model of New Form Factor RAIDER

A CAD model was constructed utilizing the scale factor of 0.669 found in Section 15.3.2. The RAIDER ducts and fairings were sized based upon the AIGM-138 Described in (Ref. 23). This resulted in the CAD model shown in Figure 72 below.

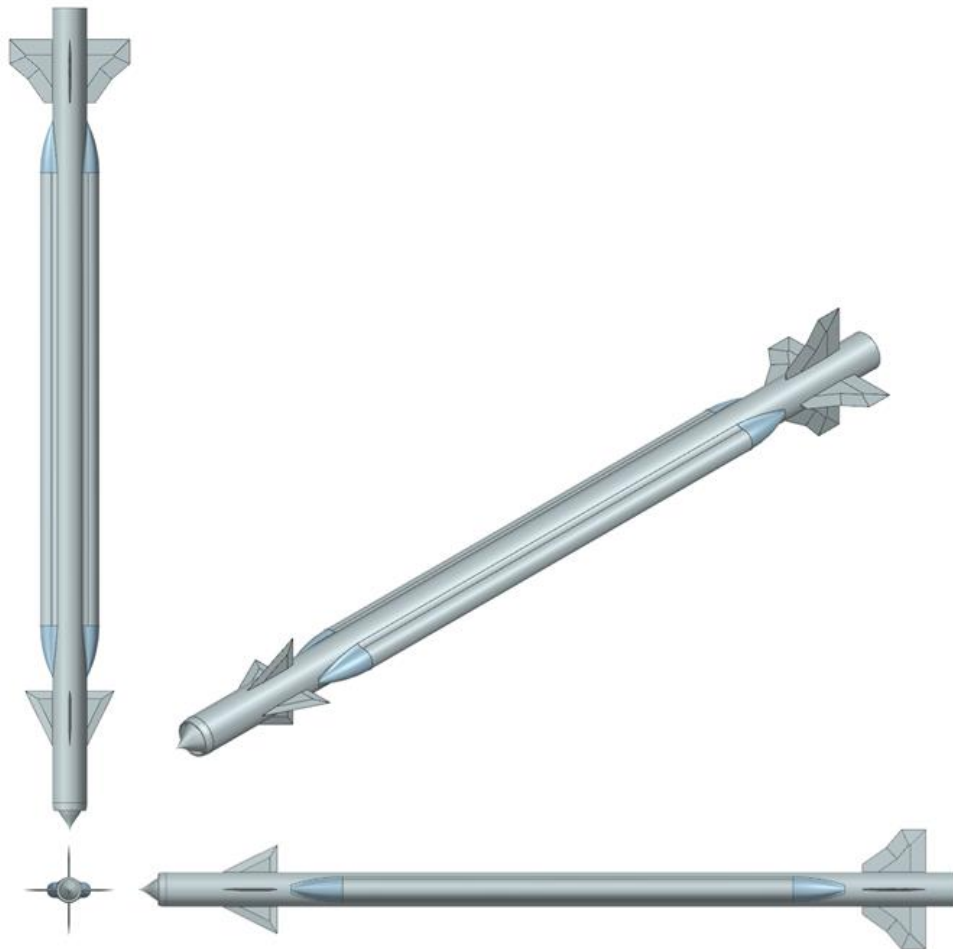


Figure 72 RAIDER AIM-9X Replacement 3 View

The newly sized replacement missile is compared to the original AIM-9X in Figure 73 below.

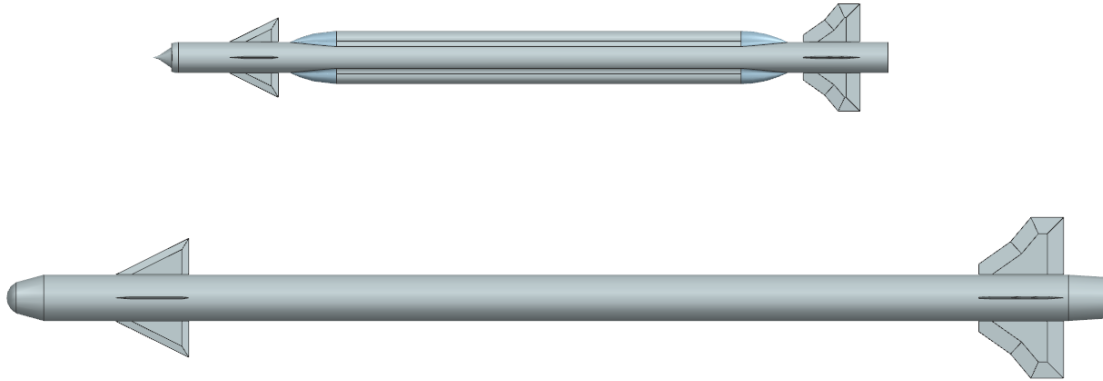


Figure 73 AIM-9X and RAIDER Replacement Comparison

16.2 Model BOM

The bill of materials (BOM) for AIM-9X RAIDER replacement will be shown in this section. Each part of the missile is listed as well as the material required to create it. The final BOM is shown in Table 8 below.

Table 8 AIM-9X Replacement Model BOM

Part No.	Part Name	Material	Qty	Unit Cost	Total Cost	Source/Supplier
1	Fuselage body	cardboard	3	\$16.52	\$49.56	apogeerockets.com
2	Duct Body	cardboard	10	\$14.42	\$144.20	apogeerockets.com
3	Inlet Body	PETG	2	\$39.99		Amazon.com
4	Planforms	1/4 in plywood	3	\$19.99	\$59.97	Amazon.com
5	Wood Filler		1	\$54.99	\$54.99	Amazon.com
6	Base Plate	32-gauge steel	1	\$14.48	\$14.48	Lowe's
7	Stand Rod	Galvanized Steel	1	\$6.45	\$6.45	Home Depot
8	Stand Connector	Galvanized Iron	1	\$5.83	\$5.83	Home Depot
9	Stand Fastener	Zinc	8	\$0.16	\$1.28	Home Depot
10	Fastener Washers	Zinc	1	\$1.28	\$1.28	Home Depot
11	Fastener Nuts	Zinc	1	\$1.38	\$1.38	Home Depot
12	Gorilla Glue	Polyurethane	1	\$12.48	\$12.48	Amazon.com
13	Sandpaper	100 grit	1	\$5.98	\$5.98	Home Depot
14	Sandpaper	220 grit	1	\$6.98	\$6.98	Home Depot
15	Spray Primer	Primer	5	\$6.98	\$34.90	Home Depot
16	Gray Spray Paint	Paint	5	\$9.98	\$49.90	Home Depot
17	Blue Spray Paint	Paint	2	\$19.98	\$39.96	Home Depot
18	Black Spray Paint	Paint	2	\$9.98	\$19.96	Home Depot
19	Epoxy	Epoxy	2	\$12.99	\$25.98	Amazon.com
20	Planform-Body Fillets	PETG	1	\$39.99	\$39.99	Amazon.com
21	Duct-Body Transition	PETG	~	~	~	
Total Cost:					\$655.53	

16.3 Components to be Ordered

From Table 8 above, all parts excluding part 3 and 20 will have to be purchased. The inlet body and planform body fillets will be 3D printed from PETG plastic, a sandable and



durable thermoplastic. All other parts can be sourced from Amazon, Home Depot, and Apogee Rockets.

16.4 STL Files for 3D Printing

STL files were generated from the CAD model for all 3D printed components, these include the inlet, duct-body fairings, as well as fin-body attachment fairings. All these components will be printed on a conventional 3D printer of PETG thermoplastic. The generated files are attached in the submission.

16.5 Assembly Methods

The assembly method for the RAIDER AIM-9X is discussed within this section. The fuselage and inflatable ducts for the RAIDER missile will be composed of cardboard tubes. These cardboard tubes will be attached by gorilla glue against the combined skin sections, as well as 3 wooden pegs on each side that connect the two tubes. These pegs will be composed of scrap balsa sheet wood and will be no more than 0.5 inches long and 0.25 inches wide. These pegs will reinforce the gorilla glue and hold together the fuselage to the inflatable ducts.

The shock inlet cone/seeker will be attached with epoxy. The 3D printed section will be made of PETG filament and will attach just as a model rocket nose cone would be. The inlet cone will be skim coated with wood filler and sanded smooth to eliminate the printing layer lines.

The planforms will be attached to the main body using 3D printed planform-body fillets. The 3D printed fillets will provide a slot for the 0.25" plywood to sit, and a larger surface with which to bond the planforms to the missile body tube.

For the finish, the missile will be skim coated in wood filler in its entirety after bonding on all planforms, ducts, and inlet cone. The missile will then be sprayed with primer and sanded again. After the missile is fully primed, enamel spray paint can be applied using tape to mask the various color sections. Wood filler will also be used to make a fillet between the fuselage and the duct cardboard tubes.

The stand will be composed of a 24 x 36-inch steel plate, with a 1-inch floor flange attached to the bottom. This flange will be attached by 1/4 inch fasteners with a washer and nut. Four more fasteners and nuts will be attached to the corners of the steel plate to provide more



stability to the plate. Attached to the floor flange is a 10-inch threaded rod that will stand vertically and allow the missile to rest on.

The paint scheme for the missile will be colored light gray as the base, with the AIM 9 and RAIDER designation painted in black, as well as 3 light blue bands painted immediately forward of the canards, forward of the tail and aft of the tail. A picture of the preferred color scheme and new designation as given by the authors, AIM-24, can be seen on the missile below in Figure 74.

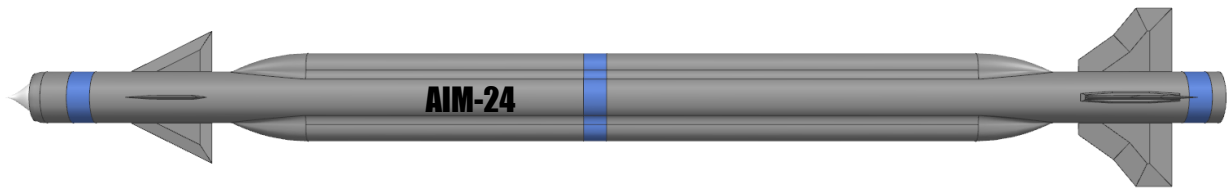


Figure 74: RAIDER AIM-9 Color Scheme

17 Conclusions and Recommendations

17.1 Conclusions

The authors conclude that:

- The first mode bending body frequency of the AIM-9X is 85 rad/s;
- The body zero-lift drag coefficient of the AIM-9X at 20,000 ft at a previously identified engagement speed of Mach 2.5 is:
 - Approximately 0.95 for a coast condition;
 - Approximately 0.87 for a powered condition;
- A larger fineness ratio leads to less body wave drag;
- The AIM-9X Block II should remain without boattail to decrease the drag at supersonic speeds as well as increase the speed of the missile;
- The lift-to-drag ratio of the AIM-9X increases if the aspect ratio increases;
- The required C_L for steady level 1g flight at 20,000 ft at an engagement speed of Mach 2.5 is about 0.30;
- The AIM-9X Block II has low $(L/D)_{max}$ and high radar cross section because the missile is short range and performance driven;
- As angle of attack increases the aerodynamic center moves back;
- The use of a flare significantly shifts the missile's AC back;
- The canard non-dimensional normal force coefficient slope with angle of attack for the AIM-9X is 1.75 at an engagement speed of Mach 2.5;
- The tail non-dimensional normal force coefficient slope with angle of attack for the AIM-9X is 1.75 at an engagement speed of Mach 2.5;
- The total normal force coefficient for the AIM-9X at an $\alpha = 9.4$ deg., canard deflection of five degrees up, tail deflection of two degrees down and an engagement speed of Mach 2.5 is 5.26;
- As Mach number increases past Mach 2, the aerodynamic center of both the front and aft planforms move to 49% of the mean geometric chord;



- As $AR > 3$, convergence curve for AC to 50% is identical as Mach increases past Mach 2;
- The HM when Mach is 2 at an altitude of 20,000 ft for the AIM-9X Block is 26,200 lbf-in (2,960 N-m);
- The AIM-9X Block II has an unstable HM at Mach less than 1.5, but this is acceptable as the missile has an engagement speed of Mach 2.5;
- The AIM-9X Block II has a $(C_{D0})_{Surface,Friction}$ value of 0.11 at Mach 2.5 and at an altitude of 20,000 ft;
- The leading edge section angles of the AIM-9X are 5 and 10 degrees which results in planar surface wave drag of 0.01 and 0.05 respectively at Mach 2;
- The planar surface zero-lift drag coefficient of the AIM-9X is 0.13;
- A grid fin tail is undesirable for the RAIDER AIM-9X;
- Larger tail area is required for stability given smaller static margins;
- Larger tail area is required for stability as the cruise Mach increases;
- The total normal force coefficient at 5 degrees angle of attack is 2.5 with the tail contributing to 60 % of the total normal force coefficient;
- The total normal force coefficient at 20 degrees angle of attack is 14 with the tail contributing to 50% of the total of the normal force coefficient;
- The reverse engineered propellant weight for the AIM-9X is 71.75 lbs;
- The reverse engineered TSFC of the AIM-9X is 13.6 lbf/lbf-hr;
- The reverse engineered TOF of the AIM-9X is 4.75 s;
- The reverse engineered time to accelerate from launch for the AIM-9X is 0.72 s and the range for the acceleration phase is 0.3 mi;
- The reverse engineered time of flight for the dash phase of the AIM-9X is 43 s and the thrust required for the dash is 376 lbf;
- The reverse engineered $(L/D)_{cruise}$ for the AIM-9X is 0.48;
- The reverse engineered empty weight ratio for the AIM-9X is 51%;



- The reverse engineered cruise Mach number and cruise angle of attack are Mach 2.5 and 1.4 degrees;
- The reverse engineered $C_{L_{cruise}}$ for the AIM-9X at the cruise angle of attack of 1.4 degrees is 0.57;
- The reverse engineered cruise mid-point air density is 2.66×10^{-4} slug/ft³ which corresponds to a mid-point cruise altitude of 56,500 ft;
- To achieve the same performance as the AIM-9X Block II, each linear dimension on the RAIDER AIM-9 can be shrunk to 66.9% of the original dimensions;
- The new RAIDER AIM-9 variant weighs only 62.6 lbs with the same performance as the AIM-9X Block II.

17.2 Recommendations

The authors recommend that:

- A more detailed and accurate basis for geometry should be found for estimations of weight, volume, and internal arrangement to eliminate errors in estimation;
- Higher fidelity codes be used to carry out computations of key characteristics, and resizing and assumptions be revised for accuracy and consistency;
- The authors recommend designating the new RAIDER variant of the AIM-9 Sidewinder the AIM-24 Viper.



18 References

1. Parsch, A., “Raytheon (Philco/General Electric) AAM-N-7/GAR-8/AIM-9 Sidewinder,” *Designation-Systems, Designation-Systems.net* [<http://designation-systems.net/dusrm/m-9.html>] Lawrence, Kansas 66044, 10 September 2023, 5:30 pm.
2. Anon., “AIM-9X Sidewinder,” *Forecast International, AeroWeb* [<http://www.fiaeroweb.com/Defense/Sidewinder.html>] Lawrence, Kansas 66044, 10 September 2023, 5:46 pm.
3. Defense Flash News, “AIM 9X Sidewinder Live-Fire Missile Exercise,” [<https://www.youtube.com/watch?v=E5az7tiuF0o>] YouTube, 4 October 2022, Lawrence, Kansas, 66044, 10 September 2023, 3:15 pm.
4. Moore, T., "Solid Propulsion Enabling Technologies and Milestones for Navy Air-launched Tactical Missiles," AIAA 2011-6941. *AIAA Centennial of Naval Aviation Forum "100 Years of Achievement and Progress"*. September 2011. [<https://doi.org/10.2514/6.2011-6941>] Lawrence, Kansas 66044, 10 September 2023, 3:56 pm.
5. Stoneman, J., “AIM-9X Block II Sidewinder (AIM-9X Blk II),” Department of Defense, DD-A&T(Q&A)823-442, March 23, 2016. [<https://apps.dtic.mil/sti/citations/AD1018971,AD1018971.pdf> (dtic.mil)] Lawrence, Kansas 66044, 10 September 2023, 3:27pm.
6. Dawley, S., “Diversified Submarine Weapon Suite a Systems Engineering Approach,” Thesis, Naval Postgraduate School, Monterey, California, December 2008.
7. Saballa, J., “Raytheon to Supply Over 500 AIM-9x Sidewinder Missiles to Us, Allies.” *TheDefensePost*, 6 June 2023, [<https://www.thedefensepost.com/2023/06/06/raytheon-sidewinder-missiles-us-allies>] Lawrence, Kansas 66044, 10 September 2023, 6:15 pm.
8. Youssef, N., Viswanatha, A., “Pentagon Spent At Least \$1.5 Million on Missiles to Down Three High-Altitude Objects; Defense officials are still analyzing debris from suspected Chinese surveillance balloon,” *The Wall Street Journal*, February 22, 2023, *The Wall Street Journal Website* [<https://www.wsj.com/articles/pentagon-spent-at-least->



- [1-5-million-on-missiles-to-down-three-high-altitude-objects-b358e522](#)] Lawrence, KS 66046, September 10, 2023.
9. Anon., “Depart of Defense Fiscal Year (FY) 2021 Budget Estimates,” Department of Defense, Volume 1, February 2020.
[\[https://web.archive.org/web/20201219025102/https://www.secnav.navy.mil/fmc/fmb/Documents/21pres/WPN_Book.pdf\]](https://web.archive.org/web/20201219025102/https://www.secnav.navy.mil/fmc/fmb/Documents/21pres/WPN_Book.pdf) Lawrence, Kansas 66044, 10 September 2023, 4:42 pm.
10. Fleeman, Eugene L., “*Missile Design and System Engineering*,” American Institute of Aeronautics and Astronautics, Inc, 2012, Chapter 2.
11. Anderson, J “*Fundamentals of Aerodynamics*” 6th ed., McGraw Hill, New York, 2017, pp 1103-1109.
12. Anon., “Short range guided missile AIM-9X Sidewinder,” *Missilery.info*,
[\[https://en.missilery.info/missile/aim9x\]](https://en.missilery.info/missile/aim9x) Lawrence, Kansas 66044, 17 September 2023, 5:07 pm.
13. Cavallo, Christian, “All About 4130 Steel (Properties, Strength, and Uses),” *Thomas*,
[\[https://www.thomasnet.com/articles/metals-metal-products/all-about-4130-steel-properties-strength-and-uses/\]](https://www.thomasnet.com/articles/metals-metal-products/all-about-4130-steel-properties-strength-and-uses/) Lawrence, Kansas 66044, 17 September 2023, 5:11 pm.
14. Verver, Gary. “The AIM-9R Sidewinder,” *Flickr*,
[\[https://www.flickr.com/photos/skyhawkpc/6280829621\]](https://www.flickr.com/photos/skyhawkpc/6280829621) Lawrence, Kansas 66044, 17 September 2023, 5:20 pm.
15. Anon, “AIM-9X Sidewinder Air To Air Missile – Fully RD Printable” *Artstation*,
[\[https://www.artstation.com/artwork/NGnP9z\]](https://www.artstation.com/artwork/NGnP9z) Lawrence, Kansas 66044, 17 September 2023, 5:50 pm.
16. Anon., “Probabile Andamento Interno Dello AIM-9M Sidewinder”, *pngwing Website*
[\[https://www.pngwing.com/ar/free-png-nwtdm\]](https://www.pngwing.com/ar/free-png-nwtdm) Lawrence, Kansas 66044 17 September 2023, 3:34 pm.
17. Roskam, J., “*Aircraft Flight Dynamics and Automatic Flight Controls Part I*”, DARCorporation, Lawrence, 2018, pp. 42.



18. Munawar, S., “Analysis of Grid Fins as Efficient Control Surface in Comparison to Conventional Planar Fins,” *AIAA Atmospheric Flight Mechanics Conference*, 2009.
19. Anon., “Raytheon AIM-9 Sidewinder,” *Estrella Warbirds Museum*.
[<https://www.ewarbirds.org/missiles/aim9sidewinder.shtml>] Lawrence, Kansas 66044,
16 October 2023, 1:18 pm.
20. Anon., “63rd Fighter Squadron (USAF AETC),” *F-16.net*. [https://f-16.net/units_article223.html] Lawrence, Kansas 66044, 16 October 2023, 1:25 pm.
21. Zvereva, A., “Sukhoi Design Bureau, 054, Sukhoi Su-57,” *Flickr*.
[<https://www.flickr.com/photos/130961247@N06/49581303977/>] Lawrence, Kansas
66044, 16 October 2023, 1:29 pm.
22. Barrett, R., “Reverse Engineering of Baseline Missiles & Proverse Engineering of RAIDER Missiles,” *AE 721 Design Lab I, aerodoc.tech*
[https://www.aerodoc.tech/files/ugd/aae7b4_12ea37f6b05e4c3da2bc53a6efa1d936.pdf
] Lawrence, Kansas 66044, 16 October 2023, 12:30 pm.
23. Andresen, A, Chen, K, Knickenberg, J, Mba, C, Sandusky, N, and Yakaqu, M, “AIGM-138 Chimera” University of Kansas, Lawrence, Kansas, May 2023.



Appendix A: Off Rail Speed Calculations

Off Rail Speed Calculation Reference



Figure A.1: Off-Rail Speed Calculation Screenshot (Ref. 3)

The off-rail launch speed of the AIM-9X was estimated using publicly available footage of a live fire exercise off the coast of Japan. The missile was measured to be 478.66 pixels long, allowing us to set a scale of 48.25pixels/ft based upon the true missile length. Analyzing the frames of video where the missile comes off the rail, it was measured that the missile travelled 186.13 pixels. One frame of 30 frames per second source video is 0.033 seconds, meaning the missile moved 186.13 pixels/0.033s, or about 100ft/s. This is reported to one significant figure due to inaccuracies of measurement and video quality.



Appendix B: AIM-9M Weight and Volume Calculations

AIM-9M Weight and Volume Calculations

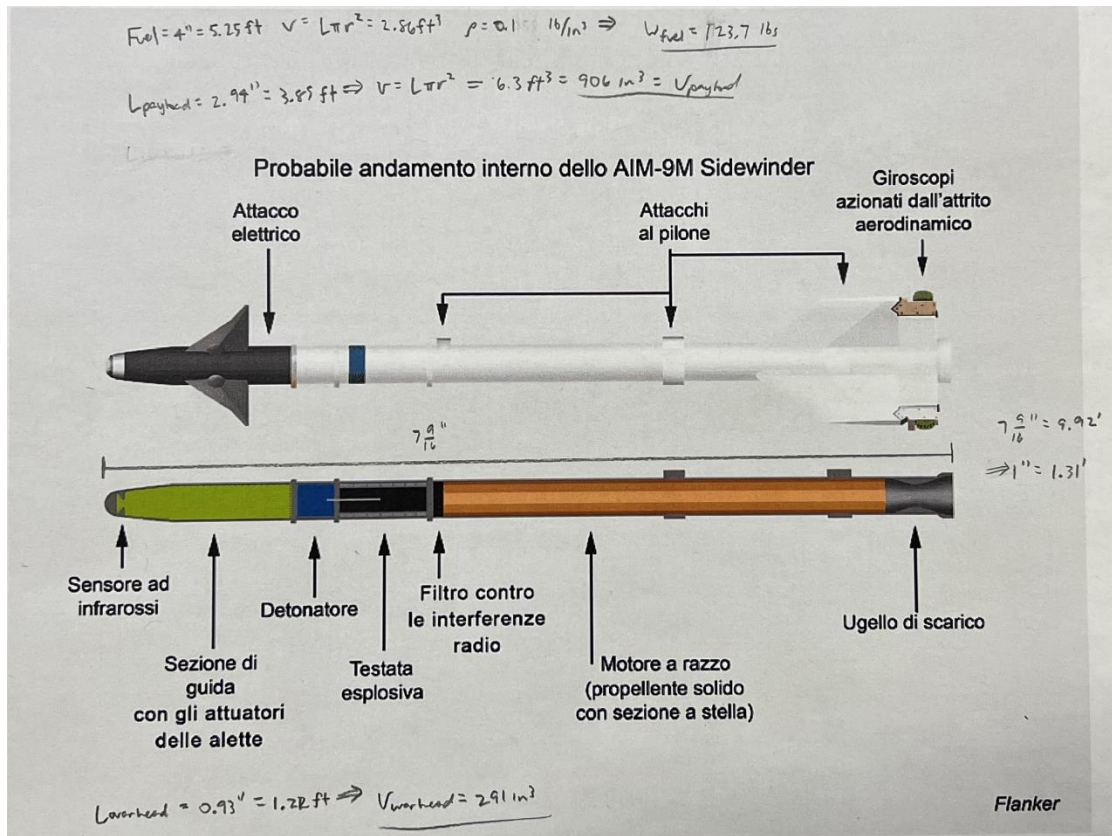


Figure B.1: AIM 9X Block II Side Profile for Calculations (Ref. 16)

The AIM-9X weight at half fuel was estimated using the cross-section cutaway of an AIM-9M from Ref. 16. While this isn't the same missile, the configuration is similar. The volume of the fuel in the missile was found by scaling the length of the missile as pictures to the actual length of the missile. Next, the length of the fuel within the missile was found and the volume was found using the already known diameter of the missile. Finally, the weight of the fuel within the missile was found by assuming a fuel density of 0.1 lb/in³. The final weight of the fuel when full was found to be 123.7 lbs and 61.9 lbs when at half capacity. With this, the weight of the missile when empty can be found by subtracting the weight of the fuel from the known weight of the missile. This gives an empty weight of 67.3 lbs. Finally, the total weight of the missile with half of its fuel was found by adding the empty missile weight to the half fuel weight, resulting in a weight of 129.1 lbs.



Appendix C: AIM-9X Volume and Planform Area Calculations

Fleeman's Figure 2.15 AIM 9X Calculation Reference



Figure C.1: AIM 9X Block II Side Profile for Calculations (Ref. 15)

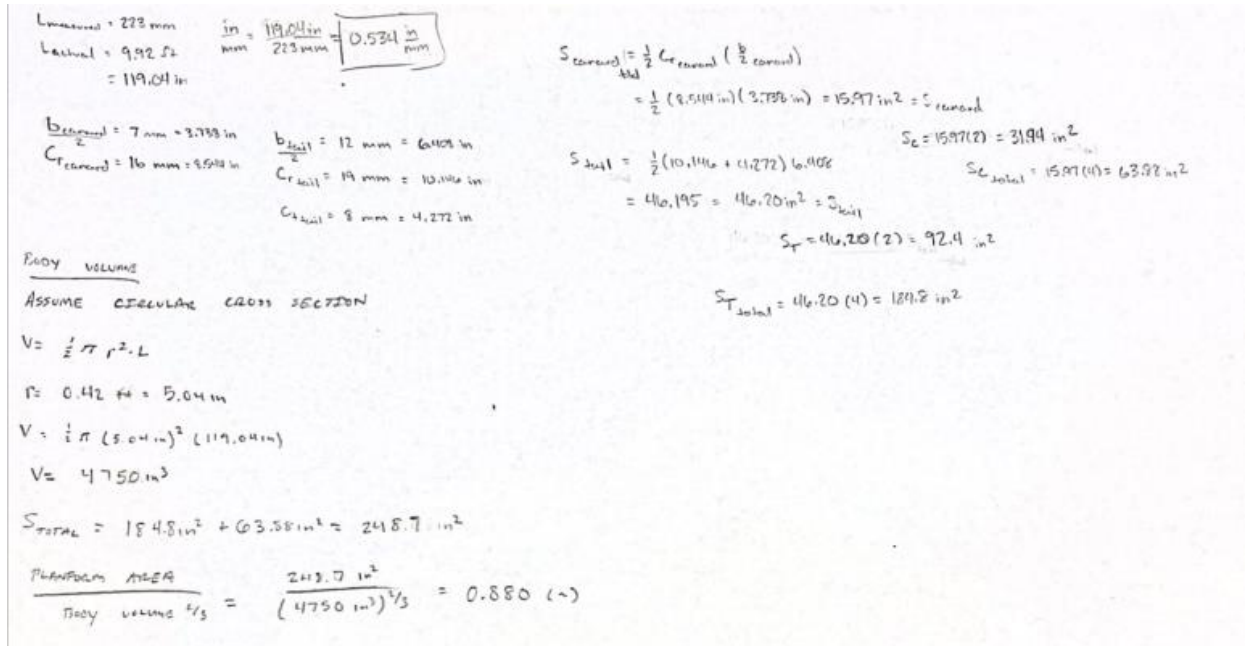


Figure C.2: AIM 9X Block II Body Volume and Ratio Calculations



Figure C.1 was taken from Ref. 15 and was used for dimensions for the calculations seen in Figure C.2. These calculations were used to find the ratio of the total planform area to *body volume*^{2/3}. The process followed was to use the actual length of the missile of 9.92 ft (3.02 m), or 119.04 in, and find the ratio of measured to actual length. The length of the missile was measured to be 223 mm and the conversion to feet was found to be 0.534 in/mm. The first step was to find the area of the four fins in the forward section of the missile. The forward fins are seen to be triangles and the area was found using the root chord length and span length of the fin. After finding the area of one fin, that area was multiplied by 4 to yield the total area for the forward fins. The same process was followed for the aft fins; however, these fins were trapezoids rather than triangles. Using the trapezoidal area equation using the root chord, tip chord, and span of the planform yielded the area. After multiplying by 4 to find the total aft fin area, the forward and aft fin areas were added together, finding that the total planform area was 248.8 in^2 (1605 cm^2). The body volume was found using the cylinder volume equation, since it was assumed the AIM 9X Block II is a uniform cylinder for the entire length. The body volume was found to be 4750 in^3 ($77,900 \text{ cm}^3$). The ratio of these two values was found to be 0.88, which is seen in Figure C.2.



Appendix D: AIM-9X Planar Surface Geometric Calculations

Fleeman Figure 2.27 AIM-9X Calculation Reference

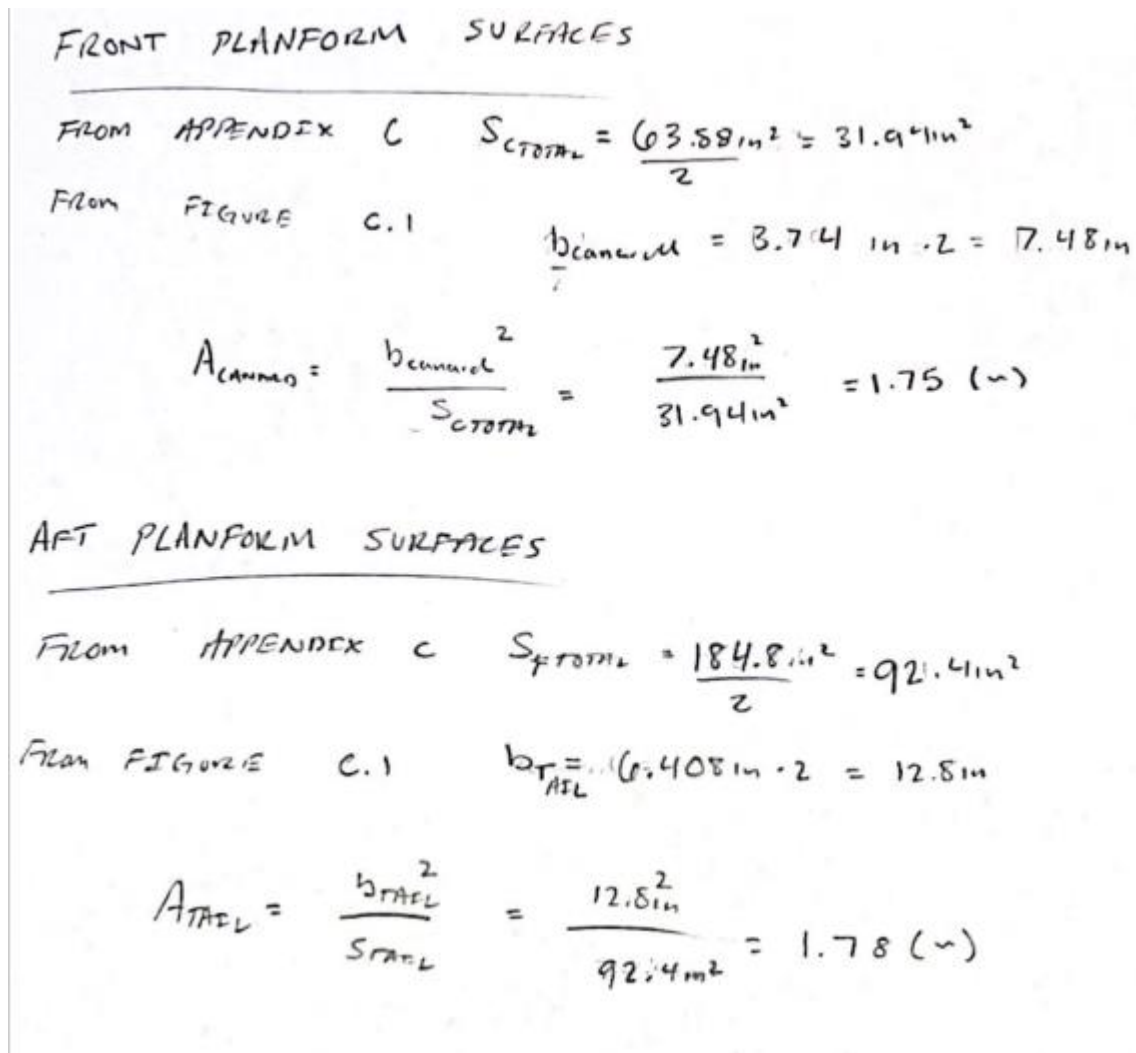


Figure D.1: AIM-9X Block II Planform Aspect Ratio Calculations

The calculations for the front and aft planforms are seen above. The value for total planform area was already found in Appendix C, and the full span of the missile was measured from Figure C.1. After obtaining those values, they were plugged into the AR equations and used for analysis.



AIM -9X Mean Aerodynamic Chord Calculation

To calculate the mean aerodynamic chord, Ref. 17 was used. This was done using the following equation:

$$c_{mac\ tail} = \frac{2}{3} * c_{r\ tail} * \left(\frac{1 + \lambda + \lambda^2}{1 + \lambda} \right)$$

However, λ must be calculated. It was calculated below using a c_t of 4.272 in and a c_r 10.146 in.

$$\lambda = \frac{c_t}{c_r} = \frac{4.272\ in}{10.146\ in} = 0.42$$

Using this λ and the previously mentioned c_r , the mean aerodynamic chord was calculated.

$$c_{mac\ tail} = \frac{2}{3} * 4.272\ in * \left(\frac{1 + 0.42 + 0.42^2}{1 + 0.42} \right)$$
$$c_{mac\ tail} = 3.203\ in$$

AIM -9X Mean Aerodynamic Chord Calculation

For section 10.1, the $\frac{M}{qc_{mac}}$ value was found using the assumptions discussed in that section. The calculations for the $\frac{M}{qc_{mac}}$ value as well as the actual $\frac{nS_{surface}}{S_{ref}}$ value can be seen below.



Assume

$M = 2.5$ (~)

Alt = 20,000 ft

$\gamma = 1.4$ (~)

$R = 1716 \frac{\text{ft} \cdot \text{lb}}{\text{slug} \cdot \text{R}}$

$C_{mac} = 13.3$ in FOUND IN SECTION 9.1

$C_{mac} = 1.11$ ft

@ 20,000 ft, $T = 4417.2$ REF 11

$\rho = 1.27 \times 10^{-3} \frac{\text{lb}}{\text{ft}^3}$ REF 11

$a_{20,000} = \sqrt{\gamma R T}$

$a_{20,000} = \sqrt{(1.4)(1716 \frac{\text{ft} \cdot \text{lb}}{\text{slug} \cdot \text{R}})(4417.2)}$

$a_{20,000} = 1036 \text{ ft/s}$

$M = \frac{V}{a}$

$V_{20,000} = M \cdot a = 2.5(1036 \text{ ft/s})$

$V_{20,000} = 2591 \text{ ft/s}$

$$\frac{M}{q C_{mac}} = \frac{2.5}{\frac{1}{2} (1.27 \times 10^{-3} \frac{\text{lb}}{\text{ft}^3}) (2591 \text{ ft/s})^2 (1.11 \text{ ft})} = 0.00053 \frac{\text{ft}}{\text{lb}}$$

FROM APPENDIX C. $S_{L \text{ TOTAL}} = 63.98 \text{ in}^2 = 0.4441 \text{ ft}^2$

$S_{T \text{ TOTAL}} = 184.81 \text{ in}^2 = 1.28 \text{ ft}^2$

$S_{\text{SURFACE}} = 0.4441 \text{ ft}^2 + 1.28 \text{ ft}^2 = 1.72 \text{ ft}^2$

$S_{\text{REF}} = 0.349 \text{ ft}^2$

$n_{\text{surface}} = 4$

$$n_{\text{surface}} \cdot \frac{S_{\text{SURFACE}}}{S_{\text{REF}}} = \frac{4 \cdot 1.72 \text{ ft}^2}{0.349 \text{ ft}^2} = 19.7$$
 (~)

Figure D.3: Planar Surface Area Reference and $\frac{M}{q C_{mac}}$ Calculation

The $\frac{M}{q C_{mac}}$ value was found using the assumption of Mach 2.5 at 20,000 ft. Using the 20,000 ft, Ref. 11 was used to calculate the speed of sound at that altitude, and then multiplied by the Mach to find velocity, which was used to find q . C_{mac} was found in Appendix C and all values were plugged into the equation and found. The surface area and reference area values were all found in Appendix C and were found using the equation in Figure D.3.

